

ISSN 0288-4534
CODEN:KONAE7

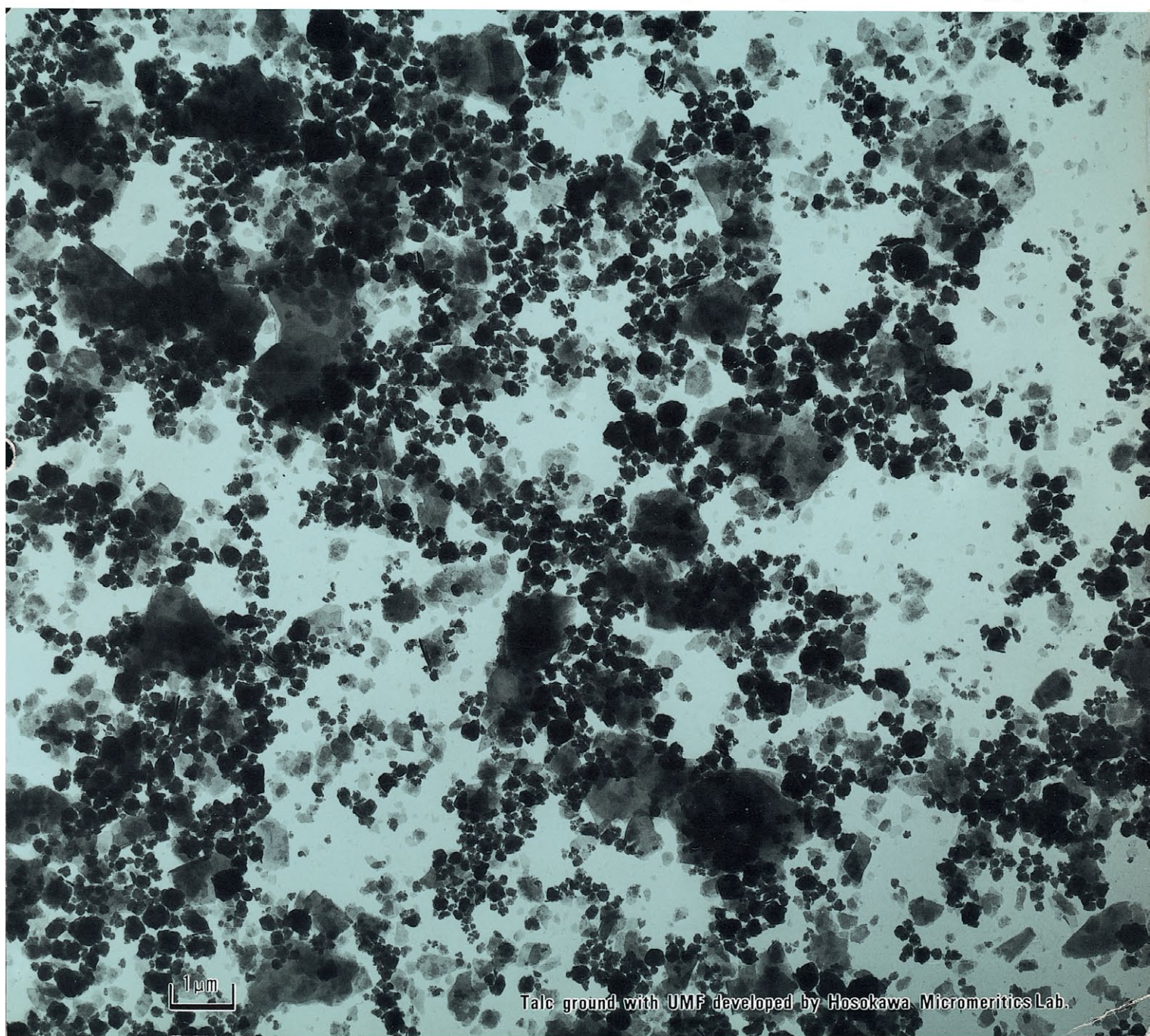
粉

KONA

**POWDER SCIENCE AND
TECHNOLOGY IN JAPAN**

No. 2 (1984)

Published by The Party of Powder Technology (JAPAN)



Talc ground with UMF developed by Hosokawa Micromeritics Lab.

Explanation of the Cover

“粉”; This Chinese character is pronounced as “KONA” in Japanese and means “Powder”.

“粉” on the front page was written by the late Mr. Eiichi Hosokawa, founder of Hosokawa Micron Corporation.

See page 6 for description of the cover photograph.

Editorial Board

Naoya Yoshioka	(Professor Emeritus of Kyoto University) Editor in Chief.
Masuo Hosokawa	(President of Hosokawa Micron Corp.)
Koichi Iinoya	(Professor of Aichi Institute of Technology)
Genji Jimbo	(Professor of Nagoya University)
Yasuo Kousaka	(Professor of University of Osaka Prefecture)
Kei Miyanami	(Professor of University of Osaka Prefecture)
Takeo Yano	(Professor Emeritus of University of Osaka Prefecture)
Tetsuo Yoshida	(Professor of Chubu University)
Tohei Yokoyama	(Managing Director of Hosokawa Micromeritics Lab.)

Editorial Assistants

Shigesumi Kobayashi	(Hosokawa International Inc.)
Toyokazu Yokoyama	(Hosokawa Micromeritics Lab.)
Tomoyuki Yamaguchi	(Hosokawa Micromeritics Lab.)



Hosokawa Micromeritics Laboratory & Hosokawa Micron Corporation

Publication Office and Owner of Copyright
The Party of Powder Technology (Japan)
in Hosokawa Micromeritics Laboratory
9, Shodai-tajika 1-chome, Hirakata, Osaka 573 Japan

(Complimentary Copy)

Printed in Japan

Contents

Grinding Behavior and Powder Characteristics of Si_3N_4 as a Raw Material for Ceramics	<i>Kazuo Suzuki and Yoshitaka Kuwahara</i> . . . 2
The Sieving Rate of Cylinder Particles	<i>Shigehisa Endoh, Jiro Koga and Kenji Yamaguchi</i> 7
Flow Behavior of Particles in a Storage Vessel of a Table Feeder	<i>Hiroaki Masuda, Zhong-qi Han, Takashi Kadowaki and Yuji Kawamura</i> . . . 16
Reduction of Power Consumption in Pneumatic Conveying of Granular Materials through a Pipeline	<i>Takeshi Kano</i> 24
A New Particle Size Distribution Apparatus based on Unbalance by Centrifugal Sedimentation	<i>Masafumi Arakawa, Gen Simomura, Akira Imamura, Naohiko Yazawa, Noriyoshi Kaya and Hiromi Kitai</i> 35
Short History of Grinding Implements for Domestic Use in Japan	<i>Shigeo Miwa, Atsuko Shimosaka and Jusuke Hidaka</i> 43
The Role of Adsorbed Water on Adhesion Force of Powder Particles	<i>Masatoshi Chikazawa, Takafumi Kanazawa and Toshihide Yamaguchi</i> 54
Measurement of Pore Distribution by Utilizing Equilibrium Moisture Content Curve	<i>Chikao Arai, Yoshiki Sano and Tadami Hanakawa</i> 62
Effects of Tensile Strength and Tensile Breakup Energy on Mulling Processes of Wet Powders	<i>Keijiro Terashita, Teruo Kimura, Hideyo Tsukaguchi and Kei Miyanami</i> 71
< Review >	
A Review of the Investigations into Powder Bed Mechanics Based on a Microscopic View in Japan	<i>Jun-ichiro Tsubaki</i> 78
Informational Articles	87

Grinding Behavior and Powder Characteristics of Si_3N_4 as a Raw Material for Ceramics[†]

Kazuo Suzuki* and Yoshitaka Kuwahara*

Government Industrial Research Institute, Nagoya
Agency of Industrial Science and Technology

Abstract

It is well known that powder characteristics of high-performance ceramics have great influence on the sintering activity of the powders and the properties of the final products. Since grinding process is essential for such materials in many cases, it is important to grasp the change in powder characteristics by grinding.

In this study, Si_3N_4 powder was ground with a vibration ball mill under several experimental conditions to examine grinding characteristics such as wear behavior of a mill and grinding media, particle size distribution, specific surface area, and X-ray diffraction intensity. Consequently the following results were obtained; ultra-fine grinding of Si_3N_4 was possible using a vibration ball mill and grinding behavior was considerably affected by the materials constructing the mill and the grinding media (especially by the hardness of the materials).

1. Introduction

High-performance ceramics which have received considerable attention as heat-resisting or corrosion-resisting material are usually produced through sintering process at high temperature. In this case, their final quality and performance are greatly dependent on the powder characteristics such as morphology, chemical composition, crystallographic phase, etc.

Grinding is an essential operation for the improvement of the morphological characteristics such as size reduction, increase of surface area and deagglomeration. In a vibration ball mill system, the relative actions of particles and grinding media bring about normal and shear stresses caused by impact and friction forces. These physical processes cause not only mor-

phological but also chemical and crystallographical changes¹⁾. In addition these changes may have much influence on various properties such as the packing structure, the sintering activity, the quality of final products, etc.

In this paper, several powder characteristics of Si_3N_4 were experimentally investigated with a vibration ball mill. In particular, the wear of a mill and grinding media from the viewpoint of chemical composition due to the contamination as well as the distribution, the specific surface area and the X-ray diffraction intensity from that of morphology and crystallographic phase were examined.

2. Experimental method and sample

A mill (a pot) and grinding media (balls) made of alumina were chiefly used in this experiment under the conditions indicated in **Table 1**. The grinding tests were carried out in three environmental states; one was a dry grinding for 200 hours, and the others were wet grindings with Fleon 113 for 200 hours and ethyl alcohol for 300 hours.

Particle size distributions of the ground products were measured by a photo extinction

* 1 Hirate-machi, Kita-ku, Nagoya, Aichi, 462
TEL. 052 (911) 2111

Received June 6, 1984

† This report is based mainly on the previous paper printed in *Journal of the Society of Powder Technology, Japan*, 20, 82 (1983).

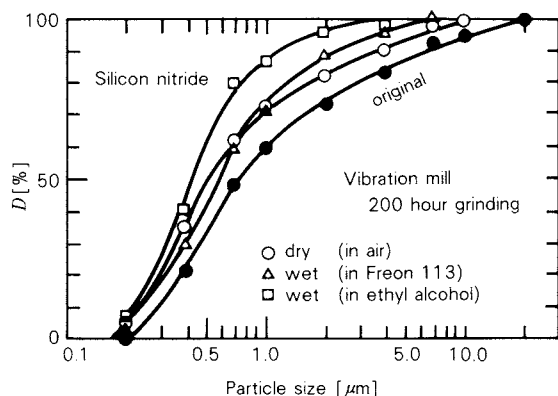


Fig. 1 Particle size distribution of 200 hour ground Si_3N_4 powder by vibration ball mill using the pot and the media made of alumina

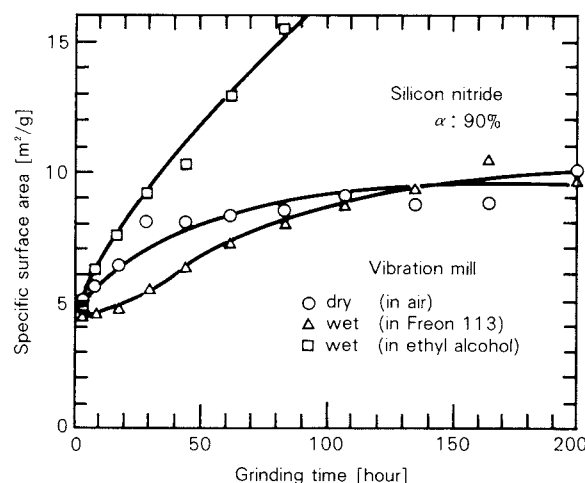


Fig. 2 Increasing characteristics of the specific surface area of ground product

Table 1 Experimental conditions

Vibration ball mill		
Amplitude of circular vibration	1.5 mm	
Frequency of vibration	1800 r.p.m.	
Volume of the mill body	1100 cc	580 cc
Materials of the mill body	Alumina	Silicon nitride
Grinding media		
Materials of the media	Alumina	Silicon nitride
Size of the media	$\phi 15$ mm	$\phi 10 \times 10$ mm
Ball filling of mill	J=0.70 (1530g)	J=0.70 (830g)
Powder		
Materials	Si_3N_4 (alfa-, amorphous-, beta-)	
Density of the materials	3.18 (2.73 for amorphous- Si_3N_4)	
Powder fraction	U=1.00 (270g)	U=1.00 (70g)
Grinding fluids		
	Ethyl alcohol	Methyl alcohol
	Fleon 113	

method based on sedimentation in the gravitational and centrifugal field. On the other hand, the specific surface areas were obtained by BET method using nitrogen gas adsorption at the extinction temperature of 110°C .

X-ray diffraction intensities of the ground products were measured by a step scanning method (10^4 counts) using the characteristic X-ray of $\text{CuK}\alpha$ (35V, 20 mA) with Ni filter.

In this study, Si_3N_4 powder (#325) with a density of 3.18 g/cm^3 and α -phase of 90% was employed as a test sample. Its properties are indicated as the symbol of \bullet in Figs. 1, 4 and 5.

3. Experimental results and discussion

3. 1 Wear of mill and grinding media

It is well recognized that Si_3N_4 with the Vickers hardness number of 2800 is harder than alumina with that of 2000. Since Si_3N_4 was ground in an alumina mill apparatus in this experiment, contamination of alumina caused by wear might possibly occur. In this study, therefore, the wear behavior in the grinding process was examined in advance.

The weight losses of the pot and the balls after the grinding trials in three environmental conditions such as air (for 200 hours), Fleon 113 (for 200 hours), and ethyl alcohol (for 300 hours) are summarized in Table 2. The losses were measured by a balance with a sensitivity of one gram.

As is evident from this table, a great deal of wear occurred in wet grinding with ethyl alcohol. On the other hand, remarkable wear was not observed in both dry grinding and wet one with Fleon 113. The result indicates that the use of alumina is not suitable for wet grinding of

Table 2 Weight loss of the pot and the grinding media made of alumina

	Dry	Wet	
	Air	Felon 113	Ethyl alcohol
Grinding time (hour)	200	200	300
Weight loss of the mill body (g)	4	0	7
Weight loss of the media (g)	0	1	60
Total weight loss (g)	4	1	67

Si_3N_4 with ethyl alcohol.

Although wear mechanism is not obvious, it is recognized that the wear behavior is influenced by stresses on the contact region. In dry grinding, since the inside of the pot and the surfaces of the balls were coated with a ground Si_3N_4 powder, the kinetic energy of the balls was almost absorbed in the coated layers of the powder. The resultant decrease in intensity of impact by the balls would possibly reduce the degree of the wear. In wet grinding, the particles were dispersed in the liquid medium and the wear behavior would be affected by the relative motion between particles and balls in the pot. These motions were considerably dependent on the physical properties of the liquid medium (viscosity, density, etc.) In addition, the influence of the surface energy reduction resulted from wetting with the fluids on the wear behavior should be taken into account. Such wear is supposed to be closely related with grinding mechanism and mechanochemistry.

3. 2 Particle size distribution and specific surface area

The particle size distributions of the products ground in three different environmental conditions with the above-stated apparatus, are shown in Fig. 1 together with that of the original powder. Figure 2 shows the increase of the specific surface area with increasing grinding time.

These two results apparently indicate that the size reduction of the ground products in wet grinding with ethyl alcohol was most remarkable. As described in the previous section, however, the existence of a lot of worn particles in the ground product should be taken into account. It can be presumed that a hard indenter (Si_3N_4 particles in this case) located on the surface generally produced a local damage zone, and that the size of the worn particles produced by scratch was generally smaller than that of the abrasive (Si_3N_4 particle). Based on the above discussion the actual particle size distribution would be larger than the obtained result indicated in Fig. 1 and the specific surface area would be smaller.

Grinding characteristics may be affected by the materials of a pot and balls. In Fig. 3, the specific surface areas of Si_3N_4 powder, which

was ground using the pot and the balls made of sintered silicon nitride, are shown as function of the grinding time. Three types of Si_3N_4 powders with different morphology and crystallography were ground in wet grinding with methyl alcohol. The weight losses of the pot and the balls could not be detected by balance after 200 hour grinding in any case. What is evident from this figure is that the specific surface area considerably increased compared with the case using the pot and the media made of alumina. The rapid increase in the specific surface area until 200 hours and its gradual decrease after the period were observed.

It is clear that the grindability was affected by the hardness of the materials of a pot and media. The grinding behavior would be fundamentally based on the fracture phenomenon of the individual particles. The hardness of materials is generally expressed in term of its resistance of local deformation on the contact region. Consider the contact problem based on the elasticity analysis²⁾ by Herz. When E and ν are taken as the Young's modulus and the Poisson's ratio of the particles respectively and

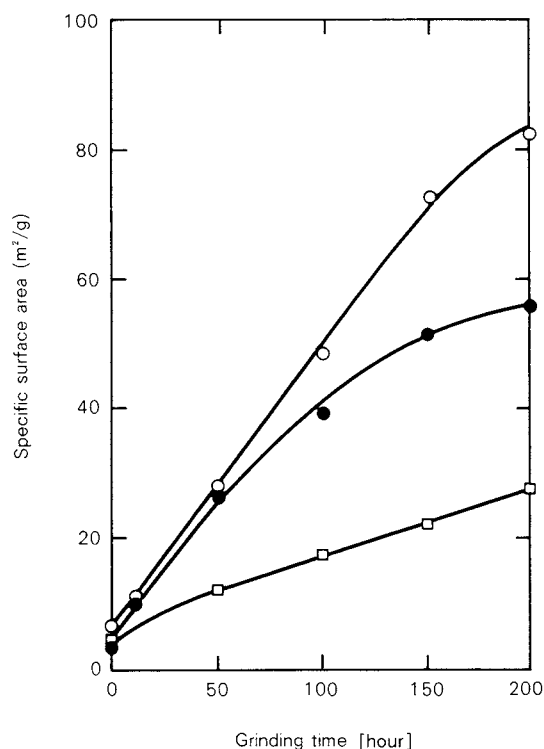


Fig. 3 Increasing characteristics of the specific surface area of three types of ground Si_3N_4 powder by vibration ball mill using the pot and the media made of sintered silicon nitride

E' and ν' as the corresponding constants for the pot or the grinding media, the radius a of the contact area is written by

$$a = \frac{4}{3} PR \left(\frac{1 - \nu^2}{E} + \frac{1 - \nu'^2}{E'} \right)^{\frac{1}{3}} = \alpha P^{\frac{1}{3}}$$

where P and R are the normal force and the particle radius, respectively³⁾. The radius a is affected by the Young's modulus and the Poisson's ratio of a pot or media, and varies with the normal load P . At the periphery of this contact region, the tensile stress reaches its maximum value

$$\sigma_m = \frac{1}{2} (1 - 2\nu)p_0$$

where $p_0 = P/\pi a^2$ is the mean normal stress, σ_m acts radially and in parallel with the surface. The maximum tensile stress is proportional to the mean normal stress. When plastic deformation occurs in brittle materials, the fracture possibly takes place at the critical stress (yield stress, Y). On the other hand, when the Vickers hardness number is about three times of the yield stress⁴⁾, the hardness of the grinding media or the pot strongly influences the grinding characteristics.

The reason of different increasing rates among three types of the powders should be considered from the viewpoint of the morphological or crystallographical state, i.e. the mean particle size, the particle size distribution, the particle shape, the degree of agglomeration, crystallographic phase and crystallite size of an original powder. Although remarkable conclusion cannot be drawn due to an insufficient number of experimental samples, it is supposed that rounded and higher crystallized particles are easily ground.

3. 3 X-ray diffraction characteristics

Crystallographic perfection of the particles is also important for a ceramic powder. X-ray diffraction intensities of the product ground by the vibration ball mill are shown in Fig. 4. The changes of the diffraction intensity ratios for [322] plane to the original powder are indicated as a function of the grinding time. The intensity ratio in wet grinding decreased linearly, though in dry grinding it decreased rapidly in the initial period of grinding.

As shown in Fig. 5, the X-ray diffraction in-

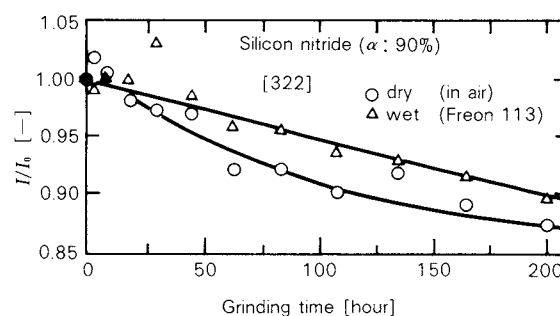


Fig. 4 Decrease of X-ray diffraction intensity as function of grinding time

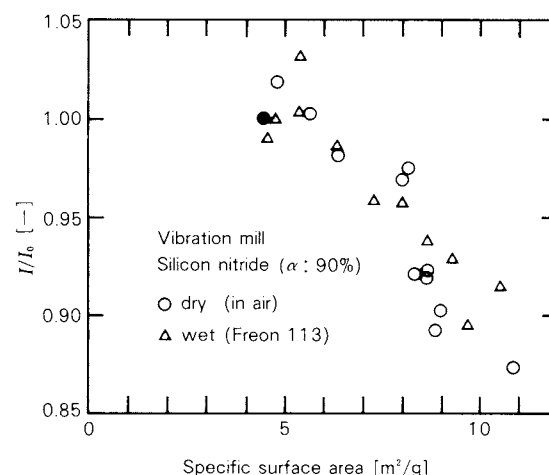


Fig. 5 Relationship between the X-ray diffraction intensity and specific surface area

tensity ratios decreased with increasing specific surface area, though the difference between dry and wet grinding was not obvious.

4. Conclusion

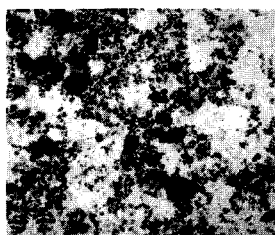
In this experimental investigation, Si_3N_4 powder was ground with a vibration ball mill to examine the grinding characteristics under several environmental conditions. The obtained results are as follows:

- (1) Large amount of wear of the mill and the grinding media took place when wet grinding was performed in ethyl alcohol. Wear behavior was considerably dependent on the grinding mechanism.
- (2) Although ultra-fine grinding of Si_3N_4 was possible using a vibration ball mill, grinding characteristics were affected by the materials constructing the mill and the grinding media (especially by the hardness of the materials).

- (3) Lattice imperfection of the ground product increased with increasing specific surface area.

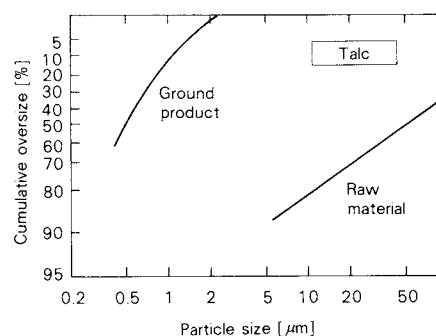
References

- 1) Kubo, T.: 'Introduction to Mechano-chemistry', Tokyo Kagaku Dojin Co., Ltd. (1978).
- 2) Timoshenko and Goodier: 'Theory of Elasticity', McGraw Hill (1934).
- 3) Lawn, B.R. and T.R. Wilsaw: 'Fracture of Brittle Solid', Cambridge Univ. Press (1975).
- 4) Bowden, F.P. and D. Tayber: 'Friction and Lubrication of Solid Part II', Clarendon Press, Oxford (1954).



Explanation of the cover photograph

The cover photograph (by TEM) shows a very fine talc powder with the magnitude of 10000X. The powder was obtained through dry grinding with UMF system developed by Hosokawa Micromeritics Laboratory. The particle size distributions of the raw material (average diameter: 50 μm) and the ground product (average diameter: 0.5 μm) are indicated in the right figure. The BET adsorption method provided the specific surface area of 43.8 m^2/g .



The Sieving Rate of Cylinder Particles[†]

Shigehisa Endoh* and Jiro Koga*

Powder Technology Laboratory,
The Institute of Physical and Chemical Research

Kenji Yamaguchi**

Department of Applied Chemistry
Hokkaido University

Abstract

The effects of particle shape and operating conditions on the sieving process were experimentally studied and the passing characteristics were discussed. Cylinder particles of unity in aspect ratio were batchwise sieved by a reciprocal shifter. The retention on a woven wire sieve of square mesh was measured and the sieving rates were obtained. The behaviour of retention with sieving time were classified into two types according as the cylinder diameter D was near the mesh size a or $D \ll a$. In the latter case, the cylinder was easily screenable and the retention exponentially decreased with sieving time. The sieving rate coefficient was independent of the initial charge. On the other hand, in the former case, the sieving rate was initially influenced by the particle mass charged on the sieve and the sieving process deviated from the exponential decrease. The sieving rate was quantitatively associated with the geometrical shape of cylinders. The sieving rate coefficients of easily screenable cylinders or in the earlier period of sieving were inversely proportional to the third power of the cylinder length. The probabilities of the cylinder passing through an opening were calculated by use of geometrical probabilities and compared with the experimental results. The number of trials of passing per unit time was almost inversely proportional to the cylinder length. Furthermore, the sieving characteristics of a set of sieves were analyzed on the basis of the rate coefficient obtained previously. It was possible to predict the change of each retention with sieving time, sufficiently. The correlation between the equivalent spherical diameter of cylinder and 50%-separation diameter measured by the multi-stage sieving gave that the separation diameter mainly depended on the cylinder diameter. In the vicinity of centrifugal effect of 1.3, the sieving rate was maximum and the empirical relationship presented by previous workers for the optimum shifting conditions was applicable to the cylinder particles.

1. Introduction

In the case of sieving of elongated or flattened materials such as woody chips, coarse particles might be mingled among undersize parti-

cles. It is important to obtain the relation between particle shape and the characteristics of passage through sieve opening.

The passing probabilities of granular materials such as sand might be estimated from those of spheres³⁾. Miwa related the size of 50%-separation of irregular shape materials to the equivalent spherical diameters⁴⁾. However, when the diameter or width of particle is smaller than the opening size or the diagonal of the opening respectively, the particles might pass through the screen even if the length is longer

* Wako Saitama, 351-1

TEL. 0484 (62) 1111

** Nishi 8-chome, Kita 13-jo, Kita-ku, Sapporo, 060

TEL. 011 (711) 2111

Received May 23, 1984

[†] This report is based mainly on the previous paper printed in *Journal of the Society of Powder Technology, Japan*, 20, 8 (1983)

than the opening size.

The sieving of elongated or flaky materials has been investigated by Markwick²⁾ and Riley⁶⁾ *et al.*. However, in those works, the effect of particle shape on sieving rate have not quantitatively been clarified yet.

In this work, therefore, it is attempted that the influence of particle shape and operating conditions on the sieving process have been experimentally examined. Cylinder particles of unity in diameter and aspect ratio are charged on a sieve and batchwise sieved. The passing probability of a cylinder through an opening has been calculated by using geometrical model and compared with experimental results. Furthermore, the multi-stage sieving process has been analyzed on the basis of the sieving rate characteristics and the measured distribution has been discussed.

2. Experimental

2. 1 Cylinder particles

Physical properties of cylinder particles are listed in **Table 1**. Used cylinder particles were spaghetti of 2mm diameter and cut in given length. The distributions of the cylinder length are shown in **Fig.1**. The length obeyed the normal distribution and the standard deviation was very small. In this paper, the ratios of cylinder length to the diameter, aspect ratio, L/D of sample 1, 2, 3 and 4 are denoted by 1, 2, 4 and 8 respectively for the sake of convenience.

2. 2 Experimental method

In **Table 2**, experimental conditions are listed. The sieves used in the experiment were square mesh woven wire sieves of 0.2m diameter. In the following part, the sieves are denoted by the numbers shown in **Table 2**.

The sieving equipment is schematically illustrated in **Fig.2**. The test sieve was fixed on

the reciprocal shifter, whose half stroke b was 0.031m and the frequency N was changeable from 1.26s^{-1} to 3.95s^{-1} . The range of centrifugal effect Z_c , defined by

$$Z_c = (2\pi N)^2 b/g \quad (1)$$

is shown in **Table 2**.

A given amount of cylinder particles with diameters smaller than the sieve opening was uniformly placed on the sieve. After given shifting duration, the undersize particles were weighted. In such a case, mechanical stop and start of shifter might cause some sampling errors. First, in order to examine this effect, preliminary experiments as follows were made.

(i) Continuous method: Particles were sampled after given duration of shifting.

(ii) Intermittent method: The shifting and stopping were repeated in each test run.

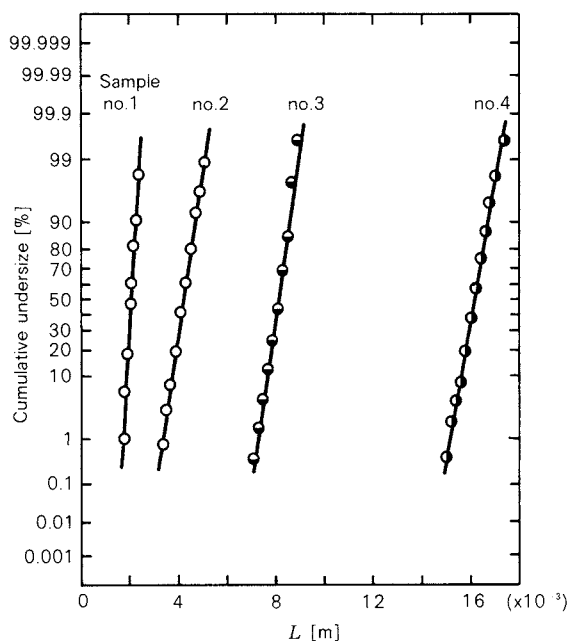


Fig. 1 Distribution of cylinder length

Table 2 Experimental conditions

Half stroke of reciprocating (b) [m]	0.031			
Frequency (N) [s^{-1}]	1.26	2.43	3.23	3.95
(Z_c [-])	(0.198)	(0.737)	(1.30)	(1.94)
Initial charge on a sieve (W_0) [kg]	0.05	0.10	0.20	
Nominal opening of sieve (a) [m]	Sieve no.9: 2.00×10^{-3} (0.525)			
(Porosity [-])	Sieve no.8: 2.38×10^{-3} (0.560)			
	Sieve no.7: 2.83×10^{-3} (0.608)			
	Sieve no.6: 3.36×10^{-3} (0.631)			

Table 1 Physical properties of cylinder particle

Sample	1	2	3	4
Material	Spaghetti			
Density [kg/m^3]	1.38×10^3			
Diameter(D) [m]	2.00×10^{-3}			
Length [$\times 10^{-3}\text{m}$]				
mean value (L)	2.04	4.16	8.10	16.13
standard deviation	0.17	0.36	0.34	0.14

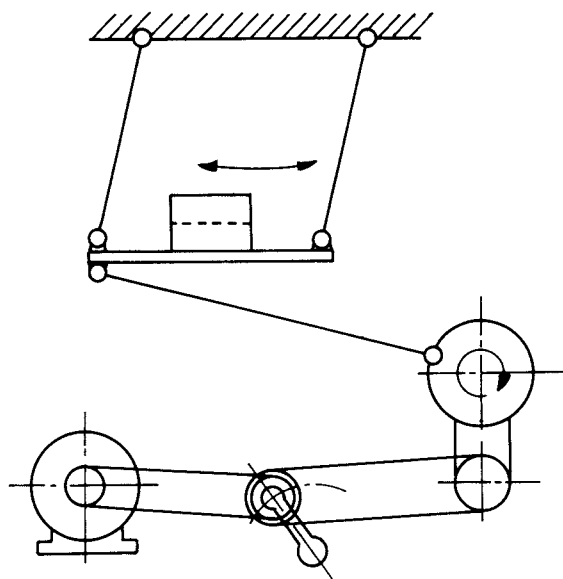


Fig. 2 Experimental apparatus (Reciprocal shifter)

Since the difference between these two methods was negligibly small, the experiments were made by the latter.

Another problem exists in the experiment. In the present work, since the opening is square and the motion of sieve is reciprocal, the orientation of the opening might influence the passage of cylinder. In order to consider this problem, two kinds of procedures as follows were carried out: in one procedure, the orientation was parallel to the direction of shifting and in another, the orientation was diagonal. Subsequently, the retention on the sieve have been determined by averaging the results of the procedures described above and used for the following analysis.

3. Result

The mass of retention of cylinders on a sieve W_r is plotted against sieving time t on semi-log charts as shown in Figs. 3, 4 and 5. Figure 3 shows the effects of sieve opening size a and aspect ratio of cylinder L/D on the sieving process. As is evident from this figure, in the case of sieve no. 7 with opening size of 2.83 mm, W_r 's exponentially decrease with sieving time t , while in the case of smaller opening, no. 8 ($a = 2.38$ mm) and no. 9 ($a = 2$ mm), behavior of W_r deviated from exponential decrease. In the following part, the sieved cylinder having diameter D near the mesh size ($0.75 \leq D/a \leq 1$) is

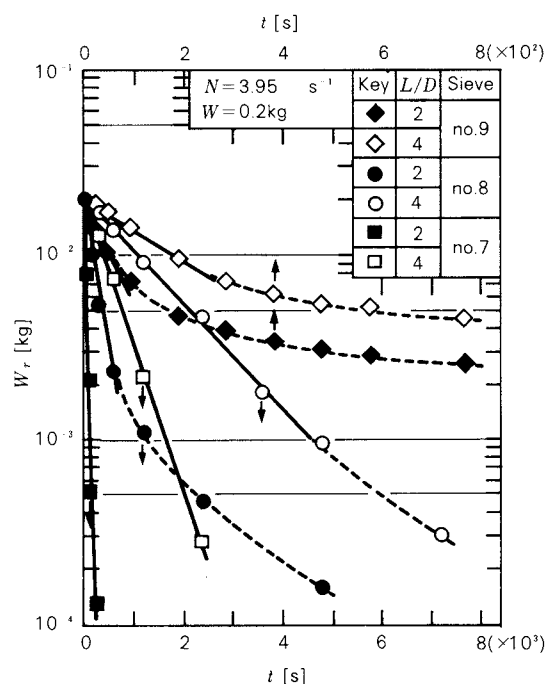


Fig. 3 Effect of sieve opening size on sieving process

called as near mesh cylinder correspondingly so called near mesh grains⁵⁾.

Figure 4 gives typical effects of initial charge W_0 , when no. 9 sieve with opening size close to cylinder diameter was employed. The exponential decrease does not appear and the sieving process might be separated into two parts. In the earlier period, the sieving rates of cylinders of $L/D = 2$ and 4 noticeably increase with W_0 . On the other hand, in the later period, the cylinder passing is steady and the behaviors of W_r are almost same. Particularly W_r of $L/D = 1$ at arbitrary sieving time seems to be proportional to W_0 .

The effects of shifter frequency N are shown in Fig. 5. At $N = 1.26 \text{ s}^{-1}$, the lag time until exponential decrease is observed. During this period, the cylinders might be rearranged in the particle layer on a sieve, and the intensity of shifting is so weak that the lag time becomes noticeable. The rate at $N = 3.23 \text{ s}^{-1}$ is the largest, consequently, it is suggested that the optimum conditions of shifting may exist.

4. Discussion

4. 1 Experimental equation for sieving process

As stated above, the sieving process might be classified into two types. The sieving process of

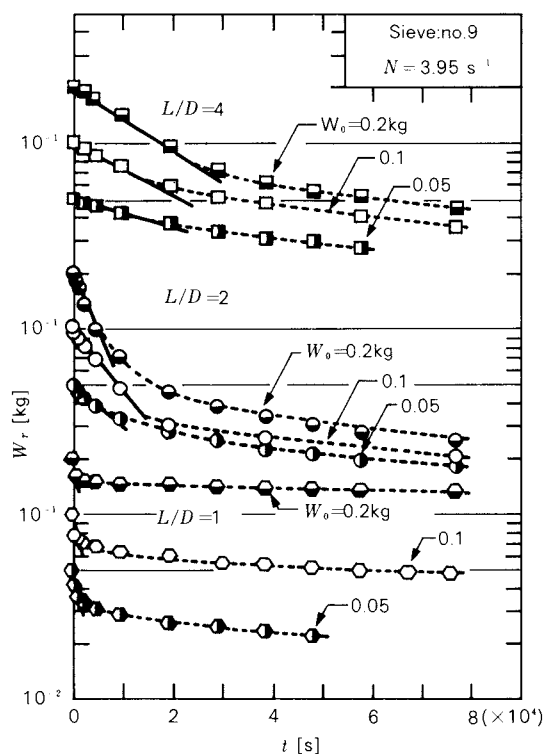


Fig. 4 Effect of initial charge W_0 on sieving process

$a \gg D$, that is, for easily screenable cylinders, is able to be expressed by the following equation.

$$W_r = W_0 \exp(-kt) \quad (2)$$

where k is a sieving rate coefficient. On the other hand, the process for the near mesh cylinder is approximately expressed as follows:

$$W_r = W_0 [K_1 \exp(-k_1 t) + K_2 \exp(-k_2 t)] \quad (3)$$

where K_1 and K_2 satisfy the following equation.

$$K_1 + K_2 = 1 \quad (4)$$

Subscripts 1 and 2 designate the earlier and the later sieving period respectively, thus K_1 and K_2 stand for the fractions of particles passing in respective period.

Those behaviors as shown in Fig. 4 and/or expressed by Eq. (3) have been observed when the material having wide size distribution has been sieved. It has been thought that those kinds of behaviors are caused by the different passing rates among particle sizes⁵⁾. However the sieving process of near mesh spherical particles measured by one-particle tracer method is expressed by Eq. (3)¹⁾. And in this work, the size and the shape of charged particles are all the same and those relations are noticed in

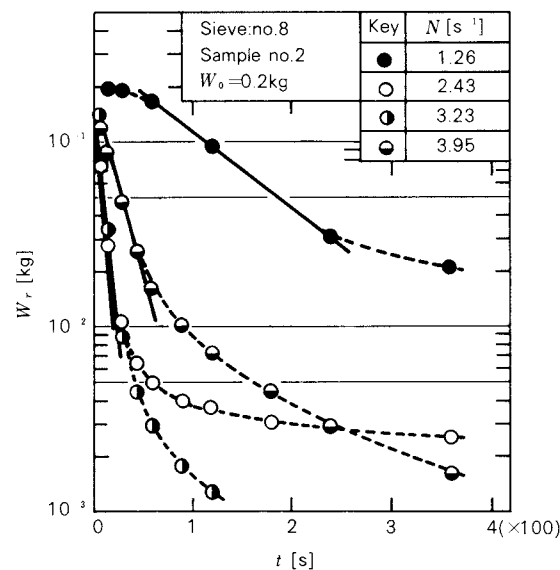


Fig. 5 Effect of frequency of shifter N on sieving process

the case of the near mesh cylinders. Therefore, the sieving process of the near mesh cylindrical particles or the near mesh grains might be expressed by Eq. (3).

4. 2 Effect of frequency

The relationships between the rate coefficient k_1 and frequency N are illustrated in Fig. 6. In this figure, the coefficient in Eq. (2) k is denoted by k_1 . Except the case of $L/D = 8$, the values of k_1 are maximum in the vicinity of $N = 3.1 \text{ s}^{-1}$. Hashimoto and Kondoh have presented the empirical relationship for the optimum shifting condition of reciprocal sieve⁵⁾, as follows:

$$NB^{0.585} = 2000 \sim 2500 \quad (5)$$

where B is a stroke of shifter in mm and N is a frequency in rpm. Then, introducing $B = 62 \text{ mm}$ of the used shifter into Eq. (5), we obtain

$$N = 2.98 \text{ s}^{-1} \sim 3.73 \text{ s}^{-1} \quad (6)$$

$$(Z_c = 1.11 \sim 1.74) \quad (6')$$

Experimental results in Fig. 6 satisfy Eq. (6), consequently, Eq. (5) is applicable to the sieving of cylindrical particles.

4. 3 Effect of initial charge

The coefficients k_1 and k_2 are plotted against initial charge W_0 in Fig. 7. The sieving rate in the case of sieve no. 8 was independent of W_0 , while in the case of sieve no. 9 ($a \approx D$), k_1 in-

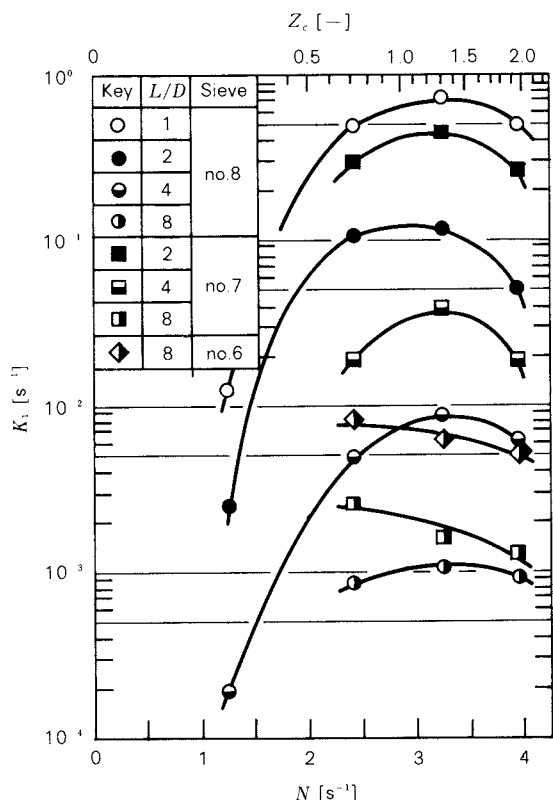


Fig. 6 Effect of frequency of shifter N on rate coefficient of sieving k_1

creased and k_2 of $L/D = 1$ proportionally decreased with W_0 . The cylinder with diameter close to the opening size could pass through the sieve opening only when the long axis of cylinder oriented perpendicularly to the sieve surface. However, the chance of perpendicular orientation is few, and on the sieve surface the orientation of most cylinders is parallel to the surface, particularly in the thin particle layer. Thus in the case of $D \approx a$, small value of k_1 was obtained for low initial charge. Furthermore, as the mean length of particles having $L/D = 1$ is 2.04 mm ($\approx a$), blinding might occur. The blinding remarkably reduces the sieving rate in the later period and the retention W_r in Fig. 4 is proportional to W_0 .

4. 4 Effect of cylinder length

Figure 8 shows the effect of cylinder length on the rate coefficient k_1 . As shown in Fig. 8, the following relationship between the sieving rate coefficient and the cylinder length is obtained.

$$k_1 \propto (L/a)^{-3} \quad (7)$$

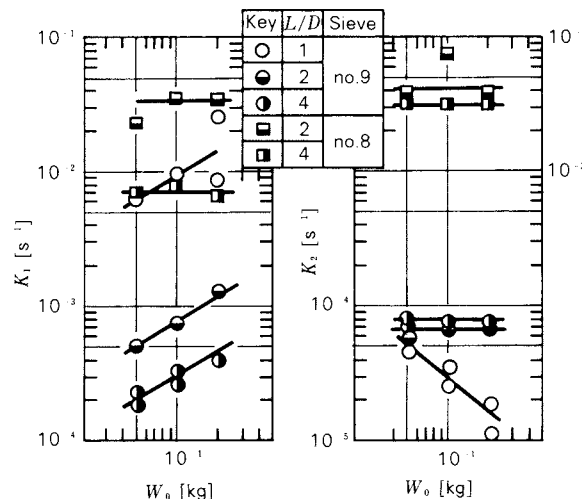


Fig. 7 Effect of initial charge W_0 on rate coefficients of sieving k_1 and k_2

In Fig. 8, the results of Markwick²⁾ are plotted and qualitatively agree with the present work.

4. 5 Passing probability of cylinder

Miwa approximately expressed the batch sieving process as follows³⁾:

$$\begin{aligned} r (= W_r/W_0) &\approx \exp(-i\epsilon P) \\ &= \exp(-\xi\epsilon Pt) \end{aligned} \quad (8)$$

where r is a fraction of retention, P is a probability of a particle passing through an opening and ϵ is an area fraction of opening. i is a number of trials of sieving and is related to the duration of sieving t , given as follows.

$$i = \xi t \quad (9)$$

Eq. (8) is corresponding to the exponential decrease, thus we obtain from Eqs. (2), (8) and (9) as

$$k = \xi\epsilon P \quad (10)$$

where the coefficient of proportion ξ is regarded as a number of trials of sieving per unit time.

Consider the probability of a cylinder passing through a sieve opening. Now it is assumed that the passing probability of a cylinder in square mesh sieve can also be defined by geometrical probability as well as spherical particle³⁾. When a cylinder whose axis orients (θ, ϕ) as shown in Fig. 9(a) falls to sieve with opening of $a \times a$, the cylinder can pass through the sieve if the center of gravity of the cylinder is in the shaded portion in Fig. 9(b). The probability of passing $p(\theta, \phi)$ of a cylinder having

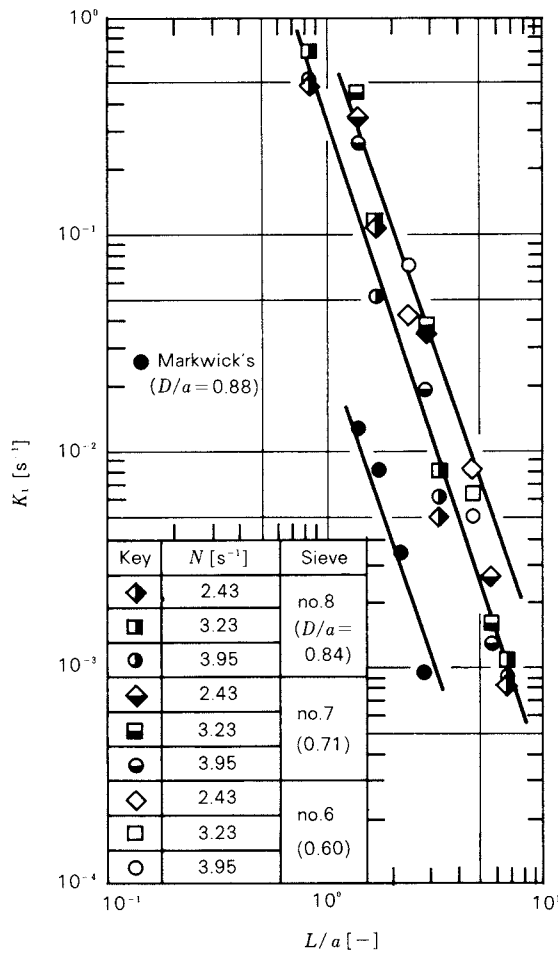


Fig. 8 Effect of cylinder length L on rate coefficient of sieving k_1

orientation (θ, ϕ) can be defined by the next equation.

$$p(\theta, \phi) = (a - l_x - d_x)(a - l_y - d_y)/a^2 \quad (11)$$

where l_x, l_y, d_x and d_y are given by the following equations:

$$l_x = L \sin \phi \cos \theta \quad (12)$$

$$l_y = L \sin \phi \sin \theta \quad (13)$$

$$d_x = D \sqrt{\sin^2 \theta + \cos^2 \theta \cos^2 \phi} \quad (14)$$

and

$$d_y = D \sqrt{\cos^2 \theta + \sin^2 \theta \cos^2 \phi} \quad (15)$$

The orientation of cylinder might be various in 3-dimensional space and the overall probability of passing can be defined by

$$P = \frac{\iint_{\Omega_p} p(\theta, \phi) f(\theta, \phi) d\theta d\phi}{\iint_{\Omega} f(\theta, \phi) d\theta d\phi} \quad (16)$$

where $f(\theta, \phi)$ is the probability density func-

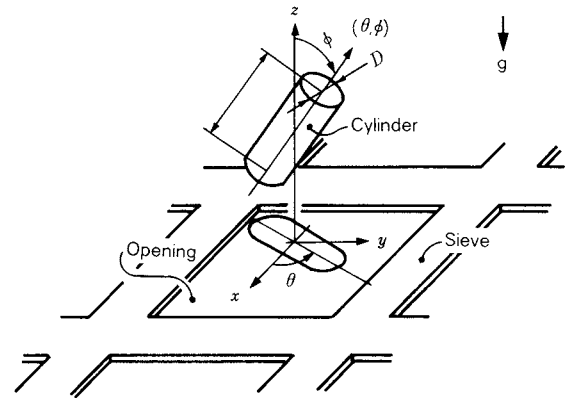


Fig. 9(a) Model of cylinder passing through sieve opening; orientation of cylinder

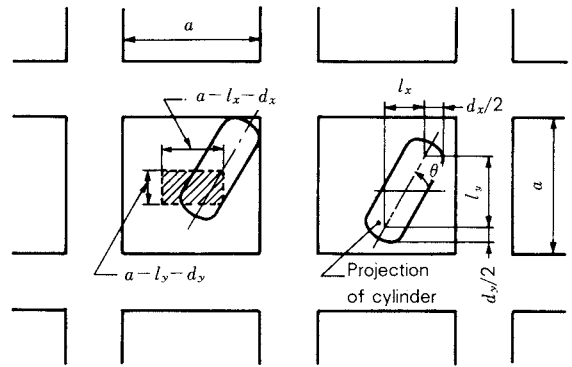


Fig. 9(b) Model of cylinder passing through sieve opening; probability of passing

tion of orientation. The region of integration Ω is

$$\Omega : 0 \leq \theta \leq \pi/2, 0 \leq \phi \leq \pi/2 \quad (17)$$

and Ω_p is the region where cylinder can pass through the opening, and depends on both L and D . We assume the following relation:

$$f(\theta, \phi) = \sin \phi / (\pi/2) \quad (18)$$

Introducing Eq. (18) into Eq. (16), we obtain

$$P = \iint_{\Omega_p} p(\theta, \phi) \sin \phi d\theta d\phi / (\pi/2) = P(L/a, D/a) \quad (19)$$

P calculated by Monte Carlo method is shown in Fig. 10, where the orientation and the center of gravity are randomly generated. For $L/a > 1.4$, the effect of L/a on the passing probability is given by the following relation:

$$P \propto (L/a)^{-2} \quad (20)$$

Figures 8 and 10 show that dependency of the experimental rate coefficients k on D/a is

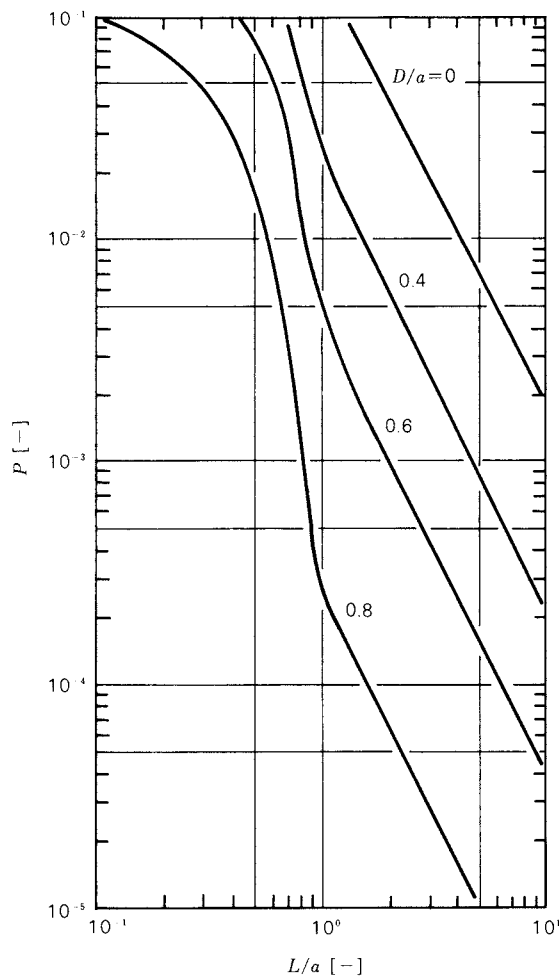


Fig. 10 Probability of cylinder passing through sieve opening

weaker than calculated one and the comparison of Eqs. (7) and (20) gives that k depends on L more strongly than P . The causes of this difference are considered as follows: although the motion of sieve was reciprocal, the orientation of the axis were assumed to be random in the calculation of P , and the number of trials of sieving might depend on the operating conditions and geometrical particle shape.

In Fig. 11, ξ calculated by Eq.(10) is plotted against L/a . ξ of the present work and Markwick are inversely proportional to L , which is roughly given as follows:

$$\xi \propto (L/a)^{-1} \quad (21)$$

5. Application to multi-stage sieving

The process of multi-stage batch sieving can be formulated when the sieving characteristics are expressed in exponential, as shown in

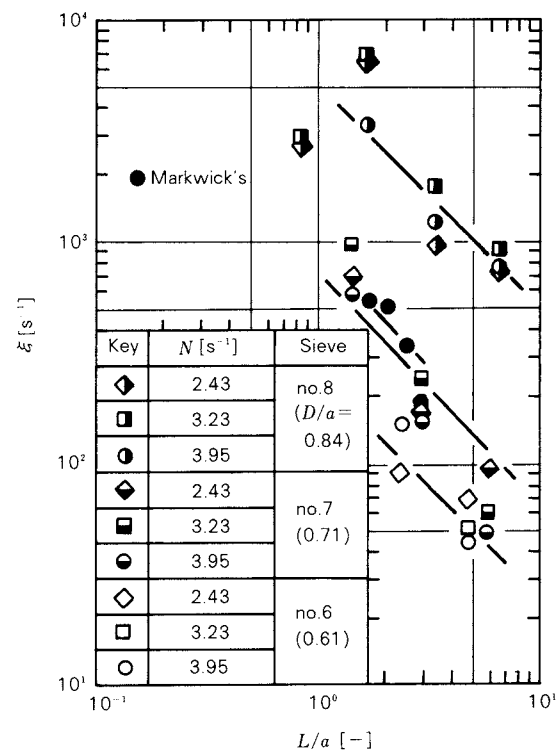


Fig. 11 Effect of cylinder length L on number of trials of sieving

Eq.(2). Consider the set of sieves which consists of sieve no. 6, 7, 8 and 9, and only cylinders of the same size are initially placed on the sieve no. 6. The behavior of retention on each sieve can be expressed by the following equation.

$$\frac{dr}{dt} = Kr \quad (22)$$

where r is a vector of residue, given by

$$r = \begin{pmatrix} r_6 \\ r_7 \\ r_8 \\ r_9 \end{pmatrix} \quad (23)$$

where r_j is a fraction of retention on a sieve number j . K is a matrix of sieving rate coefficients, as follows:

$$K = \begin{pmatrix} -k^{(6)} & 0 & 0 & 0 \\ k^{(6)} & -k^{(7)} & 0 & 0 \\ 0 & k^{(7)} & -k^{(8)} & 0 \\ 0 & 0 & k^{(8)} & -k^{(9)} \end{pmatrix} \quad (24)$$

where $k^{(j)}$ is a rate coefficient of the cylinder passing through the sieve of no. j .

Solving Eq. (22) with an initial condition r_0 , we obtain the following equation,

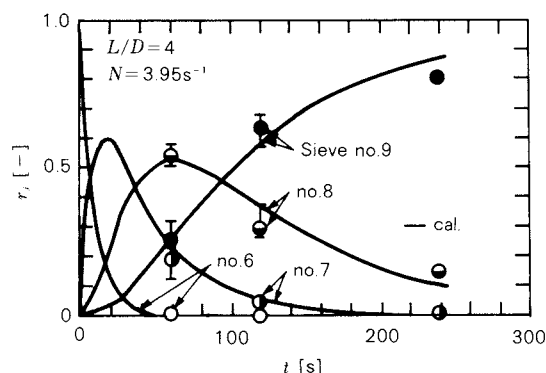


Fig. 12 Change of fraction of retention on each sieve with time

$$r = \exp(Kt)r_0 \quad (25)$$

where initial condition r_0 is given by

$$r_0 = \begin{pmatrix} 1 \\ 0 \\ 0 \\ 0 \end{pmatrix} \quad (26)$$

Figure 12 shows the change of the fraction of retention on each sieve calculated by the above equations. The values of $k^{(i)}$ used in the calculation were experimental ones. $k^{(9)}$ is so small that few particle pass through sieve no. 9. Experimental results are plotted in Fig. 12. In the experiment, 0.1 kg of cylinders having $L/D = 4$ was initially charged on sieve no. 6 and shifted with $N = 3.95 \text{ s}^{-1}$ during given duration by the procedure (i). The orientation of sieve opening was parallel to the shifting. As is evident from Fig. 12, we can obtain satisfactory agreement of the experimental residue with the calculated one. Thus the sieving characteristics in this period can be appreciated by using Eq. (2).

The cumulative oversize distribution of three kinds of cylinder are plotted in Fig. 13, when the experiments were carried out by the procedure stated above and the duration was 240 s. Obviously shown in Fig. 12, the sieving of the cylinder with $L/D = 4$ did not attain to the end point, subsequently, the retention on the sieve no. 8 was slightly higher than the other cylinders as shown in Fig. 13. The 50%-separation diameter increases with the aspect ratio.

The correlation between the equivalent spherical diameter of cylinder D_s and 50%-separation diameter D_{50} is shown in Fig. 14. The correlations do not satisfy the previous relationship of irregular shaped grains⁴⁾ and D_{50} mainly de-

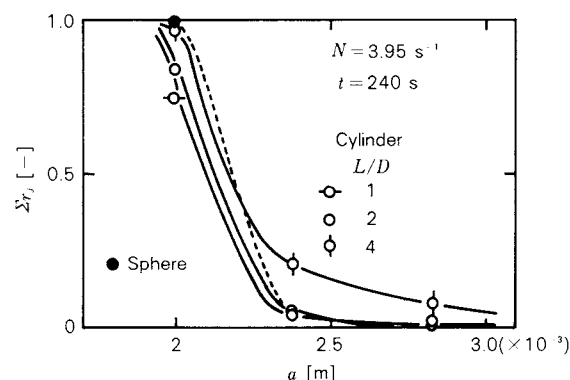


Fig. 13 Cumulative oversize distribution of cylinder

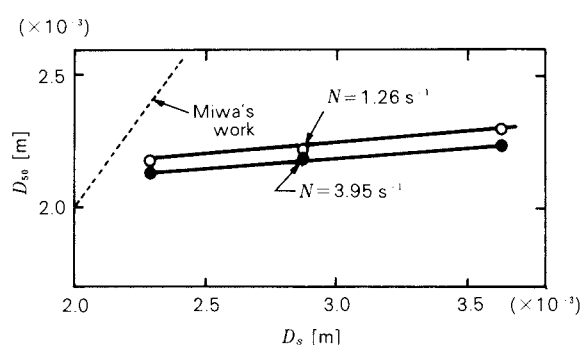


Fig. 14 Correlation between the equivalent spherical diameter of cylinder and 50%-separation diameter

pends on the cylinder diameter.

6. Conclusion

The sieving rate of cylinder passing through square mesh opening has been experimentally studied and the obtained results are as follows:

- (1) When the cylinder was easily screenable, the rate of sieving was independent of the initial charge and the retention exponentially decreased with sieving time.
- (2) For the cylinder with diameter near mesh size, the sieving rate was influenced by the initial charge and the process was expressed by experimental Eq. (3).
- (3) The sieving rate coefficient of easily screenable cylinder was inversely proportional to the third power of the cylinder length.

Nomenclature

a	: opening size of sieve	[mm or m]
B	: stroke of shifter	[mm]
b	: half stroke of shifter	[m]
D	: diameter of cylinder	[m]

D_s	: equivalent spherical diameter	[m]
D_{50}	: 50%-separation diameter	[m]
d_x, d_y	: length (see Eqs. (14) and (15))	[m]
g	: acceleration of gravity (= 9.8)	[m·s ⁻²]
i	: number of trials of sieving	[-]
K	: matrix of sieving rate coefficients	
K_1, K_2	: parameters in Eq. (3)	[-]
k_1, k_2	: sieving rate coefficients	[s ⁻¹]
$k^{(j)}$: rate coefficient of sieve j	[s ⁻¹]
L	: length of cylinder	[m]
l_x, l_y	: length (see Eqs. (12) and (13))	[m]
N	: frequency of shifter	[rpm or s ⁻¹]
P	: overall probability of passing through sieve opening (see Eq. (16))	[-]
$p(\theta, \phi)$: probability of passing through opening of cylinder having orientation of (θ, ϕ) (See Eq. (11))	[-]
r	: vector of residue	
r, r_j	: fractions of retention on a sieve (= W_r/W_0)	[-]

t	: time	[s]
W_0	: initial charge on a sieve	[kg]
W_r	: mass of retention	[kg]
x, y, z	: coordinates	[m]
Z_c	: centrifugal effect (= $(2\pi N)^2 b/g$)	[-]
ϵ	: area fraction of opening	[-]
θ	: orientation of cylinder axis	[rad]
ξ	: number of trials of sieving per unit time	[s ⁻¹]
ϕ	: orientation of cylinder axis	[rad]

References

- 1) Koga, J., S. Endoh, K. Yamaguchi and I. Inoue: *J. Soc. Powder Technol., Japan*, **18**, 755 (1981).
- 2) Markwick, A. H. D.: *J. Soc. Ind. Chem.*, **59**, 88 (1940).
- 3) Miwa, S.: *Kagaku Kogaku*, **24**, 150 (1960).
- 4) Miwa, S.: *Kagaku Kogaku*, **28**, 124 (1964).
- 5) Miwa, S.: "Huntai no Huruiwake", Nikkan Kogyo Shinbun Sha (1965).
- 6) Riley, G. S.: *Powder Technol.*, **2**, 315 (1968/69).

Flow Behavior of Particles in a Storage Vessel of a Table Feeder

Hiroaki Masuda*, Zhong-qi Han*,
Takashi Kadowaki* and Yuji Kawamura*
Department of Chemical Engineering,
Hiroshima University

Abstract

The flow behavior of particles was studied with particular attention to the effect of the inclination of a storage vessel and/or turn table of a table feeder. The effect of a converging hopper of the storage vessel and the effect of scrapers were also studied.

It was found that the particle flow was intensely distorted by slight inclination (as small as two degrees) of the storage vessel or the turn table. The distortion is found to be more intense for the vessel inclination than for the table inclination, and becomes more intense as the inclination increases. The discharge rate of the feeder increases exponentially with the angle of inclination. The flow distortion was, however, controlled by using scrapers at suitable positions.

It was also found that a new theoretical equation for a cylindrical vessel was successfully adapted for estimation of the effect of skirt clearance on the discharge rate of a table feeder.

1. Introduction

A powder feeder is one of the essential devices in the powder handling processes¹⁾. Various types of powder feeders are put to practical use according to the purpose of each. One type, the table feeder, is used widely as a continuous discharging device of moving beds of ores, coals and other particulate materials. The powder feeder is usually equipped with an ancillary storage vessel, such as a bin, a bunker, a silo, a hopper or the like. The flow behavior of the particulate materials in the storage vessel is an important factor to grasp what causes the difference in residence time of the individual particles in the vessel. Reports on this flow behavior have already been published with regard to the screw feeder²⁾, the belt feeder³⁾, the vibrating feeder⁴⁾ and the roll feeder⁵⁾. Based on those results, some methods for improving the flow behavior have been suggested. Regarding the table feeder, however, such an investigation has not yet been conducted.

In this report, some results obtained through the observation of the flow behavior of particulate materials in a model storage vessel^{6,7)} will be summarized. In addition, the change of the discharge rate of the material with the variation of the skirt clearance, and the control of the flow by scrapers, will be discussed.

2. Experimental apparatus and procedures

A schematic diagram of the experimental apparatus is shown in Fig. 1. As for a storage vessel, a rectangular vessel (Vessel 1) measuring 60mm by 18 by 500 high was used mainly, and a cylinder (Vessel 2) with a diameter of 50mm and a height of 285mm was also used. Both of them were made of acrylic resin. The feeder was set on a laboratory jack and the storage vessel was supported with clamps attached on a frame structure. The angle of inclination of the feeder from the horizontal line and that of the vessel from the vertical line could be adjusted arbitrarily. The diameter of the table was 100mm and emery paper CC-600 was stuck on the surface of the table in order to increase the friction against the powder bed.⁸⁾ The experiments were conducted in the low speed range

* Shitami, Saijo, Higashi-Hiroshima, Hiroshima, 724
TEL. 0824 (22) 7111

Received February 10, 1984

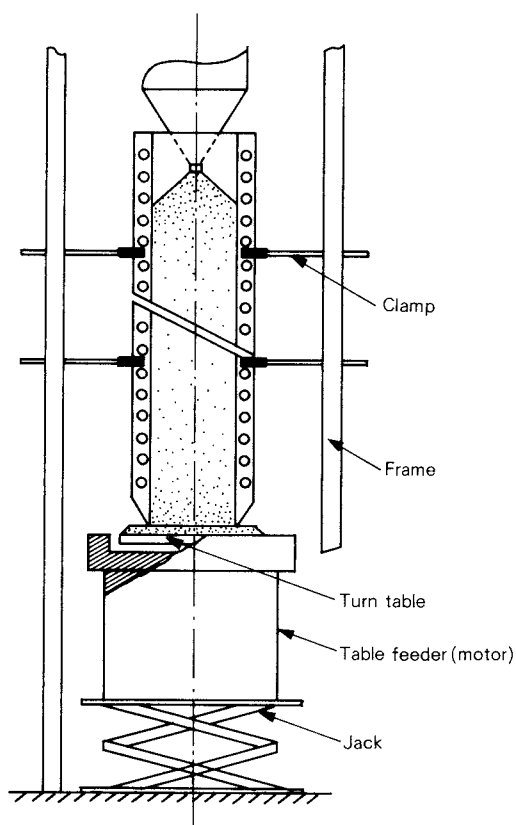


Fig. 1 Schematic diagram of experimental apparatus

Table 1 Properties of the powder materials

	Quartz sand	Morundum
True density ρ_p [g/cm ³]	2.64	3.97
Bulk density ρ_B [g/cm ³]	1.48	2.24
Angle of repose ϕ_r [deg]	37.2	39.0
Particle friction factor $\mu = \tan \phi_r$ [-]	0.76	0.81
Mass median diameter D_{p50} [μ m]	290	310

where the discharge rate was proportional to the revolution speed.⁹⁾ The observation of the flow behavior of silica sand was made by taking pictures with the aid of brown abrasive powder as a tracer (Morundum No. 54, made by Showa Denko K.K.) forming several layers in the material bed. The characteristics of these powder materials are listed in Table 1.

3. Observation of flow pattern

It is known that the flow of particulate materials in a storage vessel is roughly divided into

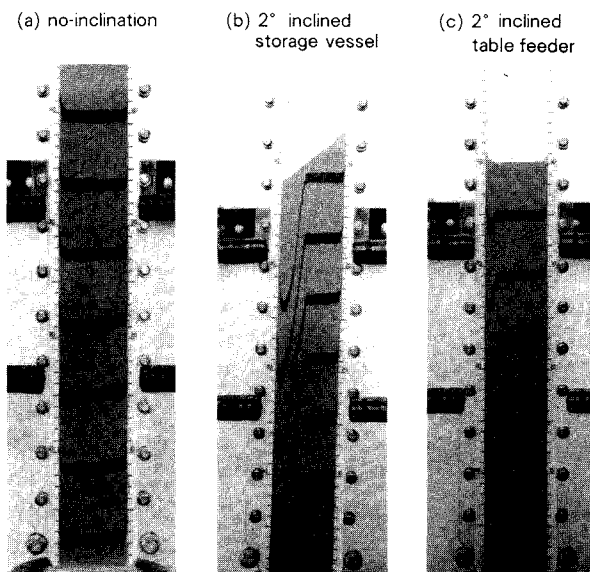


Fig. 2 Powder flow pattern in storage vessel ($H = 8$ mm, $t = 5$ min)

two types, the mass flow and the funnel flow. The flow patterns of particulate materials will be discussed in the following sections under some different conditions of the table and the vessel, that is, in the case of (1) no-inclination, (2) where either the table or the vessel is inclined and (3) using the vessel 1 with a converging outlet.

3. 1 Flow for normal conditions, no-inclination

The flow of the material is found to be a mass flow, when the skirt clearance is set between the upper limit (depending on the angle of repose of the powder) and the lower limit (depending on the particle size)⁶⁾. As shown in Fig. 2 (a), the flow of the material consists of a plug flow with uniform velocity in the core part and a deformed flow with a certain velocity profile near the wall¹⁰⁾. In practice, the plug flow region occupies a large part of the total flow and the width of the plug flow region at the bottom of the vessel assured with the tracer particles inserted at the top was about 0.85 times as broad as the vessel width (60mm). When two vessels were utilized in series in order to keep the height of the powder bed at a certain constant level in the second vessel, the width of the plug flow region decreased to about 0.82 times as broad as the vessel width. This result indicates that the width of the plug flow region changes depend-

ing on the mean stress exerted on the particulate material in the storage vessel.

3. 2 Flow for inclined storage vessel and/or inclined table

The powder flow in a storage vessel with inclination of 1° from the vertical line was the same as that of no-inclination. For the inclination of 2° , however, the powder flow was extremely distorted. The particulate material is discharged more from one side of the larger clearance between the bottom end of the vessel and the table surface and less is discharged from the opposite side. It is noticeable that such a small inclination causes a distorted flow. An example of the variation of the downward velocity v_1 of the distorted flow with time is shown in Fig. 3. In the lower section with a small z , the velocity v_1 increases rapidly with the distorted flow being propagated in a short time, while the propagation of the distorted flow is delayed in the higher section. On the other hand, the width of the distorted flow increases in a short period and then is spreading gradually⁷⁾. There is a long dead time before the particles come in motion in the higher section. It is considered that the bulk density ρ_B gets smaller¹¹⁾, and the mean stress is relaxed as the powder bed is set in motion. As this change takes place instantly in the lower section and then is propagated to the higher section, the propagation of the distorted flow is considered to be delayed in the higher section.

The powder flow in the storage vessel tilted together with the table by the same angle was

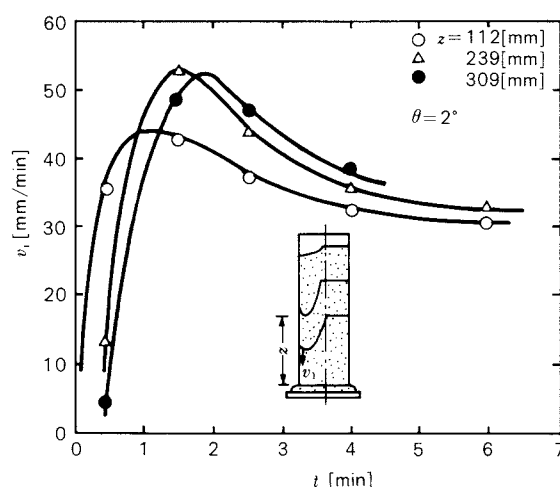


Fig. 3 Flow velocity v_1 as a function of elapsed time t

found to be a mass flow as in the case of no-inclination (§ 3-1). On the other hand, in the case where the vessel and the table were inclined on the opposite sides, more intensively distorted flow was observed than in the case where either the former or the latter was inclined, as far as the sum of the inclination of the both was within 6° . This result suggests that the relative inclination between the storage vessel and the table is the cause of the distorted flow.

3. 3 Flow in a storage vessel with a converging outlet

When the storage vessel is equipped with a converging section at its bottom, distorted flow occurs even if the vessel and the table are not inclined (which is not discussed further in this report). Figure 4 shows how the powder flow changes with time, when the table was kept horizontal and the storage vessel was inclined by 4° . The angle of the converging section at the bottom of the vessel was 45° and the width of the outlet was 30mm. The experiments with the converging angle of 60° gave almost the same flow behavior as in Fig. 4. From this result, it is assumed that the distorted flow is attributable to the contraction of the outlet width from 60mm to 30mm. As seen in Fig. 4, the distorted flow is propagated upwards in the vertical direction from the bottom.

When the table was tilted keeping the storage vessel vertical, the distorted flow region was diverted to the side of the wider skirt clearance. It is found that the particles on the side of the smaller skirt clearance have longer residence time in the storage vessel. The downward velocity of the distorted flow shows the same tendency as in Fig. 3 but the details are omitted in this report (see also Reference 7).

3. 4 With scrapers

When a scraper is attached on the table, the flow pattern changes depending on its set position, though it does not change so long as the distance between the center of the table and the scraper edge satisfies the condition described in the following equation.

$$R_s > r_0 + \frac{H}{\tan \phi_r} \quad (1)$$

Here r_0 is the radius of a circumscribed circle of the rectangular outlet of the vessel or the

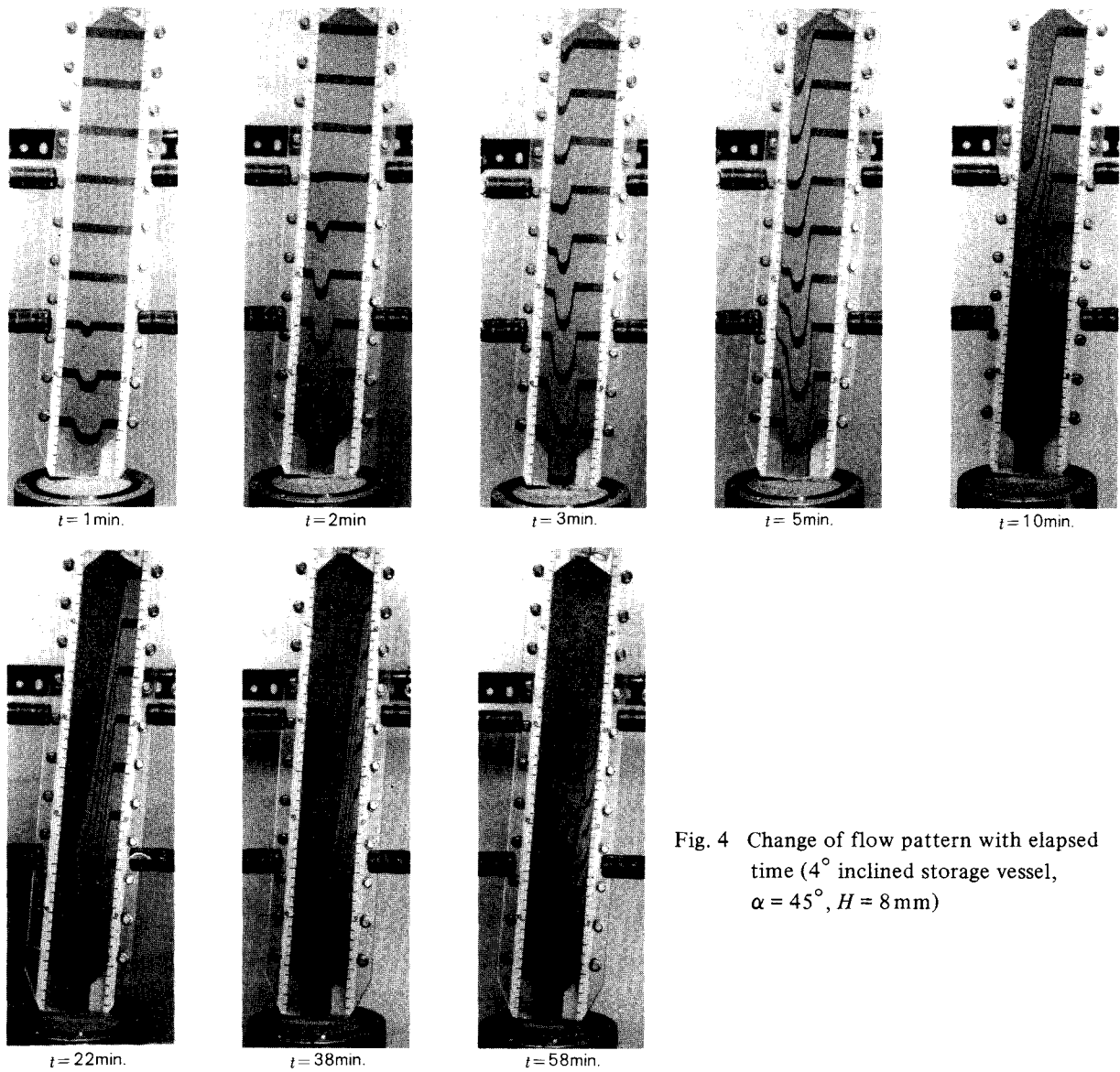


Fig. 4 Change of flow pattern with elapsed time (4° inclined storage vessel, $\alpha = 45^\circ$, $H = 8 \text{ mm}$)

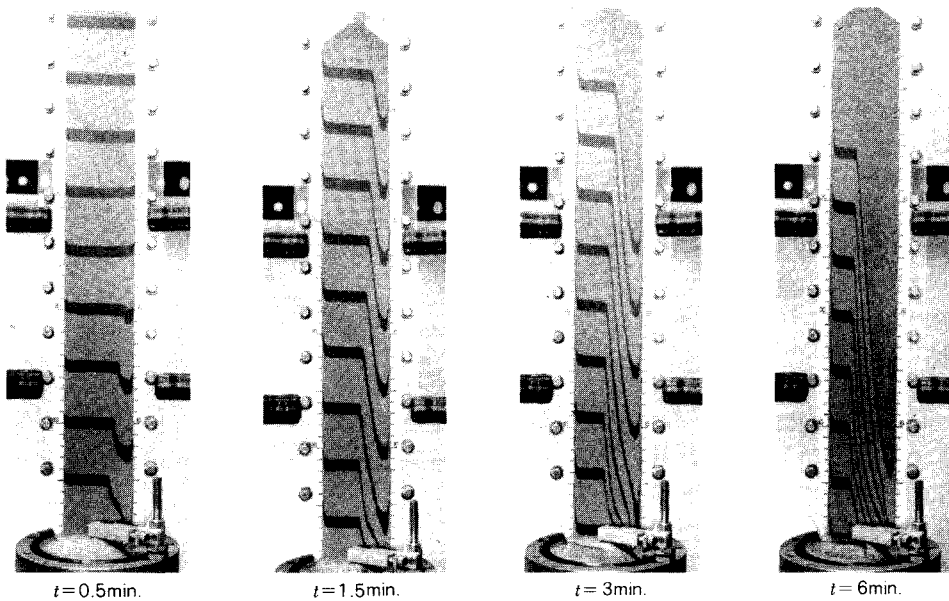


Fig. 5 Effect of a scraper on the flow pattern

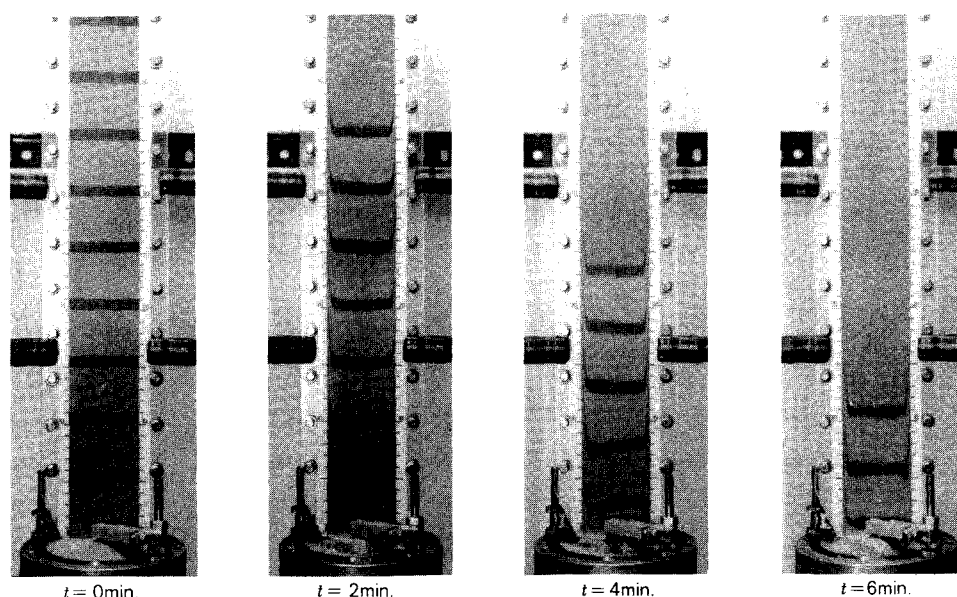


Fig. 6 Effect of scrapers on the flow pattern (two scrapers are utilized, one is behind the storage vessel)

inner radius of the cylindrical vessel, and H is a skirt clearance. Even when the scraper position R_s satisfies the condition expressed in Eq. (1), the table can be used as a powder feeder, as the particle bed spreads out with the revolution of the table.¹²⁾

In the case where R_s does not satisfy the above-mentioned condition, that is, when $R_s < r_0 + H/\tan\phi_r$, the flow is distorted as seen in Fig. 5. In this case, the residence time of the particles is shorter on the scraper side and longer on the opposite side.

As mentioned above, the powder flow is distorted when the storage vessel or the table is inclined, and the distortion becomes more violent when a scraper is set on the same side as the distorted flow. On the other hand, it is possible to realize an approximate mass flow of the particles, if the set position of the scraper is adjusted properly on the side where no distorted flow occurs. That is to say, it is possible to prevent the distorted flow and to control the powder flow by adjusting the set position of the scraper, even when the table or the vessel is inclined to some extent. Figure 6 shows the flow pattern using two scrapers, which is found better controlled compared with the pattern in Fig. 5.

Masuda *et al.*⁸⁾, previously suggested to use more than two scrapers in order to improve the accuracy in feeding small amount of powder materials. This method seems to be efficient to control the powder flow in the storage vessel as well.

4. Relation between the discharge rate and the inclination of the storage vessel

The discharge rate was measured setting the table horizontal and changing the angle of inclination of the vessel from 1° to 6° by 1° . The skirt clearance H was regarded as the distance between the center of the vessel bottom and that of the table. The result with the rectangular vessel is shown in Fig. 7, in which the discharge rate W increases with the angle of inclination θ with little effect of the skirt clearance H . On the other hand, in the cylindrical vessel, the discharge rate is affected greatly by the skirt clearance as well as the angle of inclination of the vessel as seen in Fig. 8.

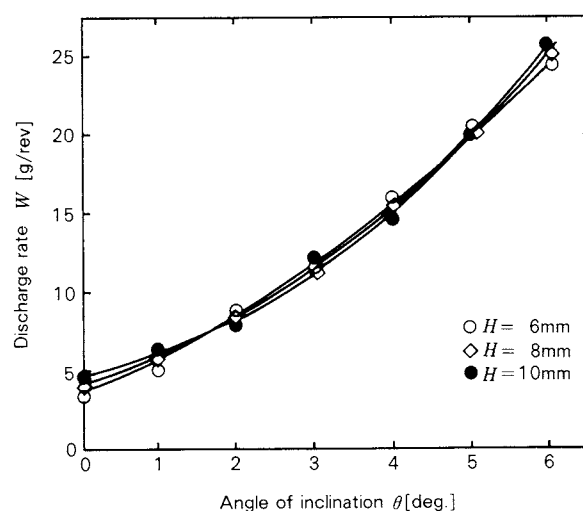


Fig. 7 Relationship between powder flow rate and the angle of inclination of vessel (Vessel-1. rectangular)

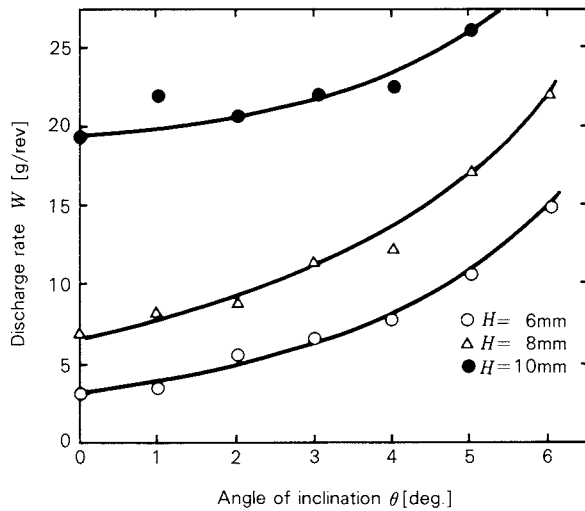


Fig. 8 Relationship between powder flow rate and the angle of inclination of vessel (Vessel-2. cylindrical)

The ratio of discharge rate W at the inclination θ to that W_0 without inclination in the cylindrical vessel is plotted against $\sin\theta$ ($\cong \theta$) in Fig. 9. This figure shows that the ratio W/W_0 of the discharge rate differs with varying skirt clearance H and that the effect of the inclination on the discharge rate becomes larger, as H reduces. The experimental result is expressed in the following equation.

$$\frac{W}{W_0} = \exp(k \sin\theta) \quad (2)$$

where a factor k depends on the skirt clearance and is 10.9 (—) at $H = 8\text{mm}$.

The discharge rate from the table feeder with the tilted table corresponded nearly to that with the tilted storage vessel, and the discharge rate increased exponentially with the angle of inclination in both cases.

The variation of the discharge rate with the skirt clearance H (for the cylindrical vessel without inclination) will be analysed in the following.

According to Masuda and Inoya¹³⁾, the spread-out length of a powder bed δ defined in Fig. 10 satisfies the following condition.

$$\int_{\delta}^{\delta+\Delta\delta} \delta^3 d\delta = \text{const.} \quad (3)$$

From Eq.(3), the following equation will be obtained.

$$\delta^3 \Delta\delta = K \quad (4)$$

Meanwhile, the discharge rate W_0 is obtained

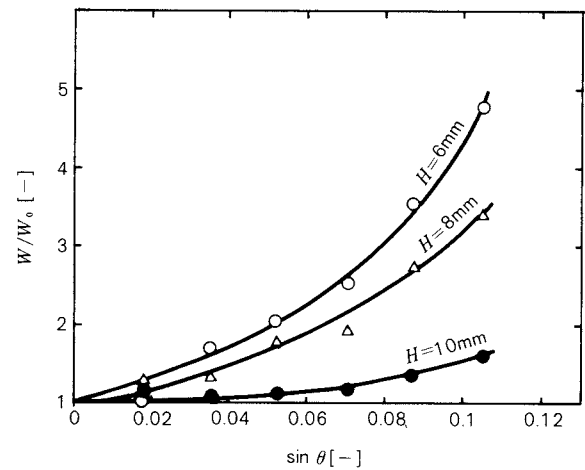


Fig. 9 Relationship between powder flow-rate ratio W/W_0 and the inclination $\sin\theta$ (Vessel-2. cylindrical)

by the integration of the spread-out part around the cylindrical vessel;

$$W_0 = \pi \rho_B H (2R - \frac{H}{\tan\varphi_r}) \Delta\delta \quad (5)$$

Substituting Eq.(4) for Eq.(5), W_0 is represented by

$$W_0 = K \frac{\pi \rho_B H (2R - \frac{H}{\tan\varphi_r})}{\delta^3} \quad (6)$$

There is a geometric relation found in Fig. 10.

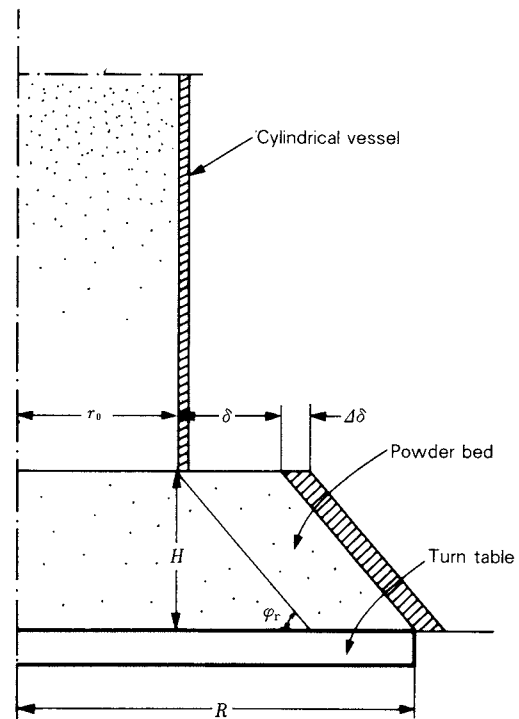


Fig. 10 Schematic diagram of powder bed on the table feeder

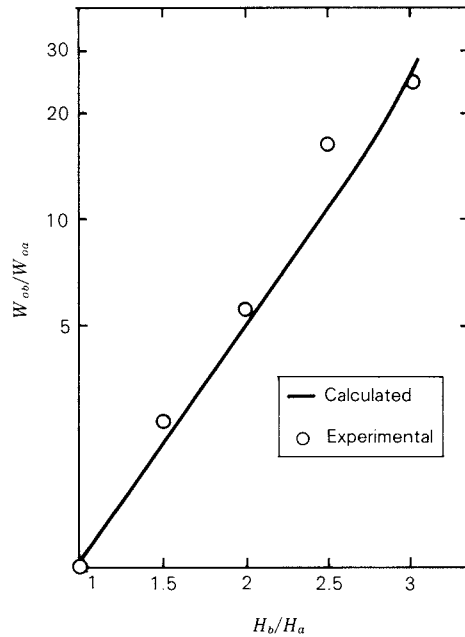


Fig. 11 Comparison between calculated and experimental W_{ob}/W_{0a} as a function of H_b/H_a (Vessel-2, cylindrical)

$$\delta = R - r_0 - \frac{H}{\tan \varphi_r} \quad (7)$$

Therefore the ratio of the discharge rates W_{ob} to W_{0a} with the respective skirt clearance of H_b and H_a is calculated in the following equation obtained from Eqs. (6) and (7).

$$\frac{W_{ob}}{W_{0a}} = \frac{H_b}{H_a} \left(\frac{R - r_0 - \frac{H_a}{\tan \varphi_r}}{R - r_0 - \frac{H_b}{\tan \varphi_r}} \right)^3 \left(\frac{2R - \frac{H_b}{\tan \varphi_r}}{2R - \frac{H_a}{\tan \varphi_r}} \right) \quad (8)$$

In Fig. 11, the result calculated with Eq. (8) is compared with the experimental data. The calculated line fits the experimental values fairly well as a whole, though the former is slightly smaller than the latter. This means that the variation of the discharge rate with the skirt clearance can be estimated by Eq. (8).

5. Conclusion

The flow behavior of the particulate material in a storage vessel attached on a table feeder was studied with particular attention to the effect of the inclination of the table and/or the vessel. Effects of the contraction of the vessel outlet and the scraper were also discussed. The obtained results are summarized in the follow-

ing.

- 1) When the table and the vessel are set normally (without inclination), the powder flow in the vessel is a mass flow. The width of plug flow region becomes a little smaller under the continuous supply of the powder into the vessel.
- 2) When either the table or the vessel is tilted a little (more than 2° or so), the flow is intensively distorted. The distortion becomes more intensive with increasing relative inclination between the table and the vessel.
- 3) The flow pattern in the vessel can be controlled to some extent by using more than two scrapers.
- 4) It is possible to estimate the discharge rate as a function of the skirt clearance.

Nomenclature

D	: width of a storage vessel	[m]
D_{p50}	: mass median diameter of particles	[m]
H	: skirt clearance	[m]
K	: proportional constant in Eq.(4)	[m ⁴ /rev]
k	: experimental constant in Eq.(2)	[-]
L_1	: width of the plug flow region in a mass flow	[m]
R	: radius of a table	[m]
R_s	: scraper position	[m]
r_0	: inner radius of the cylindrical vessel, radius of circumscribed circle of the rectangular vessel	[m]
t	: elapsed time	[s]
v_1	: downward velocity of distorted flow region	[m/s]
W	: discharge rate (with inclination of vessel and/or table)	[kg/rev]
W_0	: discharge rate (without inclination)	[kg/rev]
z	: vertical position in the powder bed in the storage vessel	[m]
α	: angle of the converging part	[deg]
δ	: spread-out length of powder bed	[m]
θ	: angle of inclination	[deg]
ρ_B	: bulk density	[kg/m ³]
φ_r	: angle of repose	[deg]

References

- 1) Iinoya, K. and H. Masuda: "Funryutai Process no Jidoka (On the Automation of Particulate Processes)", *Nikkan Kogyo, Tokyo* (1975).
- 2) Johanson, J.R.: *Chem. Eng.*, **76**, 75 (Oct. 13, 1969).
- 3) Doekson, G.: *CIM Trans.*, **123**, 257 (1970).
- 4) Miles, J.E.P. and C. Shofield: *Paper presented to symposium on solid handling, Inst. of Chem.*

- Engrs.* (Sept., 1969).
- 5) Maeda, I. and I. Tanaka: *Kagaku Kogaku Ronbunshu*, **2**, 277 (1976).
 - 6) Han, Z., T. Kadowaki, H. Masuda and Y. Kawamura: *J. Soc. Powder Tech. Japan*, **20**, 479 (1983).
 - 7) Han, Z., T. Kadowaki and H. Masuda: *J. Soc. Powder Tech. Japan*, **21**, 199 (1984).
 - 8) Masuda, H., K. Iinoya, M. Hirota and H. Kurahashi: *Kagaku Kogaku Ronbunshu*, **2**, 286 (1976).
 - 9) Masuda, H., K. Iinoya and K. Miura: *J. Soc. Materials Sci. Japan*, **21**, 577 (1972).
 - 10) Takahashi, H. and H. Yanai: *Kagaku Kogaku*, **35**, 357 (1971).
 - 11) Takagi F. and M. Sugita: *J. Soc. Powder Tech. Japan*, **19**, 542 (1982).
 - 12) Iinoya, K. and H. Masuda: *Proc. 1st International Conf. in Particle Tech., IITRI, Chicago – Illinois*, p.39 (1973).
 - 13) Masuda, H. and K. Iinoya: *J. Res. Assoc. Powder Tech.*, **9**, 227 (1972).

Reduction of Power Consumption in Pneumatic Conveying of Granular Materials through a Pipeline

Takeshi Kano*

Department of Chemical Engineering
Shizuoka University

Abstract

Pneumatic conveying of granular materials generally requires a great deal of power consumption in spite of its excellent advantages which are not obtainable with other transport methods. The purpose of this study is to examine the behavior of pneumatic conveying systems from both theoretical and experimental perspectives and find out an optimum way of reducing power consumption.

It is concluded that the application of vibration to pipes or bends is effective for this purpose. In addition several improvements to obtain economic conditions are discussed.

1. Introduction

It is well-recognized that pneumatic conveying of granular materials is more advantageous in many ways than other transport systems but it still has the fault of large power consumption in spite of endeavors for its improvement, such as the development of a dense-phase conveying^{1,2,3,4)}.

The aim of this paper is to find a suitable method for reducing the amount of power consumption in a pneumatic conveying system as follows:

- The theoretical equations were derived to be related to the air pressure required for a pneumatic conveying, and the economic conditions could be obtained, compared with experimental results.
- It was found that alternately intermittent injection of air into a top side of a blow tank and an initial point of a pipeline made it possible to let plugs with a constant length flow with a small amount of air in a stable state. In addition, the desired improvements in reduction of the power consumption by this system were to be achieved by an application of vibration to the pipeline.

2. Theory

2. 1 Air pressure required for plug conveying

The theoretical analysis of air pressure required for conveying plugs in succession was carried out, using a model shown in Fig. 1 (b) which would express the general conditions of transport shown in Fig. 1 (a). In the model, plugs with length of l_p slide successively on a stagnant bed of thickness h piled up at the bottom of a pipe with diameter of D which is inclined at angle θ to the horizontal. Based on the force balance in the flow direction of solids and air, the pressure loss of a plug Δp_p can be related to the component of gravity $M_p \cdot g \cdot \sin \theta$, wall friction resistance R_w , and friction resistance at the surface of a stagnant bed R_h as:

$$\Delta p_p \xi_p A = M_p g \sin \theta + R_w + R_h \quad (1)$$

and

$$M_p = \xi_p A l_p \rho_b \quad (2)$$

$$R_w = \xi_w p_r A_w \quad (3)$$

$$R_h = \xi_i (M_p g \cos \theta + p_r A_h) \quad (4)$$

$$A_w = \left\{ 1 - \frac{\cos^{-1} \left(1 - \frac{2h}{D} \right)}{\pi} \right\} \pi D l_p \quad (5)$$

$$A_h = 2 l_p \sqrt{(2D - h)h} \quad (6)$$

where A = cross-sectional area of a pipe
($= \pi D^2 / 4$)

* 3-5-1 Johoku, Hamamatsu, Shizuoka, 432
TEL. 0534 (71) 1171

Received March 27, 1984

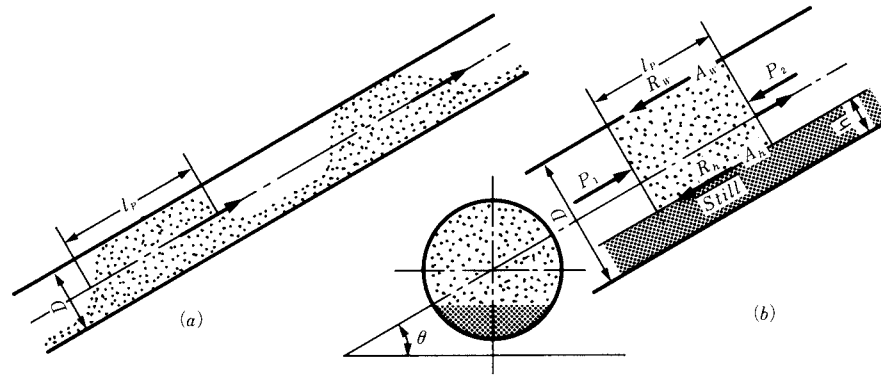


Fig. 1 Schematic diagrams of horizontal and vertical pipe

ξ_p = ratio of cross-sectional area of a conveyed plug to that of a pipe

ρ_p = bulk density of a plug

p_r = normal pressure to a pipe wall

ξ_w = wall friction factor

ξ_i = internal friction factor

A_w = contact area between a plug and a wall

A_h = contact area between a plug and a stagnant bed

Substituting Eqs. (2) to (6) for Eq. (1), pressure loss across a plug is given as

$$\Delta p_p = \left[\rho_b g \sin \theta + \xi_w \frac{4p_r}{\xi_p D} \left\{ 1 - \frac{\cos^{-1} \left(1 - \frac{2h}{D} \right)}{\pi} \right\} + \xi_i \left(\rho_b g \cos \theta + \frac{8p_r \sqrt{(2D-h)h}}{\xi_p \pi D^2} \right) \right] l_p \quad (7)$$

while Δp_p is also written by another expression:

$$\Delta p_p = \Delta p_k + \frac{\rho_a (u_a^2 - u_k^2)}{2} \quad (8)$$

where Δp_k denotes a permeating pressure loss through a pipe, which Ergun derived as:

$$\Delta p_k = \left\{ 1.75 + \frac{1.50(1-\epsilon)}{Re_u} \right\} \frac{\rho_a U}{d_s} \left(\frac{1-\epsilon}{\epsilon^3} \right) l_p \quad (9)$$

where ρ_a denotes an air density. U and u_p satisfy the following relations:

$$U = u_k - u_p = \frac{u_a}{\epsilon} - u_p \quad (10)$$

$$Re_u = \frac{U \rho_a d_s}{\mu} \quad (11)$$

where u_a = air velocity (conveyed air volume divided by a cross-sectional area

of a pipe)

u_k = permeating air velocity

u_p = plug velocity

ϵ = plug porosity

Based on the assumption that each plug and each air cushion between plugs have the same length of l_p and l_a respectively, the number of plugs through a total length of a pipeline is given by $L/(l_p + l_a)$. In this case a conveying pressure Δp_p related to a single plug is obtained by total conveying pressure p as follows:

$$\Delta p_p = \frac{p}{L/(l_p + l_a)} \quad (12)$$

2. 2 Wall friction factor in a vibratory field

The horizontal plane with vertical simple harmonic vibration of half amplitude a and frequency f is observed at time t as follows:

displacement

$$Z = a \sin 2\pi f t \quad (13)$$

displacement velocity

$$\dot{Z} = a (2\pi f) \cos 2\pi f t \quad (14)$$

displacement acceleration

$$\ddot{Z} = -a (2\pi f)^2 \sin 2\pi f t \quad (15)$$

$$= -g A \sin 2\pi f t \quad (16)$$

where A denotes a ratio of vibratory acceleration to the gravitational one given by

$$A = \frac{a (2\pi f)^2}{g} \quad (17)$$

The vibration of grains of mass M seemingly causes the following force in the vertical direction.

$$M\ddot{Z} = -M A g \sin 2\pi f t \quad (18)$$

This force periodically changes with the range of its absolute value from $M_g (1 - A)$ to $M_g A$.

When the materials are moved on the plane, a wall friction factor is given as follows:

$$\text{in static state} \quad \xi_{w0} = \frac{F_{02} - F_{01}}{(M_2 - M_1)g} \quad (19)$$

$$\text{in vibrating state} \quad \xi_w = \frac{F_2 - F_1}{(M_2 - M_1)g} \quad (20)$$

where F_0 denotes the horizontal drag force in the static state, and F in the vibrating state. The subscripts 1 and 2 imply different masses of the solids. Since F_1 and F_2 can be expressed as

$$F_1 = F_{01} - \xi_{w0} M_1 g A \quad (21)$$

$$F_2 = F_{02} - \xi_{w0} M_2 g A \quad (22)$$

Eqs. (17) to (20) give the following relation.

$$\xi_w = (1 - A) \xi_{w0} \quad (23)$$

The friction factor of a solid on a vibrating plane ξ_w was obtained by Yokoyama⁶⁾ as:

$$\xi_w = \frac{\xi_{w0} (1 - A \sqrt{1 + \xi_{w0}^2 - \xi_{w0}^2 A^2})}{1 - \xi_{w0}^2 A^2} \quad (24)$$

The approximation of the curve expressed by Eq.(24) with a straight line would provide Eq.(23).

2. 3 Additional pressure loss coefficient

In general the total pressure loss of the plug conveying or conveying pressure p can be obtained from the summation of the pressure loss caused by air flow Δp_a and the pressure loss added by the presence of plugs Δp_s :

$$p = \Delta p_a + \Delta p_s \quad (25)$$

$$\text{and} \quad \Delta p_a = \lambda_a \left(\frac{L}{D} \right) \left(\frac{\rho_a}{2} \right) u_a^2 \quad (26)$$

$$\Delta p_s = \lambda_s \left(\frac{L}{D} \right) \left(\frac{\rho_m}{2} \right) u_p^2 \quad (27)$$

where λ_a = wall friction factor

λ_s = additional friction factor

ρ_a = air density

ρ_m = average density of a plug in a unit volume of a pipe

The value ρ_m of a given plug is expressed as $\rho_m = M_p / (A l_p)$ where l_p is length of a plug and M_p is the mass of the solids. The coefficient λ_s in Eq.(27) is calculated from the following expression.

$$\lambda_s = \frac{(p_m - \Delta p_a) \pi D^3}{2 M_p u_p^2} \quad (28)$$

2. 4 Requisite power consumption and transport efficiency

Required power consumption N_c is generally written as:

$$N_c = \frac{p Q_a}{1000} \quad (29)$$

where p denotes the pressure required to convey plugs, or the conveying pressure in [Pa], and Q_a denotes the air volume rate in [m³/s]. The degree of conveying capacity, or that contribution by conveyed air, can be obtained from the following indices, mixing ratio Γ and transport efficiency η :

$$\Gamma = \frac{M_s}{\rho_a Q_a} \quad (30)$$

$$\eta = \frac{g M_s L}{p Q_a} \quad (31)$$

where M_s denotes a mass flow rate of solids.

3. Experimental

3. 1 Measurement of the wall friction factor

The measurement of the wall friction factor was carried out using the equipment shown in Fig. 2. A test sample of millet indicated in Table 1, packed in a cubic acrylic vessel with each side 100mm long ④, on an acrylic plate

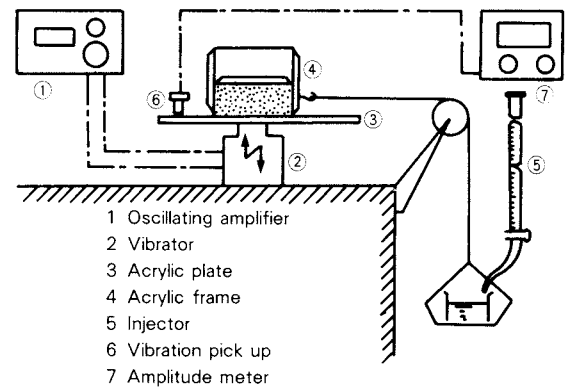


Fig. 2 Schematic diagram of apparatus to measure friction factor

Table 1 Properties of millet

Particle diameter	d_s [um]	1570
True density	ρ_s [kg/m ³]	1386
Bulk density	ρ_b [kg/m ³]	824 ~ 857
Wall friction factor	ξ_w [—]	0.421
Internal friction factor	ξ_i [—]	0.580

③, was vertically vibrated by means of a vibrator ②. The wall friction factor was obtained from the ratio of a horizontal force required to move the vessel horizontally, which was measured by ⑤, to a vertical force. An indicated value on an oscillating amplifier ① was used as a frequency. The amplitude of vibration was measured by an amplitude meter ⑦ through a non-contact type vibration pickup ⑥. In these experiments, the effects of packed amounts in the vessel, and vibrating conditions, on the wall friction factor were examined.

3. 2 Conveying experiment

Experiments were carried out in a closed-circuit conveying system having a blow tank as illustrated in Fig. 3. The total length of the system was 16.3m, containing a horizontal acrylic pipe 52mm in diameter ⑩, horizontal bend ⑪, vertical bend I (horizontal to vertical direction) ⑫, vertical pipe, vertical bend II (vertical to horizontal direction) ⑬, and so on. Several radii of curvature were employed for each bend so as to examine the effects of radius of curvature on the pressure drop.

Compressed air from a compressor ① was alternately fed into the top side of a blow tank ⑦ (initial section) and a start point of a pipe (secondary section) through a diversing solenoid

valve ⑤ after reduction with a regulator ②. In this experiment 170 kg of millet, mentioned previously, was used for each test run.

The values of partial and total pressure loss in the system were successively recorded with an electromagnetic oscillograph through a differential pressure gage and a strain gage. Plug number was counted by a photocell and recorded with pen recorder. Plug velocity was calculated from measuring time required to pass through specified sections, while lengths of a plug and an interval of plugs (air cushion) were measured by means of a photographic observation.

In addition to this test, vibration was applied on both a horizontal and a vertical pipe (the length of each is 5m) by an air vibrator (piston diameter of 19mm, maximum air pressure of $(2.4 \sim 6.4) \times 10^5$ Pa, and air consumption of $(0.65 \sim 1.33) \times 10^{-3}$ m³/s) to examine the effect and the most suitable condition. The degree of vibration was adjusted by air pressure introduced into the vibrator. Exhausted air was introduced into a start point of a pipe so as to examine whether it might be able to be utilized as conveying air.

3. 3 Improvement of transport capacity

When there was a very slow flow of air in the

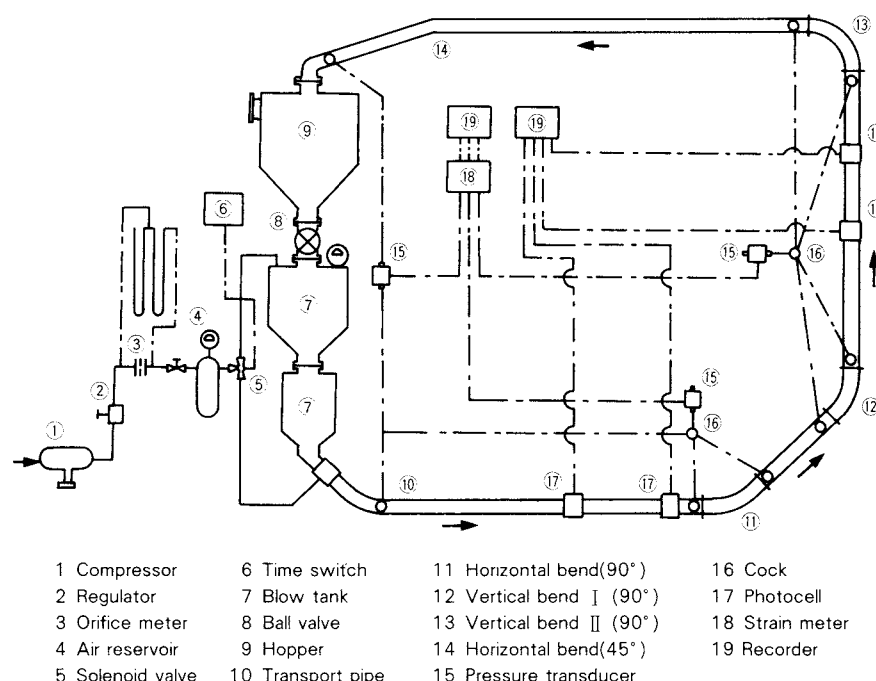


Fig. 3 Schematic diagram of experimental apparatus

steady state, at a rate of 1.2 m/s or less, it was observed that solids hardly moved due to blocking at the bottom of the tank. With increased air flow rate, solids filled in a pipe began to move, though stable transport could not be achieved because of blocking at bends. It was found that continuous conveying was impossible unless the air flow rate exceeded 10 m/s or so. In this case the flow pattern observed was that of floating transport.

Contrary to this, the following method was found to improve on such a problem. First the flow of compressed air was divided into two sections, the top side of the blow tank and the start point of the pipeline. Then these two supplies of air in an alternately intermittent way, could cause the continuous transport of relatively well-formed plugs according to the intermittent interval. In such a case the length and interval of plugs could be determined by a timer which adjusted the air supplies to the two sections. Mass flow rates of solids were found to be dependent on the air flow rate and the allocation of air supplies to the two sections. In this experiment the air flow rate was 1.4 to 2.3 m/s, the mass flow rate was 0.65 to 1.3 kg/s, and the mixing ratio was 130 to 290.

4. Results and discussion

4. 1 Wall friction factor

Figure 4 shows the relationship between wall friction factors, both measured and calculated from Eq. (23), and the acceleration ratio Λ defined by Eq. (17). Although the measured values were smaller than calculated ones, the trends of both were similar and they could be approximated by each straight line. It is clear that the friction factor will become zero when the acceleration ratio Λ in Eq. (23) is a unit or the straight line is extended in Fig. 4. Actually obtained values, however, were finite because of remarkable damping resulting from the relative motion and random action of particles.

The experimental results could be summarized as follows:

$$\xi_w = (1 - k\Lambda)\xi_{w0} \quad (32)$$

where a constant k was dependent on properties of the solids and conditions of the vibrating plates.

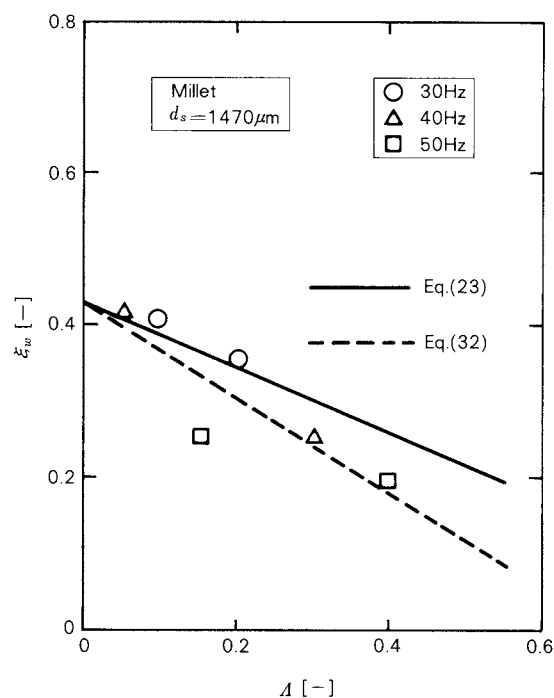


Fig. 4 Relationship between ratio of acceleration Λ and surface friction factor ξ_w

For instance,

millet: $k = 1.44$ ($d_s = 1570 \mu m$)
 polystyrene pellet: $k = 1.90$ ($d_s = 977 \mu m$)
 calcium carbonate: $k = 1.31$ ($d_s = 16.6 \mu m$)

4. 2 Effect of air supply time in the initial section on a conveying performance

Figure 5 shows the relationship between an air velocity u_a and a pressure loss through the whole line Δp . In this investigation a time of the air supply to the initial section Δt_1 varied from 0.5 to 1.5 second, while that to a secondary section Δt_2 was kept constant at 0.9 second.

The value of Δp was observed to increase with increasing Δt_1 . This is because the plugs would tend to be longer with increasing time for pushing samples out of the tank. A similar trend is shown in Fig. 6, in which the mixing ratio Γ increases with increasing Δt_1 . It is shown that a pressure loss would have a minimal effect in both cases. This is because a larger air flow rate might cause flow resistance and a smaller one might result in flow stagnation. The mixing ratio decreased with increasing air flow rate. The plots of a conveying efficiency η calculated by Eq. (26) against u_a are shown in Fig. 7. The experimental results suggested that efficient transport might be pos-

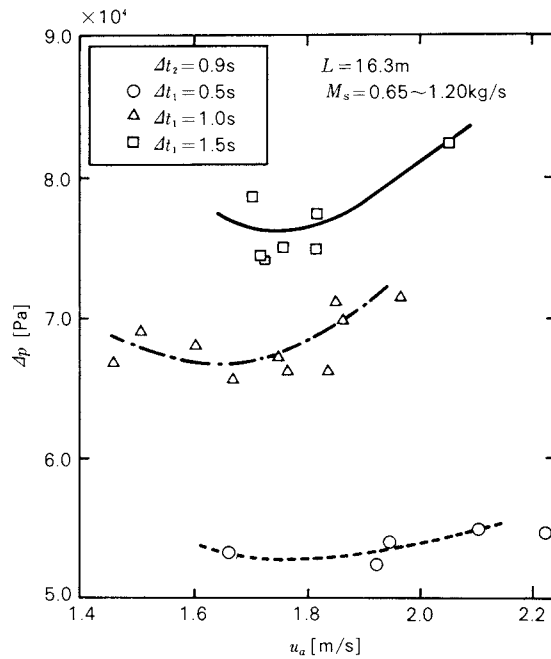


Fig. 5 Transition of total pressure drop according to air velocity in pipe in case of Δt_2 const.

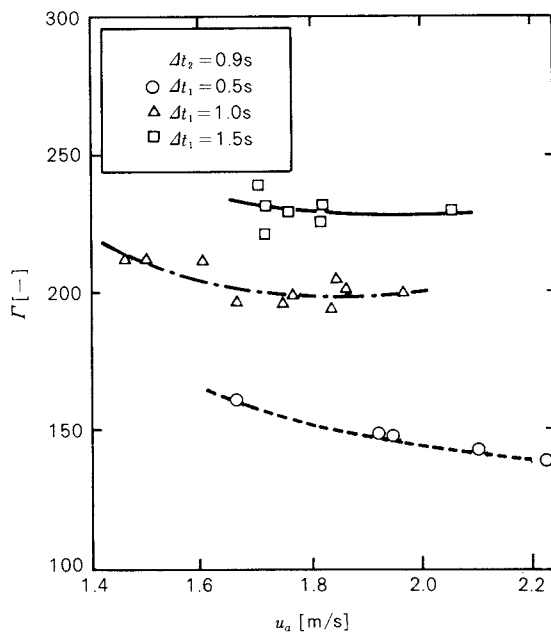


Fig. 6 Transition of mixing ratio according to air velocity in case of Δt_2 const.

sible under the condition of low air velocity and long supply time of an initial section as long as the pipeline was not blocked.

4. 3 Effect of air supply time in a secondary section on a conveying performance

Figure 8 shows the relationship between an air

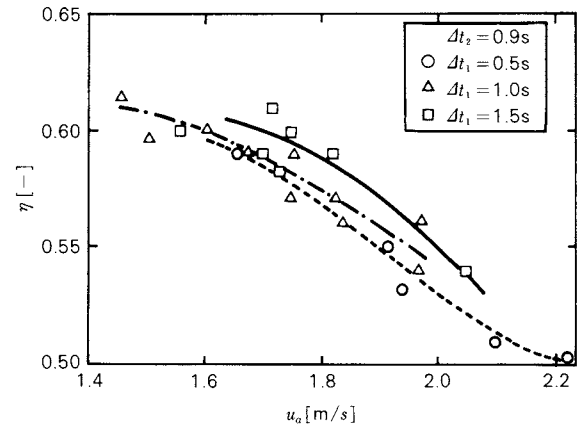


Fig. 7 Transition of transport efficiency according to air velocity in pipe in case of Δt_2 const.

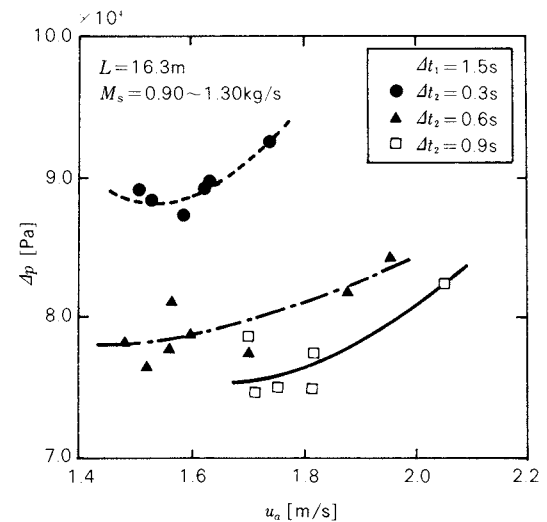


Fig. 8 Transition of total pressure drop according to air velocity in case of Δt_1 const.

velocity u_a and a total pressure loss Δp when Δt_1 was kept constant at 1.5 second. It was found that Δp would decrease with increasing Δt_2 . This is because the longer an air supply to a start point of a pipe was, the longer an air cushion would be or the shorter a solid plug would be. Expanding the length of the air cushion was observed to reduce the mixing ratio or the transport rate, which is also shown in Fig. 9.

The plots of u_a measured against η are shown in Fig. 10. Although η increased with decreasing u_a , the influence was found to be negligible. In addition, it was found that this result was nearly independent of the length of Δt_1 .

It follows from above discussion that η may

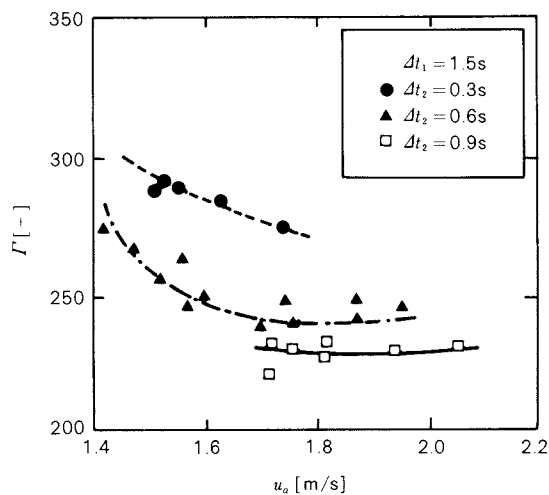


Fig. 9 Transition of mixing ratio according to air velocity in pipe in case of Δt_1 const.

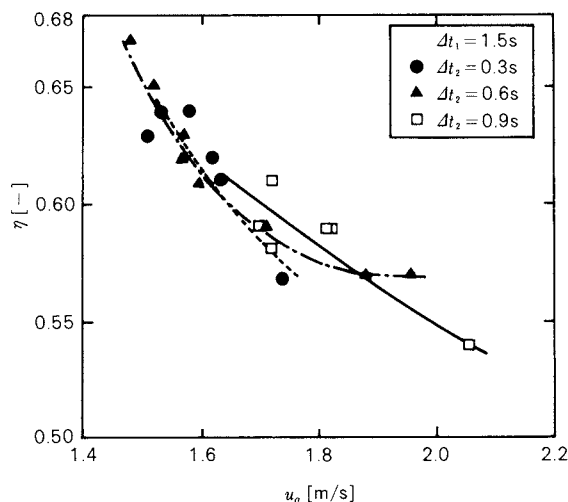


Fig. 10 Transition of transport efficiency according to air velocity in pipe in case of Δt_1 const.

be almost independent of Δt_2 but Δt_2 should be reduced in order to obtain a desired transport rate as long as stable conveying would be possible.

4. 4 Pressure loss distribution

The distribution of pressure loss across the whole system was observed as illustrated in Fig.11, in which the slope of the straight line is equal to the pressure loss in each section. Vertical bend I showed the steepest slope of the pressure loss curve which was nearly three times as large as that of a horizontal straight pipe. The slope of the pressure loss curve of the vertical straight pipe, vertical bend II, and

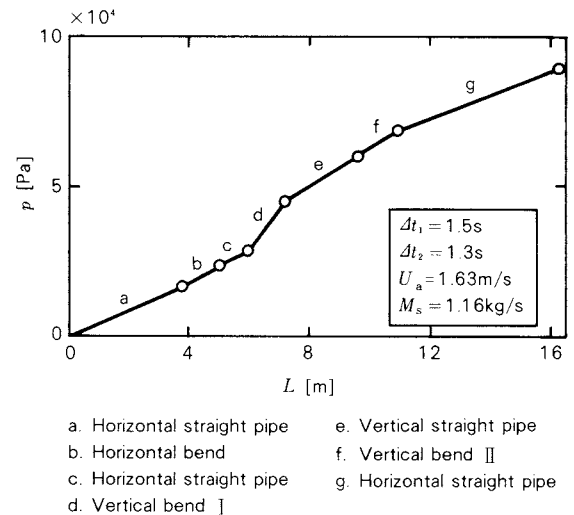


Fig. 11 Diagram of pressure drop along the pipe length

the horizontal bend pipe were almost 1.4 times as large as that of a horizontal straight pipe. It was observed that rates of plugs were slightly reduced at bends where air cushions push plugs. This trend was seen especially at vertical bend I, and it could be estimated that this would result in the maximum pressure loss at this section. Similar results to the above-mentioned were obtained with varied air velocities and intervals of air supply.

4. 5 Pressure loss and additional pressure loss coefficient

As above-mentioned, the pressure loss in the vertical pipe was found to be almost 1.4 times as large as that of a horizontal pipe.

Figure 12 shows the relationship between the length of a plug and the pressure loss across a plug l_p . It is natural that pressure loss should increase with increasing plug length. The figure shows that the solid lines calculated from Eqs. (8) to (11) could agree with the measured values with a porosity of 0.42 to 0.53. From this result a certain amount of air might be considered to pass through the plugs.

The relationship between the additional pressure loss coefficient λ_s and the Froude number related to u_p , $Fr_p = u_p / \sqrt{gD}$ is shown in Fig. 13 (horizontal pipe) and Fig. 14 (vertical pipe). It is well-known that the Froude number represents a measure of inertial to gravitational forces acting on particles in the flow. For larger Froude numbers, the additional

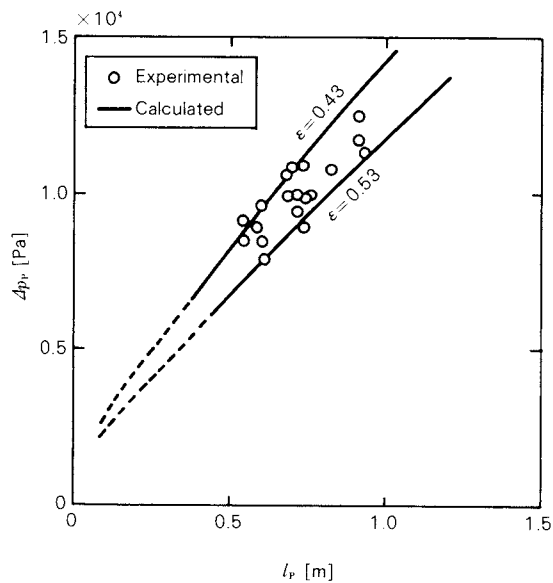


Fig. 12 Relationship between pressure drop across plug and length of plug

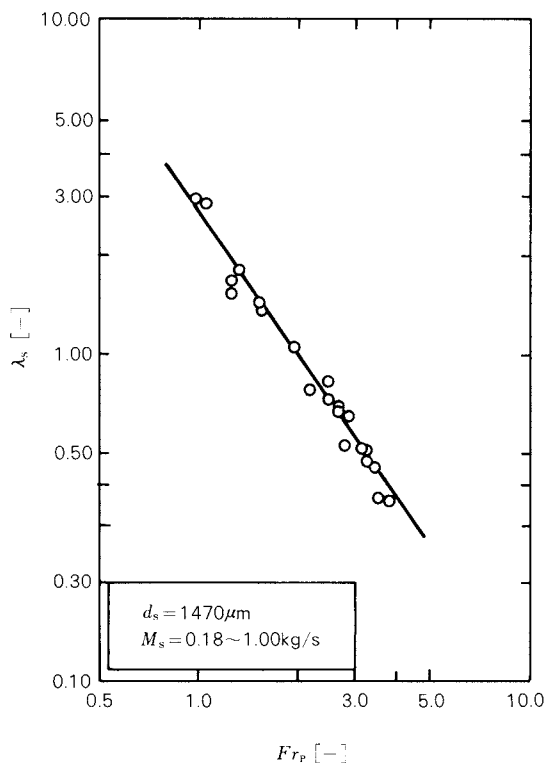


Fig. 13 Relationship between additional friction factor and Froude number in horizontal pipe

friction factors were reduced. Resultant expressions were experimentally obtained as follows:

For horizontal pipe:

$$\lambda_s = 2.62 Fr_p^{-1.43} \quad (0.9 < Fr_p < 4.0)$$

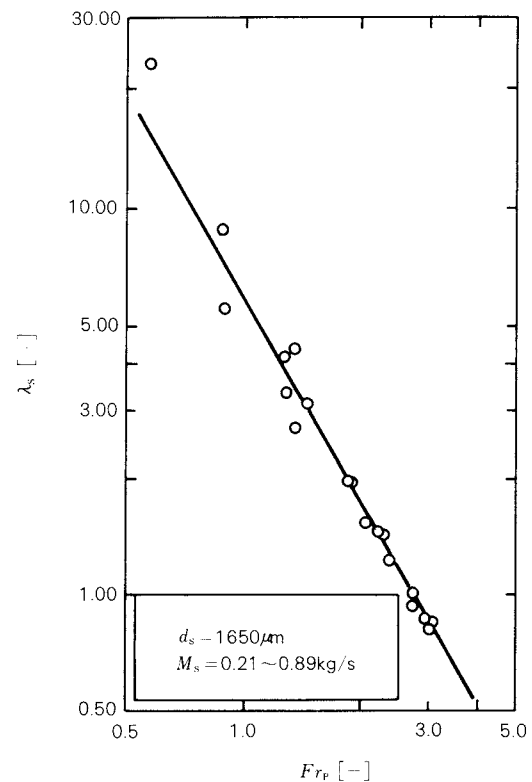


Fig. 14 Relationship between additional friction factor and Froude number in vertical pipe

For vertical pipe:

$$\lambda_s = 5.70 Fr_p^{-1.73} \quad (0.5 < Fr_p < 4.0)$$

4. 6 Stability of a plug

In this investigation it was found that alternately intermittent injections of compressed air into two different sections made it possible to transport solid plugs with air cushions in a well-ordered form of which the length could be adjusted by a solenoid valve. However such plugs were observed to repeatedly collapse and reform according to given conditions in progress.

The author introduced a ratio of plug number S_p to express the stability of plugs. This ratio S_p , which implies the apparent number of plugs compared with the number of on-off times of the solenoid valve, is calculated from:

$$S_p = n_p (\Delta t_1 + \Delta t_2) \quad (33)$$

where n_p is the number of plugs actually observed in a unit time.

Figure 15 shows the relationship between plug velocity u_p and the ratio of plug number S_p . At $\Delta t_1 = 0.5$, S_p was around one, while it increased with increasing u_p at $\Delta t_1 = 1.5$ second.

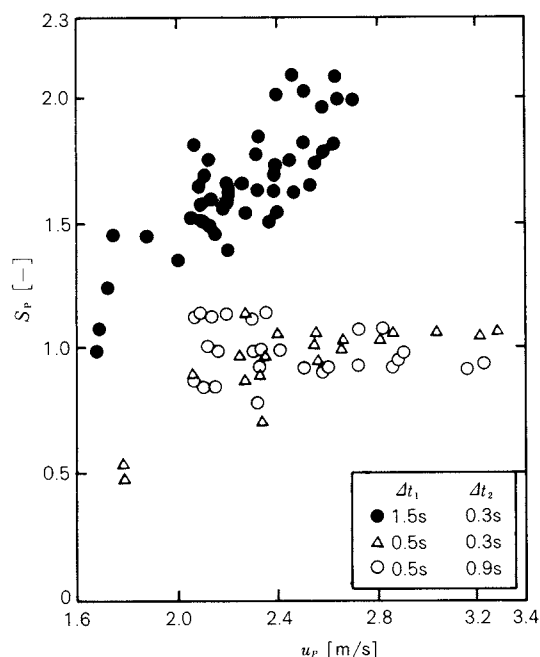


Fig. 15 Relationship between ratio of plug-number and plug velocity

This is probably because the length of plugs pushed out of an initial section would increase with increasing u_p and the plugs would be divided into plug fragments due to the penetration of compressed air.

In this paper the discussion is limited to the condition of $\Delta t_1 = 0.5$ and $\Delta t_2 = 0.3$ because of the formation of stable plugs.

4. 7 Desirable bend shape

The pressure drop in a bend Δp_b is shown to depend both on the frictional resistance and on the resistance resulting from the change in flow direction. The former is related to the length of pipeline, while the latter to the ratio of the curvature of radius R to the pipe diameter D , R/D . In this investigation the relationship between air velocity u_a and pressure loss Δp was examined using three kinds of bends with R/D ratios of 4.0, 7.5 and 11.0.

Experimental results are shown in Fig. 16 for a horizontal bend, in Fig. 17 for vertical bend I, and in Fig. 18 for vertical bend II. It was observed that there was a great deal of a pressure loss Δp_p and it fluctuated in all cases.

It is reasonable that a suitable bend shape should reduce a pressure loss, which is desired for efficient pneumatic conveying of materials. The experimental results imply that the small-

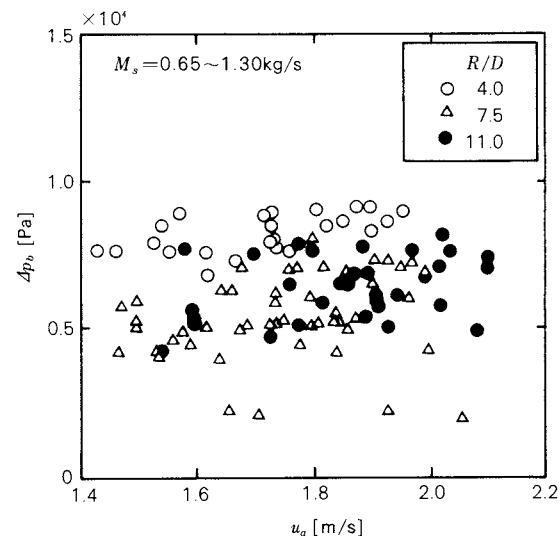


Fig. 16 Transition of pressure drop in horizontal bend according to air velocity in pipe

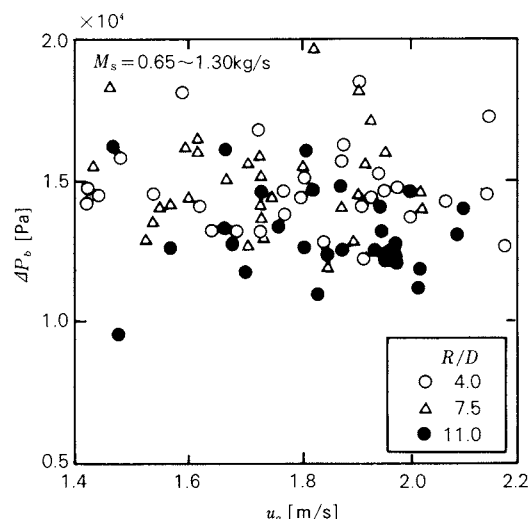


Fig. 17 Transition of pressure drop in vertical bend I according to air velocity in pipe

est pressure loss was obtained from the construction with $R/D = 7.5$ for a horizontal pipe as shown in Fig. 16 and $R/D = 11.0$ for a vertical bend I as shown in Fig. 17. In the latter case, the resistance was large because of the change in the flow direction from horizontal to upward, so that a larger radius of curvature could possibly provide a smoother flow. For vertical bend II, on the other hand, remarkable correlations could not be observed as shown in Fig. 18. It might be because the pressure drop in such a case was more susceptible to pressure fluctuation than to changes in the radius of curvature.

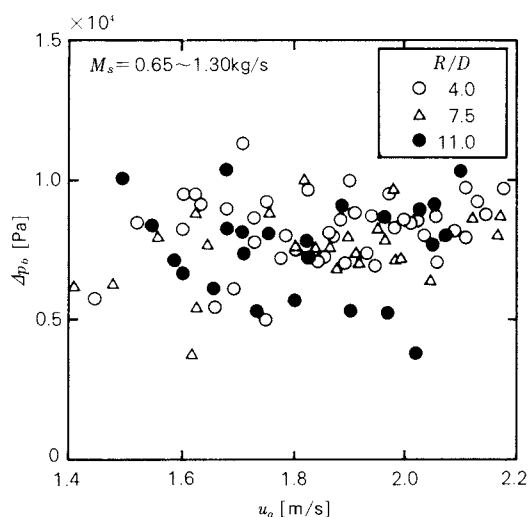


Fig. 18 Transition of pressure drop in vertical bend II according to air velocity in pipe

4. 8 Effect of vibrating bend on pressure drop

The effects of vibrating bends on the pressure drop were examined experimentally. A typical comparison of Δp_b related to u_a is shown in Fig. 19. In this experiment, when vibration with A of 4.5 was applied at the upward horizontal-vertical bend I with R/D of 11.0 (which was connected directly to the bottom of the tank), Δp_b was observed to be reduced by 20%. Such effects were also observed to be independent of R/D or A . Although similar results were obtained from a horizontal

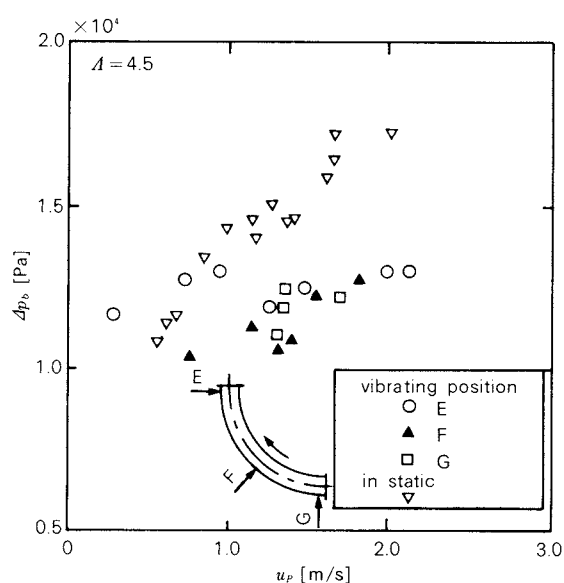


Fig. 19 Transition of pressure drop in bend according to air velocity with vibration

bend experiment, the resultant effects of vibration on vertical pipe II were ambiguous.

4. 9 Effect of vibrating horizontal pipe on pressure drop

The requisit power consumption through a horizontal pipe with length of 5.0m was examined. As shown in Fig. 20, the requisit power consumption N_c , related to u_a , was found to be reduced by 20% when vertical vibration was applied to the center of the pipe, compared with the case of the static state. Such a reduction of the power consumption might have been caused by a decrease in the wall friction resistance of solids which resulted from the vibration. In addition, a mass conveying rate M_s was observed to increase with increasing u_a .

The plots as to N_c indicated in Fig. 20 were calculated from Eq. (29), based on Q_a and N_c for transport only, without the addition of power consumption for vibrating an air vibrator. This power consumption was found to be considerably large under the given condition of 2.45×10^5 Pa and 0.65×10^{-3} m³/s because of the restricted experimental space. It is pos-

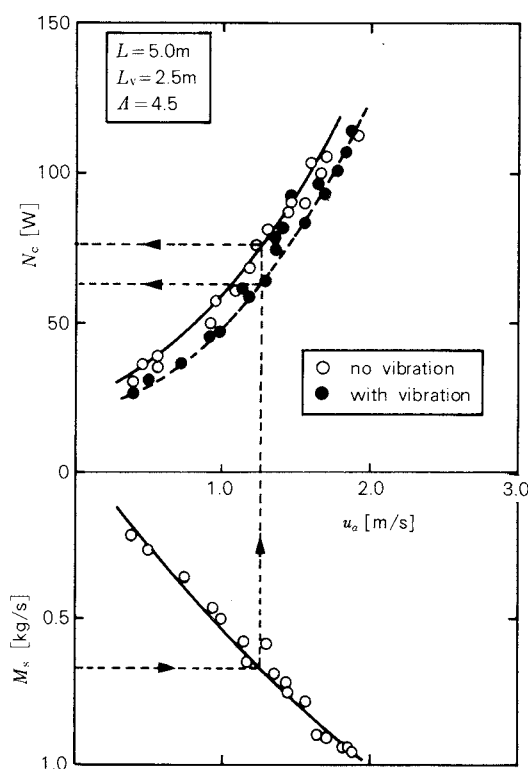


Fig. 20 Relation between power consumption and air velocity and also mass flow rate of particles

sible, however, that the effect of vibration will turn out to be satisfactory in such transport economics, if the pipeline is longer.

In addition, the exhaust gas of the vibrator was introduced to the start point of the pipeline for utilization as a part of the conveying air. The results showed that such a reuse of exhaust gas could provide a smooth and economic transport condition.

5. Conclusion

In this work, several methods to reduce requisit power consumption for dense phase plug pneumatic conveying were examined. The results obtained were as follows:

- Alternate injection of compressed air into the top side of the blow tank and the start point of the pipeline made it possible to produce plugs of the same length successively and to convey them in a stable state.
- The pressure drop in the vertical pipe was observed to be 1.4 times as large as that in the horizontal pipe. The desirable ratio of the radius of curvature to the pipe diameter was 7.5 for the horizontal bend or 11.0 for the upward horizontal – vertical bend, while a remarkable influence could not be seen for the vertical – horizontal bend.
- The vibratory pipe would result in reducing the requisit power and the exhaust air from a vibrator could be utilized as a part of conveying air.

Although the author ascertains that the results may be available to various plant designs, it is recommended that the characteristics of conveyed materials or the scale of transport systems should be taken into account.

Acknowledgement

This work was financially supported in part by a Grant-in-Aid for Scientific Research from the Ministry of Education, Science and Culture,

Japan. The author wishes to thank Masato Utsumi, Hiroki Kuroyanagi, Takuji Kawade, Taketoshi Marui, Kazunori Sugiyama and Fumiaki Takeuchi in Shizuoka University for their helps of this investigation.

Nomenclature

D	: inner diameter of pipe	[m]
L	: pipe length of transportation	[m]
L_a	: air cushion length	[m]
l_p	: plug length	[m]
M_s	: mas flow rate of particle	[kg/s]
N_c	: power consumption	[Ws]
n_p	: number of plugs per second	[1/s]
p	: cumulative pressure drop of air through the transporting pipe	[Pa]
Δp	: total pressure drop in the transporting line	[Pa]
Δp_b	: pressure drop in the bend	[Pa]
Q_a	: volumetric flow rate of air	[m ³ /s]
R	: radius of curvature	[m]
S_p	: ratio of plug-number defined by Eq.(33)	[–]
t	: transporting time	[s]
Δt_1	: regular interval of time for supplying air to the initial section	[s]
Δt_2	: regular interval of time for supplying air to the secondary section	[s]
u_a	: air velocity	[m/s]
u_p	: plug velocity	[m/s]
η	: transport efficiency	[–]
Γ	: mixing ratio	[–]

References

- 1) Aoki, R., H. Murata, H. Honma and H. Wada: *Kagaku Kogaku Ronbunshu*, **5**, 628 (1980).
- 2) Morikawa, Y., Y. Tsuji, H. Honda and H. Noguchi: *Trans. J.S.M.E. Ser. B.* **47**, 132 (1981).
- 3) Kano, T., F. Takeuchi, E. Yamazaki and H. Tuzuki: *Kagaku Kogaku Ronbunshu*, **7**, 126 (1981).
- 4) Kano, T., F. Takeuchi, Y. Kondo, M. Utsumi, T. Maeda and K. Takemura: *ibid.* **9**, 477 (1983).
- 5) Kano, T.: Unpublished
- 6) Yokoyama, Y.: *Seimitsu Kikai*, **32**, 403 (1966).

(English proof reader: S.E. Dodick)

A New Particle Size Distribution Apparatus based on Unbalance by Centrifugal Sedimentation

Masafumi Arakawa*

Kyoto Institute of Technology

Gen Simomura, Akira Imamura**
and Naohiko Yazawa****

Akashi Seisakusho, Ltd.

Noriyoshi Kaya* and Hiromi Kitai*****

Hosokawa Micromeritics Laboratory

Abstract

A new apparatus for the measurement of particle size distribution based on the unbalance caused by centrifugal sedimentation was made on an experimental bases. The size distributions obtained by this method with a constant revolution of the rotor were compared with those measured by other methods using the same sample.

Furthermore, in order to shorten the measuring time and expand the measuring size range, some additional attempts were conducted with a linear acceleration followed by a constant revolution of the rotor. They gave similar results of size distribution to the measurements at a constant revolution.

1. Introduction

The principle of sedimentation of particulate materials in a liquid phase is used most widely and reliably among various principles for the measurement of particle size distribution. One of the most popular methods based on this principle adapts the opacity with the particles settling by a centrifugal force. This method has two disadvantages. One of them is the difficulties caused by the fact that the size of particles in the submicron range becomes the same order to the wave length of light. The other is that the optical extinction coefficient varies with the particle size and the material.

A new method based on the displacement of

the center of gravity caused by particle settling was proposed to overcome the disadvantages of light extinction methods¹⁾.

In this report, we first introduce a test apparatus that was made to measure size distribution applying this method and combining a personal computer for immediate analysis. Then we show some examples of the measurement using this instrument. In order to expand the range of measuring size it was examined to increase rotor speed of the centrifuge with the measurement time.

2. Measuring principle and procedures

Pouring homogeneous suspension including a sample powder into a cell and setting it in a rotor, the balance of the rotor is arranged before measuring. The rotor being set in motion, the particles settle in the centrifugal field and the center of gravity of the cell is shifted from its initial position.

A sedimentation curve in terms of the unbalance can be obtained by the instrument which detects the deviation of the center of

* Matsugazaki, Sakyo, Kyoto, 606
TEL. 075 (791) 3211

** 2-4-1 Nishi-Shinjuku, Sinjuku, Tokyo, 160
TEL. 03 (349) 8911

*** 9, Shodai-tajika 1-chome, Hirakata, Osaka, 573
TEL. 0720 (57) 3721

Received June 27, 1984

gravity making use of a balancing machine.

The equation of motion for centrifugal sedimentation is written with an angular velocity ω and a particle radius r as follows.

$$\frac{dx}{dt} = \frac{2}{9} \left(\frac{\rho_P - \rho_L}{\mu_L} \right) r^2 \omega^2 x \quad (1)$$

where ρ_P : density of particles [g/cm³]
 ρ_L : density of dispersion medium [g/cm³]
 μ_L : viscosity of dispersion medium [g/cm·sec]

x : distance in the radial direction [cm]

Defining K as the following,

$$K = \frac{2}{9} \left(\frac{\rho_P - \rho_L}{\mu_L} \right) \quad (2)$$

Substituting Eq. (2) for (1), and applying the boundary condition $x = x_i$ at $t = 0$, we obtain

$$\ln \frac{x}{x_i} = K r^2 \omega^2 t \quad (3)$$

or

$$x = x_i e^{K r^2 \omega^2 t} \quad (4)$$

For the displacement of the center of gravity in the cell by the particle settling, we assume two processes as illustrated in Fig. 1.

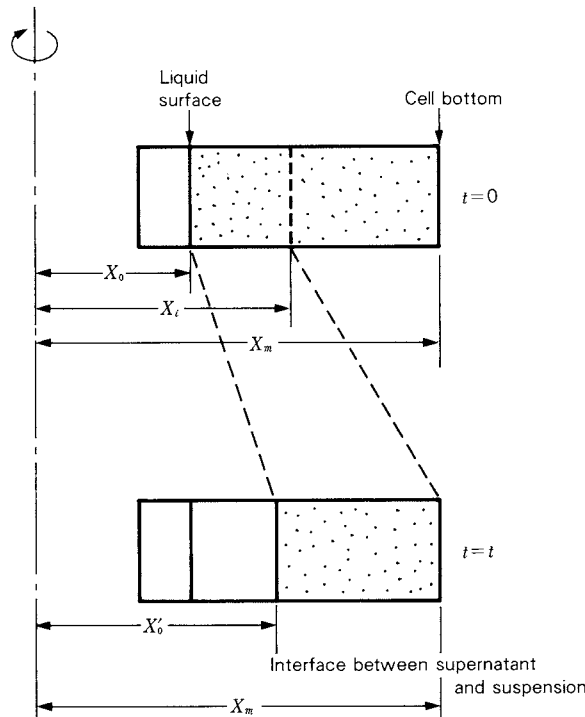


Fig. 1 Eccentric distance caused by centrifugal sedimentation

a) The displacement of the center of gravity caused by the particles which are located between x_i and x_m at $t=0$ and settle out completely by $t=t$.

b) The displacement of the center of gravity resulted from the sedimentation of the particles which are located between x_0 and x_i at $t=0$ and do not reach the cell bottom by $t=t$.

The displacements defined in above a) and b) are shown with ϵ_a and ϵ_b , respectively.

Mass of particles m_a positioned between x_i and x_m is given:

$$m_a = \frac{x_m - x_i}{x_m - x_0} m \quad (5)$$

where m is the mass of particles in the cell. Letting the initial eccentric distance be e_0 and the one after the displacement of the center of gravity be e_1 , the balancing moment takes the following forms in each case,

$$e_0 M = m_a \left(\frac{x_i + x_m}{2} \right) \left(\frac{\rho_P - \rho_L}{\rho_P} \right) \quad (6)$$

$$e_1 M = m_a x_m \left(\frac{\rho_P - \rho_L}{\rho_P} \right) \quad (7)$$

where M is the total mass of the rotating system. Combining Eq. (6) and Eq. (7)

$$\epsilon_a = e_1 - e_0 = \frac{m_a}{M} \left(\frac{x_m - x_i}{2} \right) \left(\frac{\rho_P - \rho_L}{\rho_P} \right) \quad (8)$$

For particles settling from x_i to x_m with time t

$$x_m = x_i e^{K r^2 \omega^2 t} \quad (9)$$

Reforming the above,

$$x_m - x_i = (1 - e^{-K r^2 \omega^2 t}) x_m \quad (10)$$

Substituting Eq. (10) for Eq. (5),

$$m_a = \frac{(1 - e^{-K r^2 \omega^2 t}) x_m}{x_m - x_0} m \quad (11)$$

From Eqs. (8) and (11), we obtain

$$\epsilon_a = \frac{m}{M} \frac{(1 - e^{-K r^2 \omega^2 t})^2 x_m^2}{2(x_m - x_0)} \left(\frac{\rho_P - \rho_L}{\rho_P} \right) \quad (12)$$

On the other hand, the balance moment for the mass of particles m_b positioned between x_0 and x_i at $t=0$ gives:

$$e_0' M = m_b \left(\frac{x_i + x_0}{2} \right) \left(\frac{\rho_P - \rho_L}{\rho_P} \right) \quad (13)$$

$$e_1' M = m_b \left(\frac{x_m + x_0'}{2} \right) \left(\frac{\rho_P - \rho_L}{\rho_P} \right) \quad (14)$$

where e_0' , e_1' are the initial eccentric distance and the one after the displacement of the center of gravity by sedimentation respectively and x_0' is the interface position between the particle suspension and the supernatant liquid containing no particles.

Similar to Eq. (4), we obtain the following form for x_0'

$$x_0' = x_0 e^{Kr^2 \omega^2 t} \quad (15)$$

And from this relation

$$\epsilon_b = e_1 - e_0 = \frac{m_b}{M} \left(\frac{x_m + x_0 e^{Kr^2 \omega^2 t} - x_i - x_0}{2} \right) \times \left(\frac{\rho_P - \rho_L}{\rho_P} \right) \quad (16)$$

where m_b is given by the proportional allotment of m ,

$$m_b = \frac{x_i - x_0}{x_m - x_0} m \quad (17)$$

Substituting Eqs. (9) and (17) for Eq. (16), simplification gives

$$\epsilon_b = \frac{m}{M} \left(\frac{\rho_P - \rho_L}{\rho_P} \right) \times \frac{(e^{Kr^2 \omega^2 t} - 1)(x_m^2 e^{-2Kr^2 \omega^2 t} - x_0^2)}{2(x_m - x_0)} \quad (18)$$

Total eccentric displacement ϵ for the rotor is the sum of ϵ_a and ϵ_b and given from Eq. (12) and Eq. (18),

$$\epsilon = \frac{m}{M} \left(\frac{\rho_P - \rho_L}{\rho_P} \right) \times \frac{(e^{Kr^2 \omega^2 t} - 1)(x_m^2 e^{-Kr^2 \omega^2 t} - x_0^2)}{2(x_m - x_0)} \quad (19)$$

In the balancing test, centrifugal force P located on the rotor is expressed in general

$$P = \omega^2 M e \quad (20)$$

where e is eccentric distance. The value of Me is determined by the centrifugal force P with a known ω and thus we defined an unbalance U as follows,

$$U = M e \quad (21)$$

Now assuming that the unbalanced state of the actual rotor can be realized being replaced by a completely balanced rotor with attaching a

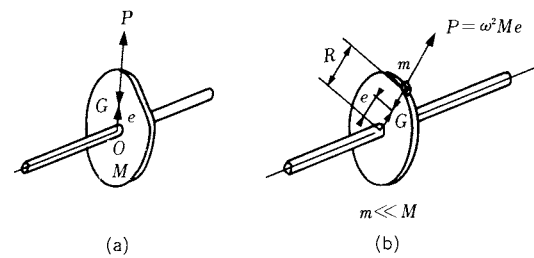


Fig. 2 Equivalent unbalance on a rotor

weight having mass of m at a radius R as illustrated in Fig. 2.

$$e = \frac{mR}{M} \quad (22)$$

The unbalance of the measuring rotor is obtained from Eq. (19) with setting $\epsilon = e$,

$$U(t) = m \left(\frac{\rho_P - \rho_L}{\rho_P} \right) \times \frac{(e^{Kr^2 \omega^2 t} - 1)(x_m^2 e^{-Kr^2 \omega^2 t} - x_0^2)}{2(x_m - x_0)} \quad (23)$$

Letting $\tau_c = Kr^2 \omega^2 t$, Eq. (23) is reformed

$$U(t) = m \left(\frac{\rho_P - \rho_L}{\rho_P} \right) \frac{(e^{\tau_c} - 1)(x_m^2 e^{-\tau_c} - x_0^2)}{2(x_m - x_0)} \quad (23)'$$

When the rotor revolution varies as shown in Fig. 3, angular speed ω is given by the following form,

$$\omega = \omega_0 + at \quad (24)$$

With this relation introduced, Eqs. (3) and (4) are rewritten as follows,

$$\ln \frac{x}{x_i} = \tau_l \quad (25)$$

or

$$x = x_i e^{\tau_l} \quad (26)$$

where τ_l is defined in the following equation,

$$\tau_l = Kr^2 \left(\frac{a^2}{3} t^3 + a\omega_0 t^2 + \omega_0^2 t \right) \quad (27)$$

The unbalance of the period before reaching constant rotation is derived from Eq. (23)' replacing τ_c by τ_l ,

$$U(t) = m \left(\frac{\rho_P - \rho_L}{\rho_P} \right) \frac{(e^{\tau_l} - 1)(x_m^2 e^{-\tau_l} - x_0^2)}{2(x_m - x_0)} \quad (28)$$

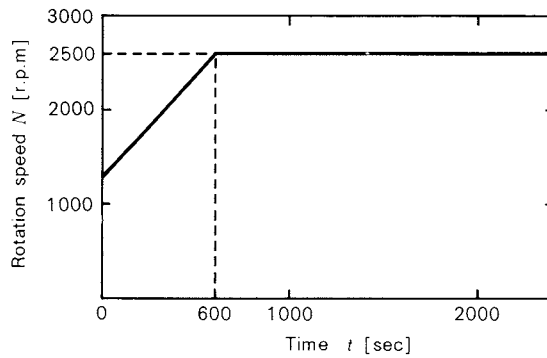


Fig. 3 Variation of rotor speed – Linear acceleration followed by constant rotation

In the period of constant rotation after $t = T_c$, the total measuring time is the sum of T_c and additional time t_c with constant rotation.

$$t = T_c + t_c \quad (29)$$

The unbalance U is given

$$U(t) = U(T_c) + U(t_c) \quad (30)$$

The first time on the right hand side $U(T_c)$ is derived from Eq. (28)

$$U(T_c) = m \left(\frac{\rho_P - \rho_L}{\rho_P} \right) \times \frac{(e^{\tau_l(T_c)} - 1)(x_m^2 e^{-\tau_l(T_c)} - x_0^2)}{2(x_m - x_0)} \quad (31)$$

$$\text{where } \tau_l(T_c) = Kr^2 \left(\frac{a^2}{3} T_c^3 + a\omega_0 T_c^2 + \omega_0^2 T_c \right) \quad (32)$$

The second term $U(t_c)$ is calculated in the same way,

$$U(t_c) = m_c \left(\frac{\rho_P - \rho_L}{\rho_P} \right) \times \frac{(e^{\tau_c(t_c)} - 1)(x_m^2 e^{-\tau_c(t_c)} - x_0'^2)}{2(x_m - x_0')} \quad (33)$$

where x_0' is the position of the interface between the supernatant part containing no-particles and the turbid part with suspended particles in the cell at $t = T_c$ and m_c is the mass of particles suspended.

When the rotor revolution reaches a constant condition, x_0' and m_c are given by the following equations,

$$x_0' = x_0 e^{\tau_l(T_c)} \quad (34)$$

$$m_c = \frac{x_i' - x_0}{x_m - x_0} m \quad (35)$$

where x_i' is the position of particles at $t = 0$ which will sediment completely at $t = T_c$, and so it can be shown that

$$x_i' = x_m e^{-\tau_l(T_c)} \quad (36)$$

Substituting Eq. (36) for Eq. (35), m_c is given

$$m_c = \frac{x_m e^{-\tau_l(T_c)} - x_0}{x_m - x_0} m \quad (37)$$

$U(t_c)$ is derived from Eqs. (33) and (37).

$$U(t_c) = \frac{x_m e^{-\tau_l(T_c)} - x_0}{x_m - x_0} m \left(\frac{\rho_P - \rho_L}{\rho_P} \right) \times \frac{(e^{\tau_c(t_c)} - 1)(x_m^2 e^{-\tau_c(t_c)} - x_0^2 e^{2\tau_l(T_c)})}{2(x_m - x_0 e^{\tau_l(T_c)})}$$

where $\tau_c(t_c)$ is given as

$$\tau_c(t_c) = Kr^2 \omega_c^2 t_c \quad (39)$$

and ω_c is given as

$$\omega_c = \omega_0 + a T_c \quad (39)'$$

From Eqs. (23), (28) and (38), we obtain the following simple equation as a general form showing the relation of the unbalance $U(t)$, coefficient A and mass of particles m for particles having uniform diameter,

$$U(t) = m A(r, t) \quad (40)$$

The unbalance $U(t_i)$ is therefore calculated as a sum of products of the mass m_j and the coefficient $A(r_j, t_i)$ of the particles having radius r_j at $t = t_i$.

$$U(t_i) = \sum m_j \cdot A(r_j, t_i) \quad (41)$$

The variation of unbalance with time is expressed by the following matrix based on Eq. (41).

$$\begin{pmatrix} A(r_1, t_1), A(r_2, t_1), \dots, A(r_n, t_1) \\ A(r_1, t_2), A(r_2, t_2), \dots, A(r_n, t_2) \\ \vdots \\ A(r_1, t_m), A(r_2, t_m), \dots, A(r_n, t_m) \end{pmatrix} \begin{pmatrix} m_1 \\ m_2 \\ \vdots \\ m_n \end{pmatrix} = \begin{pmatrix} U(t_1) \\ U(t_2) \\ \vdots \\ U(t_n) \end{pmatrix} \quad (42)$$

From the above equation, one can get the mass

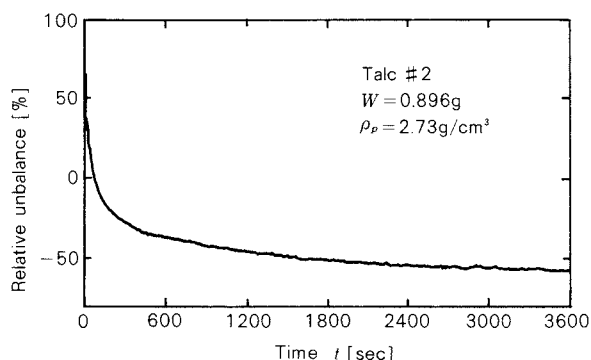


Fig. 7 Sedimentation curve of the unbalance

— Linear acceleration and constant rotation of 2500 r.p.m. shown in Fig. 3.

The last condition in the above-mentioned was planned to shorten the measuring time and to expand the measuring size range.

Figure 7 shows an example of sedimentation curve of the unbalance with a constant rotation. The horizontal axis presents the measuring time and the vertical axis indicates the relative unbalance from the base in the figure. The unbalance has a unit [g-mm] as seen from Eq. (21).

Figure 8 indicates the results of four measurements for the same sample on the condition of constant rotation to examine the reappearance. The measurements give small fluctuations of the results in the finer size range. The results are shown in Fig. 9, compared with other methods, such as sedimentation balance, electric resistance and photo extinction. The figure indicates that sedimentation balance gave the finest, having good agreement with this method, while photo extinction

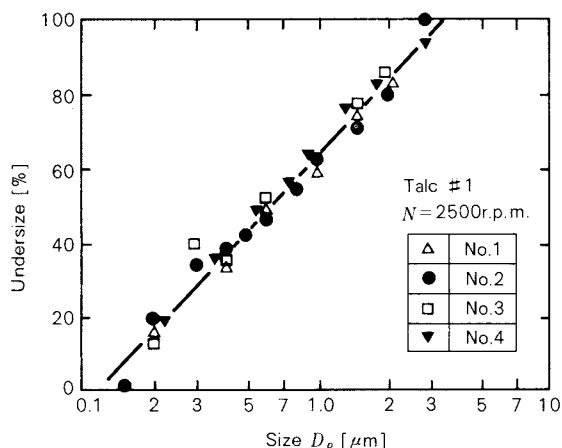


Fig. 8 Reappearance of the measurements

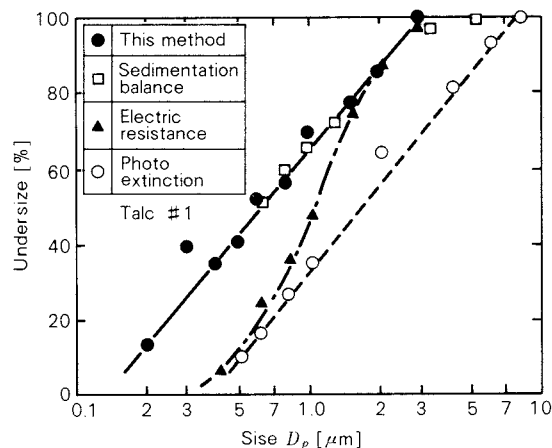


Fig. 9 Comparison of measuring methods

tended to produce a coarser result and electric resistance method had the intermediate tendency. The comparison of the methods in case of CaCO_3 gave the same feature. From these results, it is assumed that the tendency in size distribution depends on the measuring method itself.

The examples of the results in the cases of linear acceleration and constant revolution are shown in Figs. 10 and 11. The sample shown in Fig. 10 had smaller number of the coarser particles than other samples and was measured on the condition of constant rotation of 2500 r.p.m. and linear acceleration from 1300 to 2500 r.p.m. for the comparison.

Figure 11 shows the results of Kanto loam powder with mean diameter of about $2 \mu\text{m}$, the maximum diameter of $8 \mu\text{m}$ and no finer fraction of the particle less than $0.2 \mu\text{m}$. Since there was no suitable talc samples available to

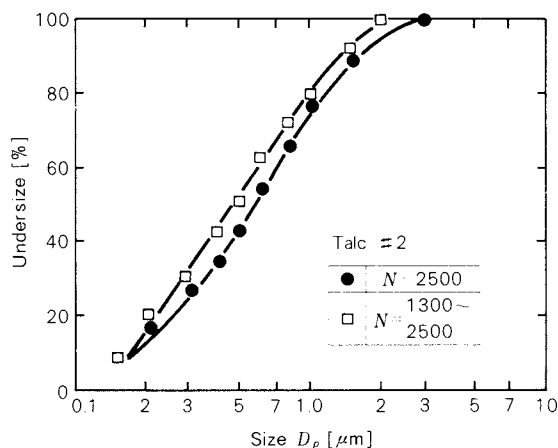


Fig. 10 Comparison of the measuring conditions

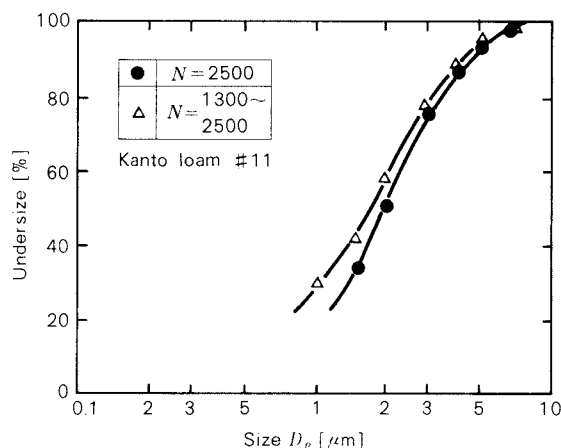


Fig. 11 Comparison of the measuring conditions

measure in the coarser particle size range, Kanto loam was employed as substitute material to compare with. The rotation speed was set at 1300 r.p.m. in this case, because the Kanto loam was relatively coarse and would have settled out immediately at 2500 r.p.m. Decreasing the rotation produces smaller vibration amplitude and so reduces the resolution of pickup as seen from Fig. 6. To avoid decreasing the resolution and rapid settling of particles, the measuring rotation was set at 1300 r.p.m. There was a little difference in the results between the constant rotation and the linear acceleration. It may come from the error in the determination of a correcting values. The signal band detected by the pickup varied with rotor revolution and therefore would require blank tests and correction of the directly obtained values. We will examine the correction more exactly.

5. Conclusion

A new method for particle size distribution measurement making use of a dynamic balancing machine was introduced and a test apparatus was made based on this method.

It has advantages of the direct relation with the displacement of the center of gravity caused by the particle settling and no connection with properties depending on the materials such as the extinction coefficient in the case of photo extinction. The other advantage of the measurement is comparatively short time required to determine the size distribution. In this instrument, as the particle settling in any

part of the suspension causes the deviation of the center of gravity, the unbalance data can be obtained without reaching specified distance for measuring.

The results of measurement by the method were similar to those by other methods and showed specially good agreement with sedimentation balance. Additionally, in order to shorten the measuring time and to expand the measuring size range, a new approach to the measurement was examined combining a linear acceleration with a following constant rotation using the same instrument. The results of the approach gave a little finer but approximately the same as those of constant rotation.

We are planning to make further developments on the measurement and improve the apparatus in order to complete a simple and precise instrument for the measurement of particle size distribution in the future.

Nomenclature

$A(r, t)$: coefficient of the matrix	[mm]
a	: constant acceleration of the rotor speed	[1/sec ²]
D_p	: particle diameter	[cm]
e	: eccentric distance	[cm]
e_0, e'_0	: initial eccentric distance	[cm]
e_1, e'_1	: eccentric distance after sedimentation	[cm]
K	: constant for a given measurement	[sec/cm ²]
k	: spring constant	[dyne/cm]
P	: centrifugal force	[dyne]
R	: equivalent radius of the rotor	[cm]
r	: particle radius	[cm]
r_i	: radius of a concerned particle	[cm]
T_c	: interval of constant acceleration	[sec]
t	: time	[sec]
t_c	: time of constant revolution	[sec]
$U(t)$: unbalance	[g-mm]
M	: total mass of the rotating system	[g]
m	: mass of particles in the cell	[g]
m_a	: mass of particles located between x_i and x_m at $t = 0$	[g]
m_b	: mass of particles located between x_0 and x_i at $t = 0$	[g]
m_c	: mass of particles suspended at $t = T_c$	[g]
x	: position in the radial direction	[cm]
x_i	: position of the particles to reach the cell bottom at $t = t$	[cm]
x_m	: position of the cell bottom	[cm]
x_0	: position of the surface of suspension	[cm]
x'_0	: position of the boundary between the supernatant and the suspension	[cm]
ϵ_a, ϵ_b	: displacement of the center of gravity	[cm]

μ_c	: viscosity of dispersion medium	[g/cm sec]
ρ_L	: density of dispersion medium	[g/cm ³]
ρ_P	: density of particles	[g/cm ³]
ω	: angular speed	[1/sec]
ω_0	: initial angular speed	[1/sec]
ω_c	: constant angular speed	[1/sec]
τ_c, τ_l	: non-dimensional variables	[—]
x	: amplitude of vibration	[cm]

References

- 1) Suito, E., M. Arakawa, T. Masuda, S. Miwa and M. Sase: "Ohyo-Butsuri (*J. Applied Physics, Japan*)", **32**, 823 (1963).
- 2) Miwa, S. and G. Shimomura: "Kaiten Kikai no Tsurawase (Balance on Rotating Machine)", **68**, Korona Co. (1976).
- 3) Arakawa, M., G. Shimomura, A. Imamura, N. Yaza-wa, T. Yokoyama and N. Kaya: *Zairyo (J. Soc. Materials Sci., Japan* **33** (1984)) (in preparation for publication).

Short History of Grinding Implements for Domestic Use in Japan

Shigeo Miwa*, Atsuko Shimosaka*
and Jusuke Hidaka*

Department of Chemical Engineering
Doshisha University

Abstract

There are many works that refer to the history of grinding implements^{1~6)}, but they are restricted mainly to the origin of Western wheat flour milling technology as a professional activity, and do not always pay attention to domestic use.

It is an interesting fact that almost all the ancient grinding implements devised by humans throughout history have continued to be used domestically even after the advent of more efficient specialized ones. We can find many examples of this in Japan as well, and some of them have survived to the present day.

On the other hand, owing to the recent dramatic change in our life-style, the familiarity of these implements is being rapidly lost in Japan. Therefore, the present work is an attempt to record them in an intelligible form, and to collate them with the Chinese and European ones from the historical viewpoint.

Another point to be cited is the very old, traditional grooving of the rotary quern which survives now in Japan. The so-called "counterclockwise revolving, eight-quarter grooving pattern" is the same as that which existed in Europe and China during the Roman period. Though we do not know where and when it originated as yet, this fact is decisive proof of its transmission.

1. Introduction

From a viewpoint of the material side of human life, a civilization was based on the material preparation technology which can be applied to provide refined materials capable of supplying human needs for everyday life from crude materials in nature. Nowadays, the technology is employed on a large scale for the production of useful constituents from various natural resources.

The origin of these technologies is presumed to be almost coexistent with the earliest humans. The most important technology for everyday life was, in the ancient world, the preparation of foods, but this technology was also used for other materials: ores and the like. Because nearly all materials used by man owe their value to the separation of useful con-

stituents, some grinding implements used for that purpose would play a most important role in the first step of the preparation process.

This paper, based on the information available today, attempts to sketch out a history of the many varieties of grinding implements for domestic use (not for professional activity) which were devised by man before modern industrial society. Although there have been many such attempts from the Western point of view^{1~6)}, they were restricted mainly to the industrial wheat flour milling for bread. East Asian peoples who do not necessarily live on wheat have been developing different varieties of grinding implements for domestic use.

2. Origin of grinding implements

In the natural world, there are resources which may be used for everyday life directly or after some comparatively simple preparation process. Foods hunted for and gathered by the earliest humans, which were various kinds of

* Karasuma-Imadegawa, Kamigyo-ku, Kyoto 602
TEL. 075 (251) 3849

Received April 11, 1984

animals, fishes, fruits, edible tubers and so on, could be easily cooked using only a simple preparation process. And, in the later period, natural copper, iron sand and alluvial gold could be used as the materials for primitive metallurgical processing by simple preparation methods, for they were naturally, though roughly, prepared resources.

However, cereals, especially wheat, barley, rice, millet and so on, required some tedious processings — threshing, hulling or milling. The wild wheat grains, like other cereals, consist of a starchy endosperm or kernel enclosed in a very hard outer sheath and bran, and they are not edible in their raw state. Similarly, with various ores, it is necessary to grind hard ores and collect the useful portion. For such similar materials, the first step of their preparation is the grinding process, which includes threshing and hulling in a broad sense.

An earliest man skinned and cut up the meat of animal with a stone knife or axe. This was also a kind of separation of useful constituents from that body, but his work was, in fact, the direct extension of his own fundamental motion. Even if the material of which the knife or axe was made, was changed from flint to bronze or iron, it would have still remained the direct extension of his teeth or nails, and the tools were only supplementary ones. Unless there had been complicated human regulation for that use, it would have been difficult indeed to accomplish the work. In modern times the knife and axe still survive in their original design, even if the material of which they are made is metal, and the style is refined.

However, in the case of grinding, the situation was quite different. The first man sampling a seed of wild grass would have cracked it with his teeth or his nail, and then, after placing the bulk of the grains in a hollow of a natural stone, he pounded it with a stone, and then blew away the husks. As a result it became easier for him to eat. Using the resulting flour, he could make rough cakes. Because the process of physical change occurring in each grain was complex, and numerous grains were simultaneously processed, he could not regulate them directly. His work was only a simple mechanical action repeated monotonously. It was not the direct extension of the human teeth or nails, but was assuredly a mass process-

ing operation, which held great possibilities for further improvement.

Even if there is evidence, which survives now with the Ainu in Japan (one of the old races of East Asia), to suggest that a wheat grain can be ground to powder with one's teeth, it would, needless to say, be difficult to satisfy the required level of productivity necessary for everyday life.

Then in the course of time, the earliest primitive grinding implement was gradually improved, enlarged and specialized for each purpose. Though there is no clear evidence to tell us what sort of implements were tried, we can easily imagine that man would take one of following three possible ways according to the characteristics of the grains he used:

- 1) Pounding which would lead to a mortar and pestle and later to a stamp mill.
- 2) Rolling which would lead to an edge-runner.
- 3) Rubbing which would lead to a rubbing stone, a saddle quern, and later a rotary quern.

The discovery — or invention — of grinding implements and grinding methods bears very special importance in the history of human beings. The most important achievement was the dramatic increase in human food supply. Many wild grass seeds which had been inedible in their raw state became the source of food when grinding could make them edible. There is a chicken-and-egg aspect to this, though; the discovery could lead to the coming of agriculture. As a matter of course this collecting seeds would have suggested the idea of growing plants for food.

Different courses of development of implements could be seen at different regions of the world, related to the grain available. For example, rice or millet was not necessarily ground to powder, because they could be cooked after only hulling, and, as in China, a mortar and pestle or an edge-runner mill was the major implement developed.

On the other hand, wheat with interpenetrated shell would not be cooked without grinding to powder. In this case, rubbing action was more efficient than pounding.

3. Mortar and Pestle

The first thing we will discuss is pounding

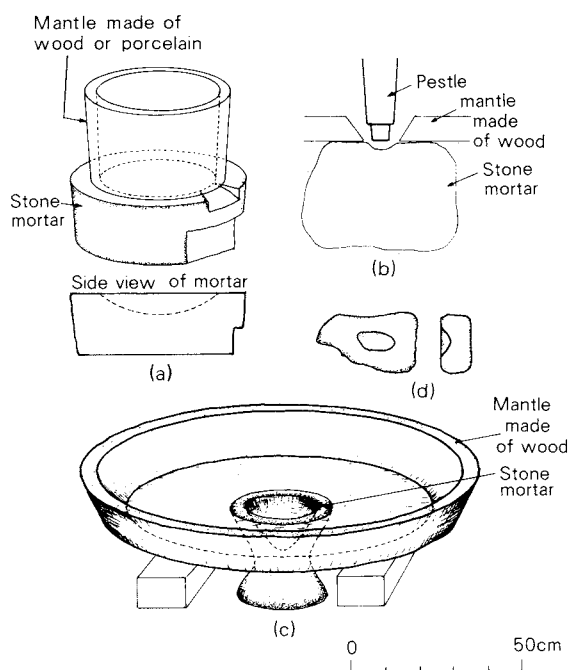
with mortar and pestle, since this would have been applied to all kinds of uses. The earliest grinding implements found from the remains of the Palaeolithic era consisted of a roundish stone which was held in the hands and a larger hollowed stone for a bed stone. The hollowness is necessary for efficient impactation and to prevent grain from falling off of the stone. Therefore, a round mantle made of hide or wood on the flat bed stone could serve the same function. Since the mantle made of perishable materials is easy to lose, it is difficult to find the certifiable relics of this type of mortar. **Figures 1 (a), (b) and (c)** are such reference examples surviving in Japan and Korea. It is interesting to compare them with the relics from the Stone Age in **Fig. 1 (d)**. If the mortar was fixed on the ground, a much larger pestel could be used.

Since the mortar and pestle covered a wide range of adaptability, they were normally not specialized for a certain single purpose for a

long time. However, they became specialized gradually as one purpose gained predominance over others. Anyone using the mortar and pestle may notice that it works in the following three ways.

- 1) **Hulling** — grain surface grinding: If grain with a relatively soft outside husk is pounded using a pestle with a flat end (**Fig. 2(a)**), the husk is gradually removed, as in hulling and polishing of rice or barleycorn. The grain is ordinarily moistened with water before being pounded, a practice which appears to have been discovered early in Roman period¹⁾. In order to promote the grains circulation, usually a ring made of rice straw (Usuwa 白輪 in Japanese) was inserted into the mortar¹³⁾.
- 2) **Impact grinding**: If the end of pestle is roundish (**Fig. 2 (b)**), it may penetrate through the bed of grains, and grind the grains to powder at the bottom of the mortar. From the remains of prehistoric period in Europe, many relics of mortar and pestle had been excavated, but thereafter they seem to have been replaced by the quern, used for wheat; though the stamp-mill has survived until the present day in mining. On the other hand, after the introduction of the foot-driven tilt-hammer or water-powered mill, impact grinding was used widely and still survives in Japan.
- 3) **Rubbing**: Rubbing the pestle against the inner side of the mortar causes reduction of the grain to powder effectively. Poppe⁷⁾ attributed the origin of the invention of rotary quern to a revolving pestle in a mortar, and his opinion was quoted by Karl Marx⁸⁾, but we remain unconvinced.

An Egyptian tomb painting of about 1450B.C., in which two persons are pounding together in a mortar, and a Greek vase painting of about 500B.C., in which a man and a woman are pounding together, are well known. Particularly interesting is the fact that the double-bell shaped pestle and tree-trunk mortar similar to these ancient Western paintings had survived in Japan until twenty years ago. Since Japanese farmers did not have the rotary quern until about the eighteenth century, the mortar and pestle were most important grinding implements for general use. The earliest excavated evidence of its use in Japan was known in the



- (a) Stone mortar for water-powered rice polishing mill. (Gifu Pref. and Hyogo Pref. Japan)
- (b) Stone mortar for water-powered stamp-mill used to grind raw materials of porcelain. (Ehime Pref. Japan)
- (c) Korean mortar surviving only in Cheju(濟州島).
- (d) Mortar in the Stone Age.

Fig. 1 Reference examples of mortars with a round mantle made of perishable materials in Japan and Korea.

Yayoi period (400B.C.-400A.D.), when rice cultivation was introduced. It is a matter of debate whether the similarity was based on the fact that a substantially identical problem can lead to very similar solutions in places widely separated in space and time, or on the result of spread in the ancient world.

In Japan, the mortar with decorated waist (Fig. 2(c)), which had ceremonial meaning, and the double-bell shape pestle gradually fell into disuse during the eighteenth century in urbanized regions, and were replaced with hammer pestle and non-decorated drum shape mortar (Fig. 2(a)) which were more efficient. At present they survive only in ceremonial use to make rice cakes.

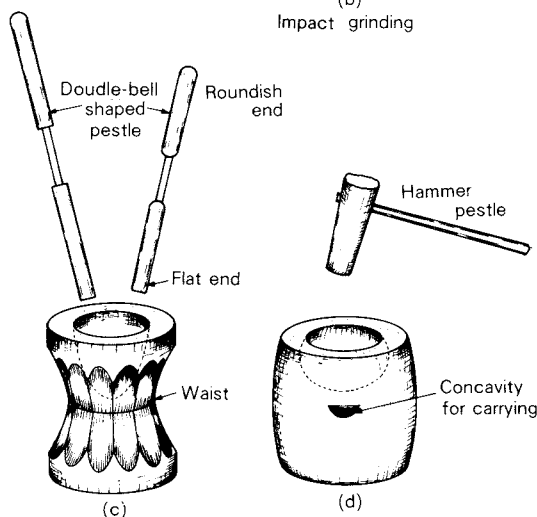
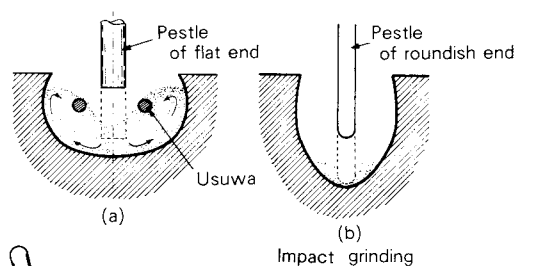
Because flour milling was a matter of primary interest in the Western world, the mortar and pestle was abandoned early, probably late in the prehistorical period. However, in other regions, especially in East Asia, they survived for a long time and developed markedly.

In China, early in the former Han Dynasty (221B.C.-9A.D.), foot-driven and water-powered tilt-hammer pestles (碓 in Chinese, Karausu in Japanese) thrive and seem to have been introduced in Japan in about the eighth century. They were used mainly for hulling and polishing rice and rarely used for making rice cake. They were a familiar sight to the people throughout rural regions and even within the cities to some extent till half-century ago.

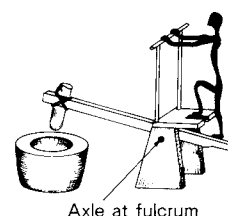
Earthenware mortar (研磨鉢 in Chinese, Suribachi in Japanese) is a type of mortar for domestic use¹³⁾. The transmission from China (Song Dynasty, 960-1279A.D.) to Japan is supposed to have taken place in the thirteenth century, and gradually replaced the stone mortars. The earthenware mortar which has fine grooving on its working surface that cooperates with a wooden pestle to bray the material, and is still widely used for various purposes of household cooking; for example wet grinding or dispersion of "miso" (bean paste), "tofu" (bean curd), yam, and dry grinding of cayenne pepper, sesame seeds and so on.

4. Edge-runner mill

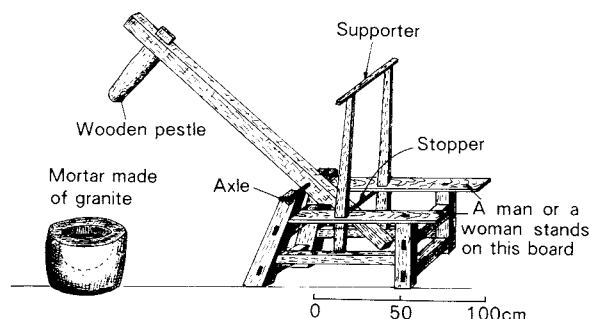
Another notable development of the primitive mortar and pestle for greatest productivity was replacement of a pestle with a roller, which



- (a) Principles of hulling of various cereals.
- (b) Principles of impact grinding with mortar and pestle.
- (c) Double-bell shaped pestle and mortar with traditional decorated waist.
- (d) Hammer pestle and drum shaped mortar.



- (e) Principle of foot-driven tilt-hammer mill.



- (f) An example of foot-driven tilt-hammer used to polish rice and to make rice cake.(Hiroshima Pref.)

Fig. 2 Some examples of mortars and pestles in Japan

might have come from the idea of a wagon wheel being used to thresh wheat or other cereals in the ancient world.

The edge-runner mill, commonly employed by Romans for professional use in olive oil production, was one of the established machines (Fig. 3 (a)). It consisted of one or a pair of broad stone wheels freely mounted on a short horizontal axle which was loosely supported with a vertical shaft. Rotation of the shaft caused the wheels to revolve on a circular stone base crushing the olives laid in their path. The mill was driven by slaves or animals and there is no evidence to suggest the use of water power. Later, in Europe, the mill was developed mainly in mining. Fret-mill, Pan-mill and Chilean-mill are now used in the modern industry.

Another fashion was taking place in China for hulling and grinding of cereals¹⁰⁾. Chinese Nien (碾) was recorded in the second century A.D.¹¹⁾, and later, there were various designs, for instance, the rotary bogie-wheel edge-runner mill with single roller and the rotary double edge-runner mill with two wheels (Shih nien, 石碾) and so on²⁾.

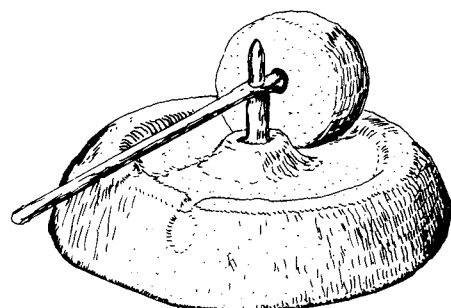
Strangely, there is no evidence of the nien

being introduced into Japan, except small scale edge-runner mills with longitudinal travel (man power) (Yen nien, 研碾 in Chinese, Yagen, 薬研 in Japanese) for herb medicine (Fig. 3 (b)). In medieval times, this implement was also used to prepare gun powder.

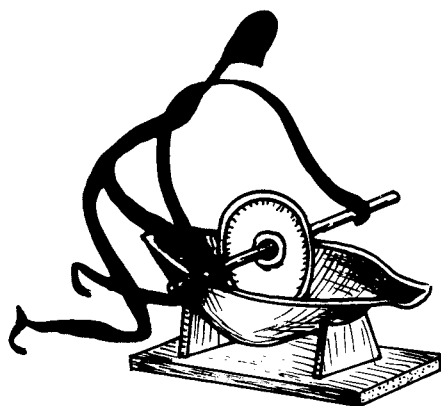
5. Saddle quern

As described before, rubbing the inner surface of the mortar with the roundish end of the pestle could be used for grinding to powder. For such use, a larger rubbing area is a basic requirement. If the size of the upper stone is restricted by the fact that one must be able to lift it with both hands, one possible way for the enlargement of the rubbing area is the use of a flat dish-shaped understone as a grinding slab. The back-and-forth motion of the grinding slab made a shearing action possible under more precise control than the mortar and pestle did. Also it held the possibility of making the grinding process continuous.

In the course of time, probably thousands of years of use, this primitive implement was gradually developed to more favored milling implement — the fully developed Saddle quern, consisting of a concave lower stone, on which a smaller stone was rubbed to grind the ma-

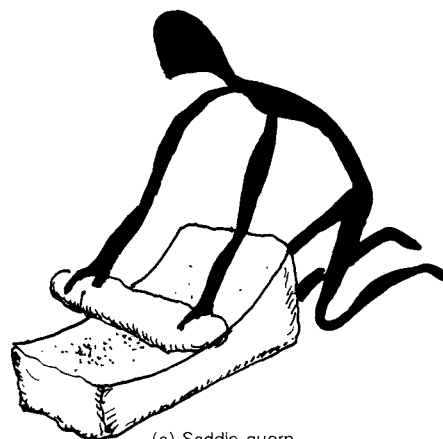


(a) Olive mill in Roman.

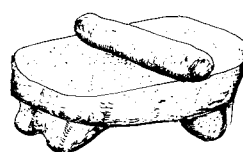


(b) Yagen in Japanese.

Fig. 3 Edge-runner mill



(a) Saddle quern.



(b) Metate used by aborigines in America.



(c) Grinding slab (Jomon period in Japan).

Fig. 4 Saddle quern

terial (Fig. 4 (a)). Numerous statuettes from Egyptian tombs depict women kneeling at the saddle querns, grinding meal to offer the dead in the after-life.

Saddle querns might have been specialized closely related with the processing of wheat and barley, and were discovered in the relics of Neolithic sites in Africa, Western and Northern Asia¹²⁾. A sort of saddle quern "Metate" which consisted of bench- or trough-like bed stone and often made of volcanic rock, was used for grinding maize by the American aborigines (Fig. 4 (b)).

Though in Korea there was some unambiguous proof of the existence of saddle quern, in Japan there is no clear evidence indicating that it was used. Though some dish-shaped relics which resembled saddle quern were excavated from the remains of the Jomon period (before the Yayoi period) in Japan in some rare cases, they are more primitive grinding slabs (Fig. 4 (c)).

6. Rotary quern

The saddle quern was an extremely advanced tool for grinding, their final form was a result of thousands of years of use and evolution. No further advances could be made in its developmental pathway.

The rotary quern, consisting of two circular stone discs was the beginning of a new era in grinding technology. However, to this day no decisive proof is available to tell exactly where and when the quern was invented. It is a matter of debate whether the step wise sequence of

improvement could have led to the rotation of the wheel, or an intellectual leap suddenly occurred.

There are two findings which are estimated to be intermediate forms in the progression from the saddle to the rotary quern. One of them is a semi-rotary quern employing a circular upper stone mounted on a bed stone which has a hollow holding the upper stone, swung to and fro along an arc by hand. Another one is a lever mill surviving in Greece.

Storck³⁾ discussed a remarkable find, an ancient and unique relic, now in the Tiflis Museum²⁾, which was discovered by the Russian archeologist Tseretheli amongst the remains of Urartu, a Kingdom centering on the highland plains around Lake Van before the eighth century B.C. But how widespread in Asia and Europe such a quern existed is still not fully known, and so only future discoveries will confirm or refute the Urartu quern.

Beyond the historical black out for many centuries, many pieces of evidences of various kinds from all over Europe, especially Rome, South-East Asia (Taxila, 600B.C.-500A.D., Parthia, 171B.C.-225A.D.), and China (Ch'in Dynasty, 221-206B.C., Han Dynasty, 206B.C.-220A.D.), show that the refinement of rotary quern was accomplished by that age.

It appears that the pot quern (Fig. 5 (a)), which survived for domestic use in medieval times, was introduced into Britain no earlier than the Roman occupation.

A wonderful technical refinement in China is

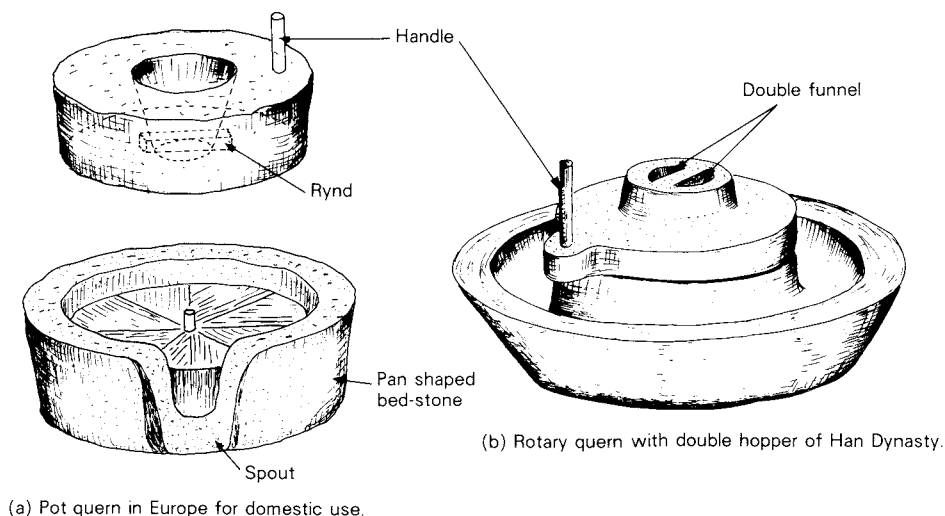


Fig. 5 Rotary quern

particularly interesting. One example is an article buried in a tomb (so-called 明器 in Chinese) (Fig. 5(b)). Also a stone mill, the diameter of which is 850mm, was excavated. Many other sites in China belonging to this period have produced several varieties of rotary querns. The earliest written evidence concerning the existence of the rotary quern and milling wheat is late Former Han Dynasty (53-19B.C.).

7. Relation to Buddhism in Japan

The introduction of the wheat and flour milling into Japan is closely related to Buddhism. In the oldest chronicle of Japan “Nihon-shoki”(日本書記 720A.D.), we find the following description: “In March of the spring of the eighteenth year of the Emperor Suiko (610 A.D.) the King of Korea presented a monk, named Doncho (曇徴), which made a mill (碾磑 Tengai in Japanese), that was really the first mill in our country,” Another piece of written evidence can be found from the word “碾磑” (Tengai) here and there in the oldest Japanese law-book “Ryo-no-gige”(令義解)(718-833A.D.), and in the document of Todai-ji (東大寺, a temple established in 745 A.D.).

On the other hand, the era corresponds to T’ang Dynasty (618-906A.D.) in China when many Buddhist temples set up water-mills in their manors and made large profits on them, the beginning of which occurred during the Pei-wei Dynasty (386-534A.D.)¹⁰⁾. An interesting relic of a large stone mill (Fig. 6) which seems to belong to that period was preserved in a temple – Kanzeon-ji 觀世音寺) in Fukuoka Pref. – which played an important role in the introduction of foreign culture mainly from T’ang. Although such a mill is a familiar one in Europe or China, in Japan the form and the size of the mill are surely strange. Of particular interest is a hemispherical pivot built in the center. Although Storck³⁾ discussed such a pivot in the early Palestinian and Hindu querns, it seems to be very rare.

Because the basic item of staple food in Japan was rice and barley, wheat was, probably, a rare or novel food for the noble personages at that time. Though the mill might have been harnessed for foreign visitors and the upper classes, it does not appear to have been widely accepted.

The introduction of such a large stone mill from Europe for commercial flour milling was curiously about a thousand years later (late the nineteenth century). It appears that the hand-operated rotary quern was introduced into Japan no earlier than the thirteenth century. Japanese Buddhist monks who went abroad to China (Southern Sung Dynasty, 1127-1279A.D.) to study imported some rotary querns, and Chinese and Korean craftsmen introduced the technology. Earliest written evidence is “大宋諸寺図” (pictures of temples in Sung) preserved in Tofuku-ji (東福寺) in Kyoto. Therefore no archaeologically reliable and undisputed fragment of a rotary quern older than that time has ever been found. Even a few centuries after that time, such relics were still rare indeed, and the hand-querns were no larger than about 360mm in diameter. It is an interesting fact that in any ruins of that time, the

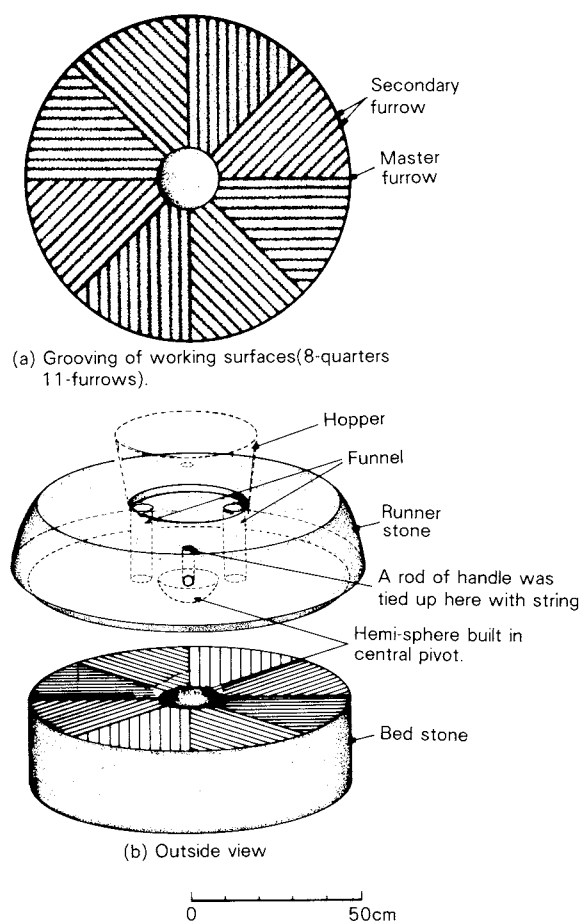


Fig. 6 A relic of the oldest and largest mill-stone in Japan probably imported from China in the seventh century (Now preserved in Kanzeonji (temple), Fukuoka Pref.)

relics of the rotary quern can be found only in the settlements of the upper classes, not in those of the farmers. Since the seventeenth century the hand-rotary quern has come into widespread use very gradually and only in the eighteenth century did Japanese farmers start to use it for general purpose like grinding of various cereals, or for Tofu making.

8. Relation to tea-ceremony

From China (Southern Sung Dynasty), Buddhist monks had introduced another novel rotary quern which was specialized for producing the green tea powder used for tea-ceremony. **Figure 7** shows the hand operated tea-mill (Chausu 茶磨 in Japanese), which was made of a somewhat harder and more beautiful stone (such as diabase or quartzite), than the ordinary querns for cereals. In China, the tradition of tea-ceremony went out of style during the Ming Dynasty (1368-1644A.D.), but in Japan the tradition still survives today. Late the sixteenth century, the tea-ceremony had been all the fashion with the commanders in chief of the Samurai (the warriors of Japan) as a status symbol and sometimes Chausu were heirlooms. The ruins of a castle and the ancient battlefields of that period produce an outstanding profusion of evidence related to the tea-mill. A notable feature of Chausu compared with other querns is an axle which is loosely inserted into the funnel. Thus the upper stone is capable of sliding on the working surface of the bed-stone, and so preliminary crushing of raw materials occurs between the axle and the funnel.

Now the stone mill (the diameter of which is

about 36cm), driven by an electric motor, survives in commercial production of the powdered green tea (particle size finer than about $10\mu\text{m}$) for tea-ceremony.

9. Rice-hulling mill in Japan

There were two words “mo” (磨) and “lung” (礮) in Chinese for the mills. The former means a stone rotary mill, and the latter means a man-operated mill specialized for rice-hulling (decorticating). The lung was made of sun-dried clay – “thu lung” (土礮 in Chinese, Tousu in Japanese), or made of wood “mu lung” (木礮 in Chinese, Kizuriusu in Japanese). These were substitutes for the stone mill because they were easy to make.

Damp kneaded clay with a little common salt was used to fix the teeth of oak or bamboo onto the working surface, so that they could act in the same way as the grooves of the stone quern. The pattern of the teeth (**Fig.8 (a)**) was according to the tradition, the same as that of the stone rotary quern, and was counterclockwise revolving, eight-quarter grooving to be described later. Rice hulling with such a mill required a cooperative and laborious effort by two or three men as shown in **Fig.9 (b)**.

The lung was introduced into Japan in the seventeenth century and has been widely accepted as an important implement of farmers for domestic use until recently (**Fig.8 (b)**).

In Japan there was another form of wooden mill which had radial grooving and was operated, not with continuous revolutions, but by swinging to and fro along an arc of a circle by pulling two strings using both hands of two men or women who sat facing each other on

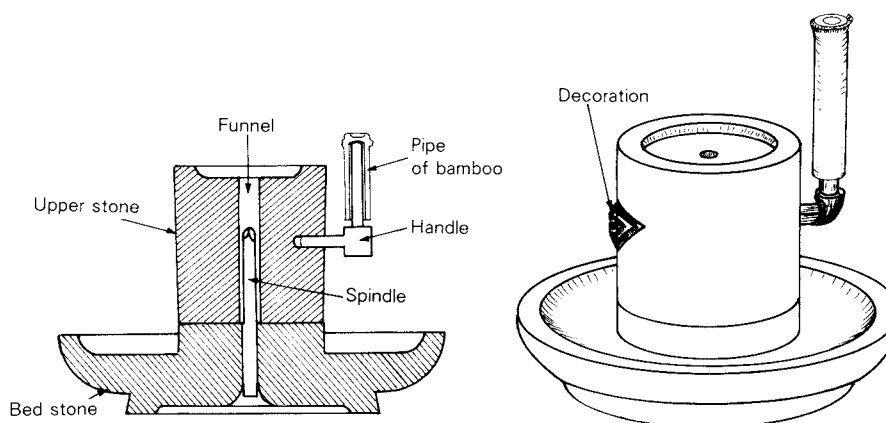
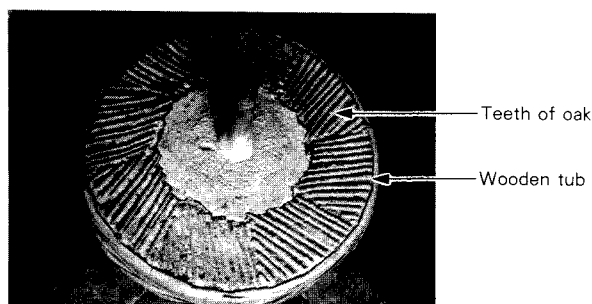


Fig. 7 Japanese Chausu



(a) Working surface was similar as the stone quern (8-quarters 13 furrows). Clay was held in the wooden tub.

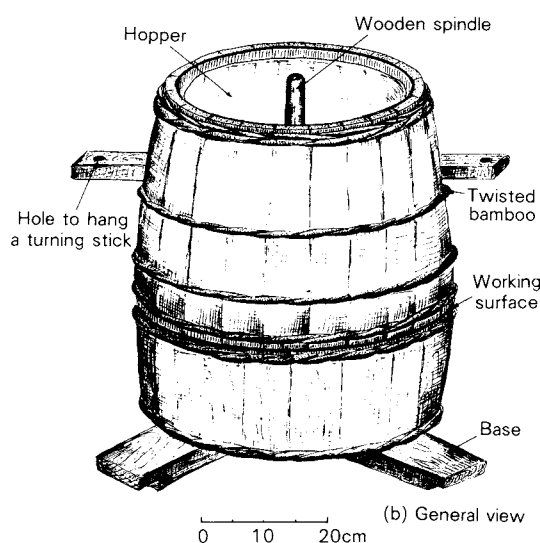


Fig. 8 An example of rice-hulling mill of Japan (Yamagata Pref.)

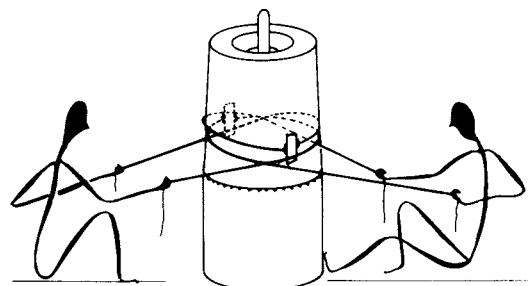
opposite sides of the mill (Fig. 9 (a)). Such an implement also has survived until recently in a mountainous district for domestic use only.

10. Principles of the rotary quern

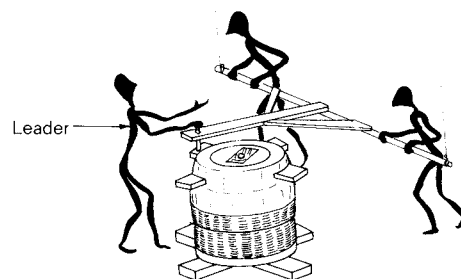
Basic principles of the rotary quern are nearly the same throughout the world, but there are subtle differences from region to region which seem to be important in considering the history of the quern, since they have survived for nearly two thousand years.

1) Bosom

The working surface of the lower stone, in principle, was perfectly flat, but that of the upper stone was slightly concave, especially near the centre to admit a little continuous flow of grains. Such an open annular space between two stones was known as a bosom ("Fukumi" in Japanese). Thus, the grains received in this bosom are gradually drawn



(a) Made of wood operated with swing to and flo.



(b) Made of clay encircled with wooden tub or twisted bamboo.

Fig. 9 Principles of operation of a rice-hulling mill

towards the circumference by the revolution of the upper stone, first being crushed by degrees, and then ground and ejected from the mill. Therefore, the upper and lower stones contact each other only at their circumference, so that when mounted they would grind the grains only near the edges.

Superficial thinking would result in the idea that the ground flour must fall down off of the stones by downward force of gravity. Hence, sometimes the lower stone was slightly conical in shape. As the true principles of the working of the appliance became recognized, however, the bed-stone seems to have been gradually flattened.

2) Grooving

An early and notable improvement was the grooving of the working surfaces. The grooves or furrows had a typical, traditional pattern which consisted of eight radial master furrows and several secondary furrows parallel to each master furrow (Fig. 10 (b)). Thus the working surface was divided into eight equal segments or harps which were called quarters. "Quarter" was a unique terminology of the millwrights in Europe, since "the quarter is not a quarter"⁹⁾. It is not certain where and when such fully a

developed and methodical system of furrowing was first evolved. There is a noteworthy fact that the pattern—counterclockwise revolving, eight-quarter grooving—seems to be widespread and common throughout Europe and Asia. For instance, the pattern of the British-Roman quern⁵⁾ (first century A.D.) is the same as the one surviving in China and Japan.

Besides the eight-quarter pattern, there was a six-quarter pattern in China and Japan. Especially in Japan, a distinct regional distribution was found in the eight—and six-quarter¹³⁾ patterns, but as yet we do not know why this distribution occurs or what it might represent¹²⁾.

3) Pivoting

A hole was drilled through the top of the upper stone, forming a kind of funnel which acted as a hopper. As the upper stone revolving, the grains fell down into the bosom.

As shown in Figs. 5 and 10, the shape and position of the funnel were different in Europe and in Asia. Consequently, the construction of the pivoting upper stone upon the lower one was different. The existence of a “rynd” (Fig. 10(a)) seems to be a prominent feature of the European quern. A pin of wood or iron stood in a hole in the centre of the lower stone, and the top of the pin fit into the rynd. A rynd was a block of wood or iron bridging across underneath the funnel, leaving a little space

on both sides of it for the grain to percolate through. The gap between the two stones is maintained uniformly. Though primitive adjusting of the fineness was done using a small piece of leather or wood of any desired thickness fixed in the socket of the rynd, a fairly efficient method of regulation was by adjustment of the pivot height. Another exception to the existence of the rynd in Japan is seen in the stone quern of the medieval gold and silver mines, the technology of which was introduced from Europe¹⁴⁾

On the other hand, Chinese and Japanese querns had the funnel at an eccentric position, and so there was a pivoting hole in the center of the upper stone. Although the querns of the rynd system were used in some rare cases, especially for “Tofu” making, they seem to have introduced the European style, since they were no more than one hundred years old.

11. Conclusion

In this paper the varieties of grinding implements for domestic use in Japan have been traced, principally excluding the ones used in professional activity, because we can see that almost all of the ancient implements survived for a long time in domestic use. In parallel with the professional activity of flour milling, domestic milling continued to be practiced. The reason for its survival was, needless to say, necessity or economy. However another point

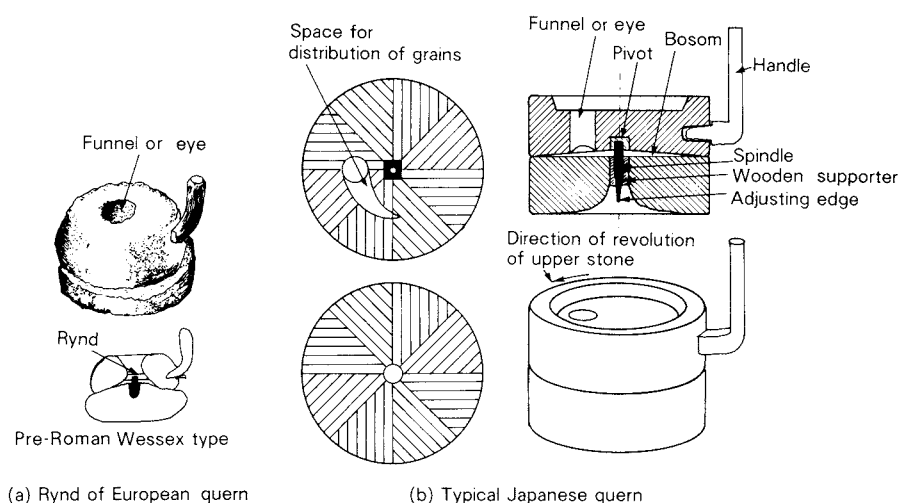


Fig. 10 Principles of rotary quern

to be remembered is that various home-made foods made from small quantities of superior materials prepared skillfully using domestic implements were undoubtedly preferred in many households which could obtain the ready-made products from a shop. Particularly in Japan many ancient implements have survived, because throughout the roughly two thousand years since agriculture was introduced into Japan in the Yayoi period, nothing has arisen to replace the old ways of raising crops, at least as far as the wet-field system of rice cultivation is concerned. And so the life-style of rural villages has been preserved while the cities have evolved a new culture. For instance, Japanese "Chausu", which was introduced from China many centuries ago, is refined in Japan, and survives today. It is indeed a beautifully made object, artistic instead of technological.

The age in which we live is one of constant change, especially in the last three decades. Everything becomes obsolete almost as soon as it is completed; modern man is prepared to accept it, and tends even to welcome this state of affairs as inevitable. However, some humanity has occasionally been lost, the humanity included in the everyday things in which the human history is condensed. The study of various grinding implements may lead to the study of "what is a preferable civilization."

References

- 1) Bennett, R., and Elton, J.: *History of Corn Milling*. Vol.1 Burt Franklin, N.Y. (1898).
- 2) Needham, J.: *Science and Civilization in China*. Cambridge at the Univ. Press (1965).
- 3) Storck, J., and Teague, W.D.: *A History of Milling – Flour for Man's Bread*. Mineapolis Minnesota Univ. Press (1952).
- 4) Maurizio, A.: *Histoire de L'Alimentation Vegetale*. Payot, Paris (1932).
- 5) Reynolds, J.: *Windmills & Watermills*. Hugh Evelyn Lond, (1970).
- 6) Freese, S.: *Windmills and Millwrighting*. David & Charles Newton Abbot, England (1957).
- 7) Poppe, J.H.M.: *Geschichte der Künste und Wissenschaften*. (1807).
- 8) «К.Маркс,Ф.Энгельс Союзненця» Том. 47 (ЛолцтиЗдат,Москва) (1973).
- 9) Speight, J.: *Milling*, 147, [18] 374-375 (1966).
- 10) Hommel, R.P.: *China at Work*. (The M.I.T. Press, 1937).
- 11) Amano, A.: *History of Chinese Agriculture*. Ochanomizu-Shobo (1962).
- 12) Fujimoto, T.: *Trans. of Archaeological Institute*, No.2, 40-75 (1983).
- 13) Miwa, S.: *Cultural History of man and materials – Mortar*. Hosei Univ. Press (1978).
- 14) Nozaki, J.: *Trans. of Tohoku Cultural Institute, Tohoku Gakuin Univ.*, No.11, 71-87 (1980).

(English proof reader: S.E. Dodick)

The Role of Adsorbed Water on Adhesion Force of Powder Particles

Masatoshi Chikazawa*, Takafumi Kanazawa*
and Toshihide Yamaguchi*

Department of Industrial Chemistry
Tokyo Metropolitan University

Abstract

Adhesion forces generated at a contact point between spherical and plate specimens of potassium halides, commercial soda-lime glass and Pyrex glass were estimated by using an electrobalance, and adsorption isotherms of water vapor and methyl alcohol on these samples were also measured. The thickness of a liquid bridge and the pressure at which a capillary condensation occurs for the first time have been investigated using porous glasses each of which has a monodispersed pore radius. The following conclusions have been deduced from the comprehensive comparison of the obtained results. The adhesion forces under low and high water vapor pressures are suggested to be ascribed to hydrogen bond and liquid bridge, respectively. A marked increase of adhesion force observed in the pressure range $0.6 < P/P_0 < 0.85$ is due to a transformation from hydrogen bond to liquid bridge and due to a change in the physical property of condensed liquid. The thickness of the liquid bridge at $P/P_0 = 0.6$ is presumed to be $29\text{-}37\text{\AA}$

1. Introduction

The powder characteristics, i.e. angle of repose, properties of packing and friction, and fluidity, are largely influenced by adhesion forces generated among powder particles. Therefore, during storage, flow and handling of powders, the adhesion forces very often cause severe problems. As a rule, these adhesion forces are classified into five major groups such as solid bridges, adhesion and cohesion forces in not freely movable binders, interfacial forces and capillary pressure at freely movable liquid surfaces, attraction forces between solid particles, and interlocking bonds¹⁾. In cases of hydrophilic powders the adhesion force due to water vapor adsorption is generally regarded to be larger than the van der Waals force, and becomes an origine of troublesome matters in handling powders under atmosphere. The force produced by water adsorption also closely relates to the

physical property of water layer, and its property varies with the thickness of water layer formed on a solid surface. However, the informations concerning the following three points, 1) the relationship between the thickness of water film formed on a solid surface and humidity of atmosphere around the sample, 2) the changes in physical properties of the water film with its thickness, 3) the thickness of a liquid bridge formed at the neighborhood of a contact point between two sample particles, are scarcely obtained. The purpose of the present study is to clarify the generation mechanism of the adhesion force due to water vapor adsorption, by discussing the above obscure points.

2. Experimental

2.1 Materials

The samples used were alkali halides (i.e. KCl and KBr), commercial soda-lime glass beads (7-20 mesh), Pyrex glass and porous glass. Alkali halides were purified by two times recrystallization in their aqueous solutions.

* Fukasawa, Setagaya-ku, Tokyo, 158
TEL. 03 (717) 0111

Received June 26, 1984

The samples for adhesion force measurement

A spherical sample of the alkali halide was prepared by covering a glass bead with the alkali halide itself as follows. A glass bead with 2-3 mm in diameter was dipped for a moment in a melted alkali halide under an atmosphere of nitrogen. In case of Pyrex glass, a spherical sample was obtained by fusing an end of its fibriform glass using a gas burner. The commercial soda-lime glass bead was used without any treatment. On the other hand, a sheet specimen of an alkali halide was made by pressing the powder sample. In case of Pyrex glass, a commercially available glass sheet was used. The commercial soda-lime glass was melted and made in a sheet-form.

The samples for adsorption measurement

A solution, 100 ml 20-30 wt%, of a purified alkali halide sample was poured in five-fold volume of ethyl alcohol cooled to $-80 \sim -90^\circ\text{C}$ with stirring. A precipitate obtained was filtered, washed four times with absolute ethyl alcohol, and then evacuated under a reduced pressure of 10^{-6} mmHg. The specific surface areas of KCl and KBr samples were found to be 1.04 and 0.71 m^2/g , respectively. For Pyrex glass, the powder samples which had large surface areas (0.2-0.4 m^2/g) were prepared by grinding hollow Pyrex capillaries and slender Pyrex rods. The porous glass sample (Thirsty Glass Corning Code 7930, 200 m^2/g) having a monodispersed pore radius of 20 Å was treated with 0.1% HF aqueous solution for a proper duration to widen the pore radius. The resulted pore radii were calculated to be 27, 30 and 33 Å from nitrogen adsorption measurements.

2. 2 Adhesion force measurement

Adhesion forces generated at a contact point between spherical and sheet specimens made of the same material were measured by using an electrobalance under various water vapor pressures. In cases of alkali halides, a caking due to water vapor adsorption occurred at high water vapor pressure, and the adhesion force suddenly increased with the strength of the caking. However, the effect of the caking on the adhesion force was unrecognized within 20 minutes since the two specimens were in contact

with each other. Therefore, the adhesion force was measured after the lapse of 5-15 minutes and 5-10 times measurements were carried out for accuracy.

2. 3 Adsorption isotherms

The adsorption isotherms of nitrogen, water and methyl alcohol vapor on the samples were determined volumetrically by using an adsorption apparatus. When the vapor pressure of an adsorbate unchanged for 15 minutes, adsorption equilibrium was regarded to be established. The equilibrium pressures of water and methyl alcohol were measured using a mercury manometer and a reading magnifier having a resolution of 10^{-2} mmHg. The effects of a tube radius of the manometer and a shape of its meniscus on the measured pressure were considered and the equilibrium pressures were corrected.

3. Results and discussion

3. 1 Adhesion force

Generally, in cases of the powder particles whose surfaces have a hydrophilic property, it is known that the adhesion force due to water vapor adsorption increases abruptly above the pressure of about 60%rH and has a maximum value in a high pressure region of 70-90%rH²⁾. However, no detailed informations concerning

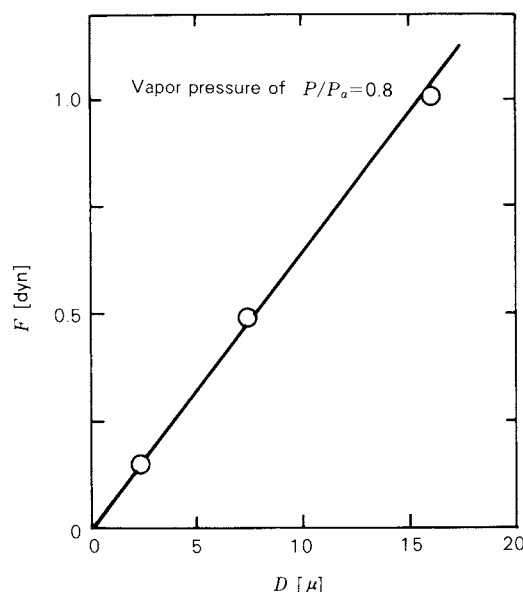


Fig. 1 Relationship between adhesion force and particle size at water vapor pressure of $P/P_0 = 0.8$

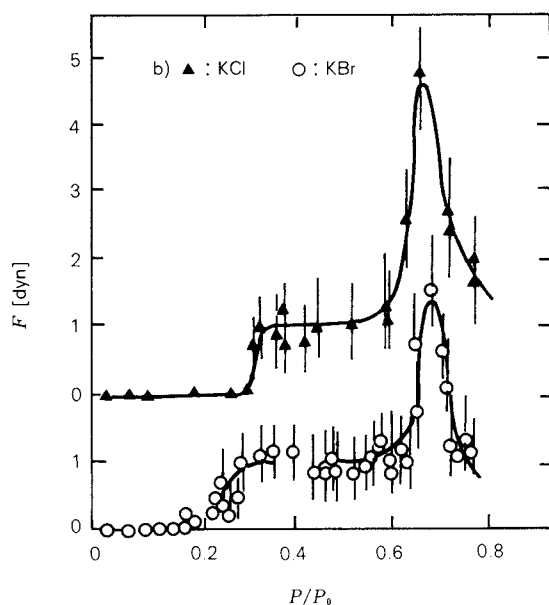
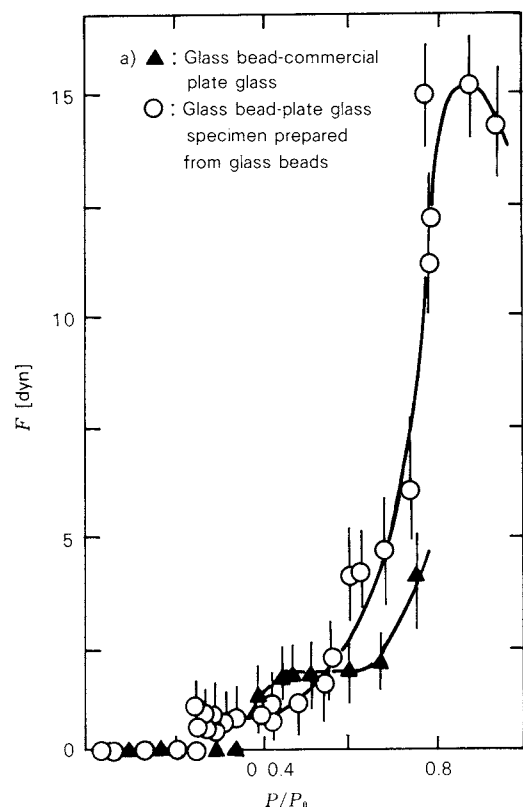


Fig. 2 Changes in adhesion forces of potassium halides at a contact point with water vapor pressure

the mechanism of such adhesion force change are obtained. According to theoretical calculations, the adhesion force generated by a liquid bridge which is formed in a gap of the separated two spherical particles³⁾ or made at a contact point between a projection of conical

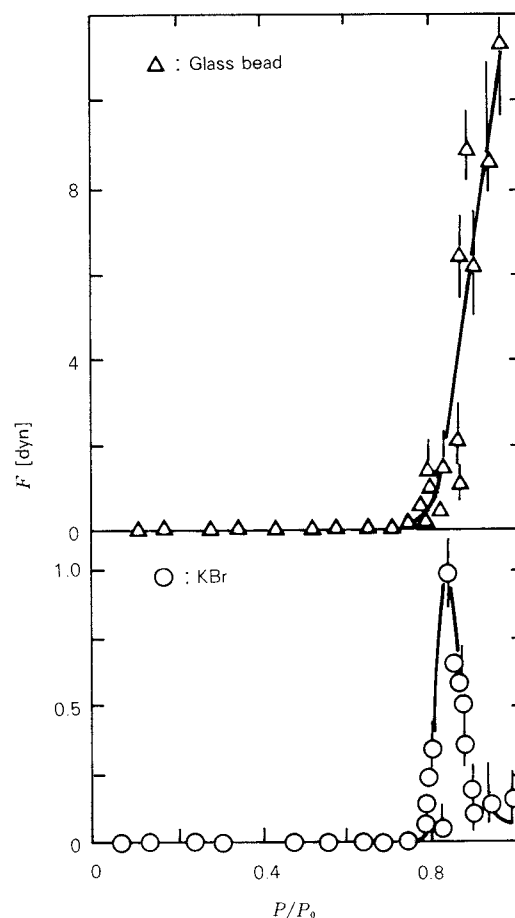


Fig. 3 Changes in adhesion forces of glass bead, and KBr with methyl alcohol vapor pressure

shape and a sheet or spherical specimen⁴⁾, increases with the amount of absorbed water. As for the former mechanism, a maximum value of the adhesion force arises in further adsorption, but in the latter case it is not observed. The effect of particle size on the adhesion force is shown in Fig. 1⁵⁾. The adhesion force increased linearly with the radius of a spherical particle. Hereafter, a spherical sample with a proper size was used. In Fig. 2 changes in the adhesion force with increase of water vapor pressure are given⁶⁾. For KBr sample, the adhesion force was detected above the pressure of $P/P_0 = 0.20$, and was roughly constant in the range of $0.2 < P/P_0 < 0.55$. At the pressure larger than $P/P_0 = 0.6$ the force increased suddenly, and then decreased markedly with increase of the pressure in the range above $P/P_0 = 0.66$. As for KCl sample, a similar phenomenon was observed. The water vapor pressure at which the adhesion force began to appear was

slightly higher than that of KBr. In cases of the glass beads, the same type of adhesion force curves were observed. From these results, the effect of varying the samples on the characteristics of the adhesion curve seems to be small.

In Fig. 3 changes in adhesion force with increase of methyl alcohol vapor pressure are shown⁷⁾. The force was recognized only above the pressure of $P/P_0 = 0.8$ and it disappeared in the lower pressure region. On the other hand, in case of water adsorption the adhesion force appeared even in the low pressure region. Such discrepancy in shape of the adhesion force curve is explained in terms of the adhesion force generated by hydrogen bond. In case of water adsorption, three dimensional hydrogen bond formation will be possible, whereas it will be difficult in case of methyl alcohol adsorption on account of the difference of molecular structure between the two molecules. A detailed discussion concerning the hydrogen bond formation will be made in the following section.

3. 2 Adsorption isotherms

Adsorption isotherms of water vapor and methyl alcohol on various samples are shown in Fig. 4⁸⁾. In the vicinity of $P/P_0 = 0.2$ at which the adhesion force was measured for the first time, the coverage $\theta = S_{H_2O}/S_{N_2}$ of KBr surface with water molecules was found to be 0.58, assuming the cross-sectional area of 10.5 \AA^2 for a water molecule, where S_{H_2O} and S_{N_2} are surface areas determined from water vapor and nitrogen adsorptions, respectively. For KCl sample, the coverage $\theta = 0.50$ estimated at the appearance of the force was slightly smaller than that of KBr. On the other hand, regarding the glass samples the coverages necessary for generating the force were obtained to be $\theta < 1.5$. In these cases the accurate coverages were not obtained on account of the presence of micropores or migration of water molecules into the glass samples. As for the alkali halides, the adhesion force was generated in spite of the small amount of adsorbed water. Moreover, the capillary condensation is considered to be difficult at a contact point since about 40-50% of the alkali halides surfaces are bare. Therefore, the formation of a liquid bridge is concluded to be impossible. From these results the other generation mechanism of adhesion force such

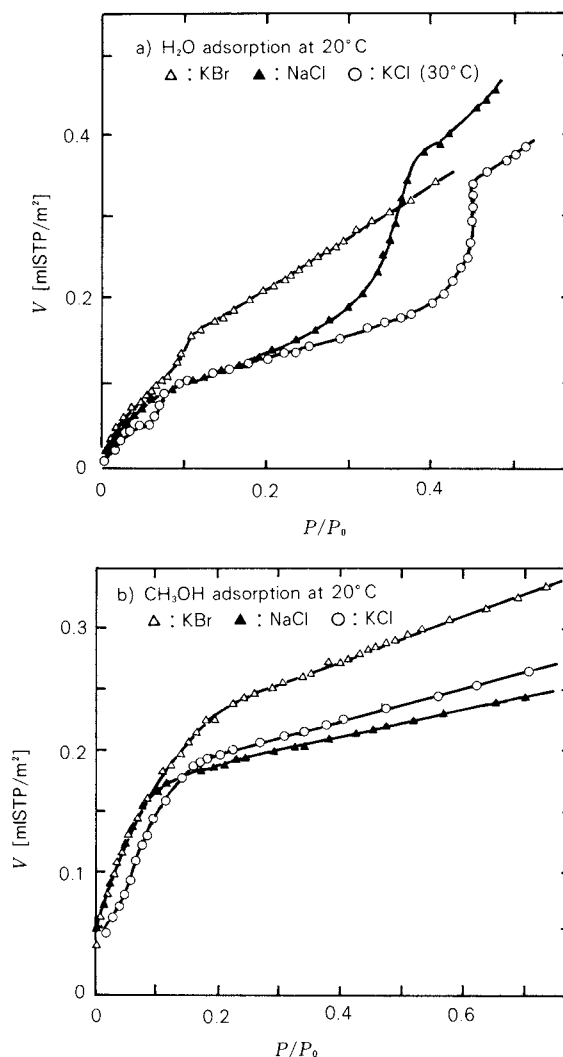


Fig. 4 Adsorption isotherms of H_2O and CH_3OH on alkali halides

as hydrogen bond must be proposed. For KCl sample, changes in adhesion force with the amounts of water and methyl alcohol are given in Fig. 5⁷⁾. In case of the water adsorption the force was detected at low coverages $0.5 < \theta < 1.5$, while the force was undetected at the same coverages in methyl alcohol adsorption. Considering these results, the difficulty of the three dimensional hydrogen bond formation will be reasonable in methyl alcohol adsorption.

The isosteric heats of methyl alcohol adsorption on KCl, NaCl and KBr are given in Fig. 6⁸⁾. In cases of KCl and NaCl samples, clear autophobic adsorptions were inferred since the isosteric heats of adsorption decreased markedly after the completions of their monolayer adsorptions. The similar phenomena are ob-

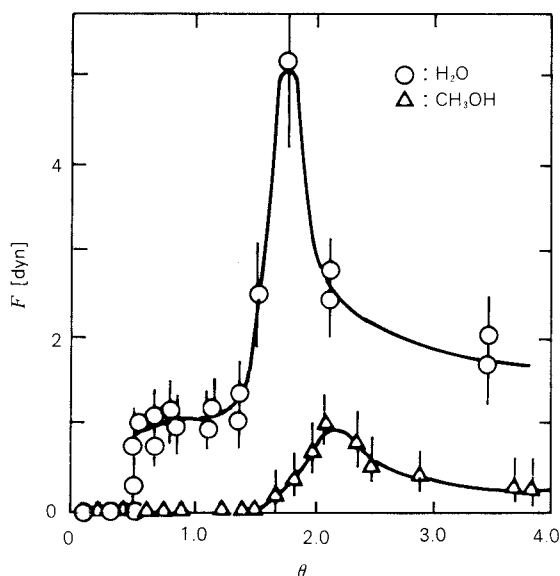


Fig. 5 Changes in adhesion forces of KCl with adsorbed amounts of water and methyl alcohol

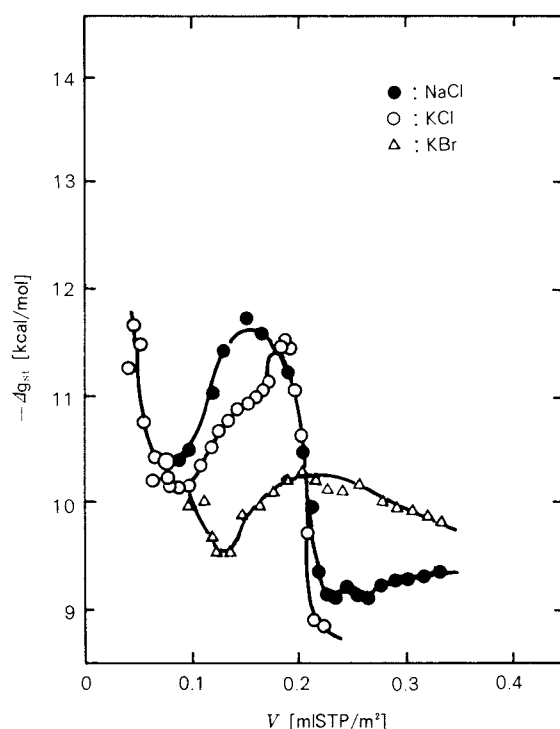


Fig. 6 Isosteric heats of adsorption of methyl alcohol on alkali halides

served for the other adsorbates⁹⁾. These facts imply that a polar group in a methyl alcohol molecule is located under its methyl group, and an interaction between a methyl alcohol molecule and the polar groups in formerly adsorbed molecules is difficult.

3. 3 Thickness of a liquid bridge

Detailed informations about the following two points, 1) the water vapor pressure at which a capillary condensation can occur and form a liquid bridge at a contact point for the first time and 2) the thickness of the liquid bridge, are not obtained yet. The adsorption isotherms of water vapor on Pyrex glass particles prepared by grinding hollow Pyrex capillaries and slender Pyrex rods are given in Fig. 7⁵⁾. The former sample is supposed to contain a great number of micropores having various pore radii. The adsorptive properties of these two samples are necessarily equal each other as the samples consist of the same components. Therefore, if the adsorbed amounts of water vapor per unit surface area estimated from nitrogen adsorption are plotted against the pressure, the two adsorption isotherms will coincide. In a pressure range $0 < P/P_0 < 0.6$, the expected coincidence was recognized. However, a discrepancy between the two isotherms were observed above the pressure of $P/P_0 = 0.6$. As the adsorbed amounts of water vapor for the sample prepared by grinding hollow Pyrex capillaries are greater than those for the another sample, a capillary condensation is considered to occur at the pressure of $P/P_0 = 0.6$ for the first time in some scale. Hence, a liquid bridge which generates the adhesion force is supposed to be formed by capillary condensation at the pressure above $P/P_0 = 0.6$. Using the Kelvin equation (1) and assuming the cylindrical pore shape, the pore radius (r_p) of the capillary is calculated to be 37\AA . This value is obtained by adding a value of multilayer thickness (t) to the Kelvin radius (r_k).

$$r_k = - \frac{2V\gamma \cos\alpha}{RT \ln P/P_0} \quad (1)$$

$$r_p = t + r_k \quad (2)$$

Where P and P_0 values are vapor pressures of adsorption equilibrium and bulk liquid at measurement temperature, respectively, and α represents a contact angle of liquid film. The values V and γ are molar volume and surface tension of the liquid condensed in a micropore. The shape of a liquid bridge formed at a contact point between the two samples is regarded approximately as a thin disk. From these results, the thickness of the liquid bridge is con-

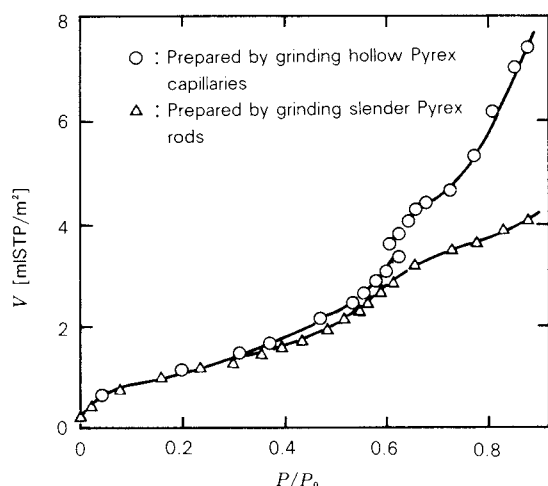


Fig. 7 Adsorption isotherms of water vapor on Pyrex glass particles at 20°C

cluded to be 37Å.

In order to obtain some further informations about the thickness of a liquid bridge, the porous glass with a monodispersed pore radius distribution (20Å) was used and the capillary condensation phenomenon was studied varying its pore radius distribution. The adsorption and desorption isotherms of nitrogen, water vapor and methyl alcohol on porous glass sample (20Å) are shown in Fig. 8⁵⁾. The pore radius distributions estimated from these desorption

isotherms are also illustrated in Fig. 8⁵⁾. A monodispersed distribution was obtained for each adsorbate. However, the discrepancy in the peak value of the distribution was recognized in spite of using the same sample. As the thickness (t) of multilayer is evaluated accurately from an adsorption isotherm, such discrepancy will be ascribed to the Kelvin radius (r_k). The r_k value is calculated based on the following three assumptions, 1) the contact angle (α) of the liquid film formed on a solid surface is zero, 2) the molar volume (V) of condensed liquid in a micropore is equal to that of bulk liquid, and 3) the surface tension (γ) of the liquid film is the same as that of bulk liquid. In a desorption process, the actual contact angle of the liquid film is considered to be zero since the angle is regarded as a receding contact angle. Moreover the molar volume of condensed liquid in a micropore is presumed to be approximately equal to that of bulk liquid¹⁰⁾. From these results, the discrepancy in the pore radius estimation will be mainly due to the change in the surface tension of the liquid condensed in a micropore. The surface tension of the condensed liquid can be determined so as to obtain the correct pore radius distribution calculated from nitrogen desorption. The influence of the pore radius on the

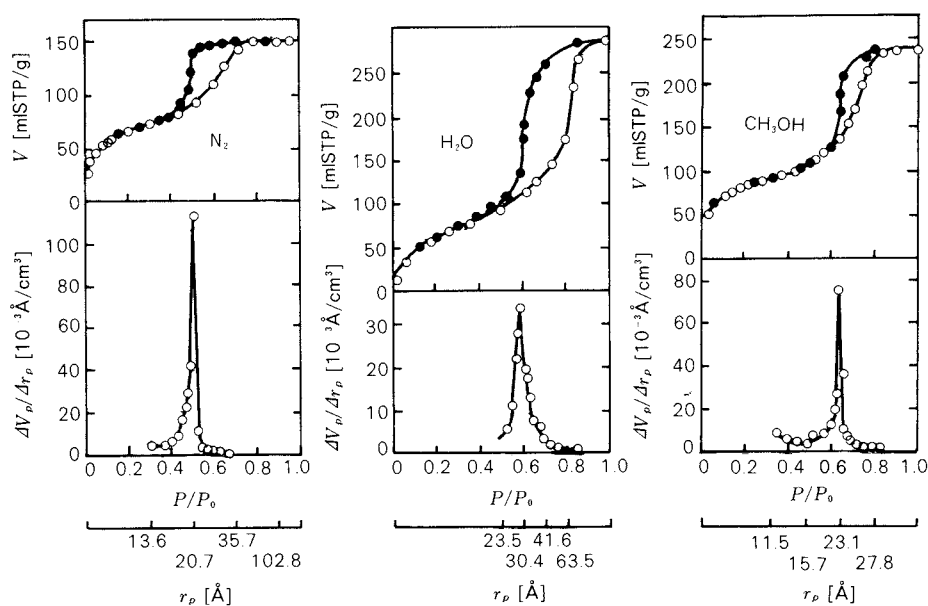


Fig. 8 Adsorption and desorption isotherms of N₂, H₂O and CH₃OH on porous glass, and pore size distributions calculated from their desorption isotherms

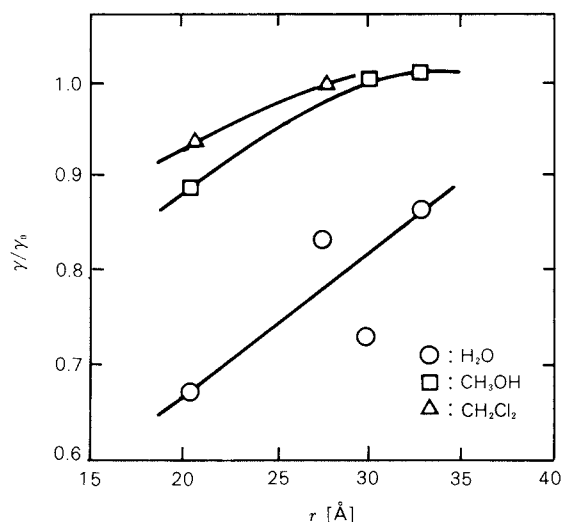


Fig. 9 Effect of solid surface on surface tension of condensed liquid

surface tension of the condensed liquid are shown in Fig. 9⁷⁾. The surface tension became large with increase of the pore radius and then equalled that of bulk liquid. The greatest change in the surface tension was observed in water vapor adsorption. This phenomenon is explained that the influence of a solid surface on the liquid structure of water layer extends to further distance comparing the other adsorbates on account of the ability of three dimensional hydrogen bond formation. As for water molecules, such affected region is presumed to be about 40 Å. Considering the change in surface tension of the condensed liquid, the thickness of a liquid bridge is revaluated to be about 29 Å at $P/P_0 = 0.6$. Hence, the thickness of a liquid bridge is concluded to be in the range from 29 Å to 37 Å at the pressure of $P/P_0 = 0.6$.

3. 4 Phase transition temperature

It is shown in the above section that the physical properties of the liquid condensed in a micropore are different from those of bulk liquid. In this section, these physical property changes are discussed again from a different angle such as variation of phase transition temperature. The relationship between measurement temperatures and water vapor pressures in adsorption equilibrium, i.e. the Clausius-Clapeyron plot, is given in Fig. 10. An intersection of two linear lines was observed. The isosteric heat of water vapor adsorption can be

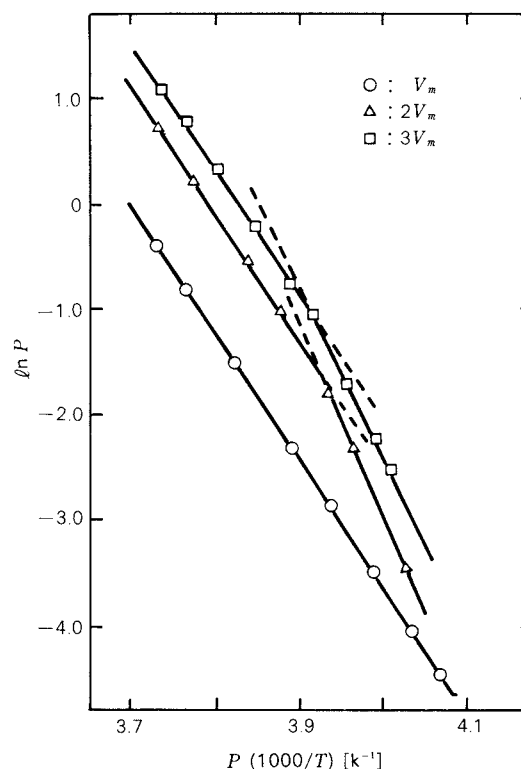


Fig. 10 Clausius-Clapeyron plots of water vapor adsorption on porous glass

estimated from an incline of the linear line. The value determined from the linear part of the high temperature region equalled approximately the liquefaction heat of water vapor. On the other hand, the heat evaluated from the low temperature region corresponded to the sublimation heat of bulk ice. Therefore, the temperature at the intersection is considered to represent a phase transition temperature of the adsorbed water layer. The obtained temperature is lower than the melting point of bulk ice since the liquid structure of the water layer is different from that of bulk water. The changes in the transition temperature with the adsorbed amount of water are given in Fig. 11⁷⁾. The temperature variation tendency with the adsorbed amount was slightly different each other. However, the abrupt increase of the transition temperature was recognized in the adsorbed range about $2 < V/V_m < 3$, where V_m represents a monolayer capacity and V is the adsorbed amount. This experimental result shows that the liquid structure of the water layer changes markedly in the same range. On the other hand, a completion of $2-3V_m$ adsorption was observed at the pressure of $0.6 <$

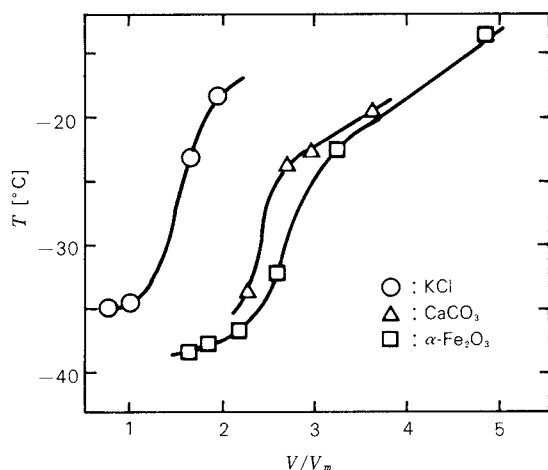


Fig. 11 Phase transition temperature of water layer formed on solid surfaces

$P/P_0 < 0.8$. In the same pressure range, the capillary condensation occurred in a micro space and the adhesion force due to the formation of a liquid bridge arose. From these results it is concluded that the abrupt increase of the adhesion force is due to the change in the generation mechanism of the force, such as from hydrogen bond to liquid bridge, and due to the variation of the surface tension of a liquid bridge.

For KCl sample no phase transition was observed at adsorbed amount below $0.18 \text{ m}\ell \text{ STP/m}^2$ corresponding to the coverage of 0.54. The obtained result indicates that water molecules are adsorbed in a dispersed state and do not form a cluster which causes a phase transition. However, the adhesion force was detected in such a condition. Therefore, the force generated in low pressure region is considered to be ascribed to the formation of hydrogen bond. This conclusion is in accord with the description in the foregoing section.

4. Conclusion

Adhesion forces generated at a contact point between spherical and plate specimens of various samples were measured by using an electrobalance, and adsorption isotherms of water vapor and methyl alcohol for those samples were also determined. Moreover, capillary condensation phenomena have been investigated in order to clarify the physical property changes

of the water layer formed on a solid surface. The following results have been obtained.

- 1) The adhesion force generated at water vapor pressure below $P/P_0 = 0.6$ is presumed to be ascribed to the formation of hydrogen bonds. As the physical properties of water layer are different from those of bulk water, a capillary condensation which forms a liquid bridge is difficult.
- 2) A marked increase of adhesion force in high pressure region $0.6 < P/P_0 < 0.8-0.9$ is explained in terms of the change in adhesion mechanism from hydrogen bond to liquid bridge, and in the same range the physical properties, i.e. surface tension and phase transition temperature, of condensed liquid vary with the thickness of water layer.
- 3) The surface tension of the water condensed in a micropore (pore radius 20\AA) at the pressure of $P/P_0 = 0.6$ was estimated to be about 68% of bulk water.
- 4) A capillary condensation occurs only above the pressure of $P/P_0 = 0.6$ and the thickness of the liquid bridge at $P/P_0 = 0.6$ is considered to be $29-37\text{\AA}$.

References

- 1) Pietsh W.B.: *Trans. ASME*, **B81**, 435 (1969).
- 2) Asakawa S. and G. Jimbo: *J. Soc. Materials Sci., Japan*, **16**, 358 (1967).
- 3) Pietsch H. and H. Rumpf: *Chem. Ing. Tech.*, **39**, 885 (1967).
- 4) K. Inoya and H. Muramoto: *J. Soc. Materials Sci., Japan*, **16**, 352 (1967).
- 5) Yamaguchi T., M. Tomita, M. Chikazawa and T. Kanazawa: *J. Soc. Powder Technol., Japan*, **16**, 514 (1979).
- 6) Chikazawa M., W. Nakajima and T. Kanazawa: *J. Soc. Powder Technol., Japan*, **14**, 18 (1977).
- 7) Chikazawa M., T. Yamaguchi and T. Kanazawa: "Proceeding of International Symposium on Powder Technology" p.202, (1982) The Soc. Powder Technology.
- 8) Chikazawa M. and T. Kanazawa: *Bull. Chem. Soc. Japan*, **50**, 2837 (1977).
- 9) Barto J., J.L. Durham, V.F. Baston and W.H. Wade: *J. Colloid Interface Sci.*, **22**, 491 (1966).
- 10) H.L. McDermot and W.G.M. Tuck: *Can. J. Res.*, **28B**, 292 (1950).

Measurement of Pore Distribution by Utilizing Equilibrium Moisture Content Curve

Chikao Arai* and Yoshiki Sano*

*Department of Textile Chemical Engineering
Shinshu University*

Tadami Hanakawa**

Hosokawa Micron Corporation

Abstract

As one of the methods of measuring the pore distributions, the equilibrium moisture content curve of porous powder was investigated owing to the facility in the measurement.

*A simple and reasonable method was developed for calculating the distribution from an adsorption isotherm. It was shown that the distribution could be evaluated by an equation which contained two coefficients. The coefficients depend only on the characteristics of adsorbate, and these values can be calculated from a *t*-curve.*

*Since it seemed impossible to measure *t*-curve on the equilibrium moisture content, the *t*-curve on water vapor adsorption was determined instead of that on moisture content. It was then shown feasible to apply the curve for pore distribution analysis by the equilibrium moisture content curve.*

1. Introduction

In the measurements of pore distributions by the adsorption method, the nitrogen isotherm at its own boiling point has been generally used, and the isotherm of water vapor adsorption is also useful in certain cases. The water vapor adsorption isotherm can be usually measured by a spring balance, and this measurement method has some advantages, for example, unnecessary of the special refrigerant such as liquid nitrogen. But the method by water vapor adsorption needs a long time to measure the isotherm because of the reasons that the adsorption rate is slow at room temperature, and that the adsorbed weight is measured stepwise by increasing the relative pressure.

In the measurements of equilibrium moisture contents by a so-called desiccator method,

not only moisture contents of various materials can be determined in a run, but it is also possible to measure the moisture contents for different humidities at the same time. Furthermore, neither complex equipment nor tedious experimental operations for completing the adsorption isotherm are required. In spite of these simplicities, only a few studies have been reported on the calculations of pore distributions from moisture content curves, moreover the estimated values on the pore radii have been known to be too small on account of disregarding the moisture adhered to the pore surface.¹⁾

Although complicated calculations are necessary to obtain a pore distribution from an isotherm, this paper describes a simplified and reasonable method for the calculation from an isotherm of water vapor adsorption. Then the equilibrium moisture content curves are shown on several porous materials. The present method on water vapor adsorption was discussed on whether the calculation of pore distributions from the curves is appropriate or not.

* 3-15-1 Tokida, Ueda, Nagano, 386
TEL. 0268 (22) 1215

** 9, Shodai-tajika 1-chome, Hirakata, Osaka, 573
TEL. 0720 (55) 2221

Received May 21, 1984

2. Calculation of pore distribution

2. 1 Calculation method of pore volume

When an adsorption isotherm is divided into many sections as shown in Fig. 1, pore volumes of porous materials have been calculated on the basis of the concepts as follows: upon increasing relative pressure from x_i to x_{i-1} , the state of multimolecular layer at the thickness of t_i changes into that of capillary condensation in the pore with radius r_i to r_{i-1} . In the pore with radius more than r_{i-1} , the thickness of the adsorbed layer increases from t_i to t_{i-1} . Then the sum of those is equal to the increment of adsorption volume, Δv_i , on an isotherm, that is,

$$\Delta v_i = \int_{r_i}^{r_{i-1}} \left(\frac{r - t_i}{r} \right)^2 V(r) dr + \sum_{j=1}^{i-1} \int_{r_j}^{r_{j-1}} \frac{(r - t_i)^2 - (r - t_{i-1})^2}{r^2} V(r) dr \quad (1)$$

where $V(r)$ is the distribution function of pore volume. The first term of the right hand side of Eq.(1) corresponds to the increase in adsorption volume on account of pore filling, the second term indicates the increase in thickness of the adsorbed layer in the pore not yet filled by capillary condensation.

Complexities of the conventional calculation methods are in the evaluation process of pore volume from Eq. (1), and various methods have been presented. Cranston and Inkley²⁾, Doll-

more and Heal³⁾ assumed that the thickness of adsorbed layer, t_i , in Eq.(1) depends only on relative pressure, and that the values of t_i are equal to those of t -curve. On the other hand, Broekhoff and De Boer^{4,5)} showed on the basis of thermodynamical considerations that t_i depends not only on the relative pressure but on the pore radius, as indicated on Fig. 2. They calculated the pore volume by employing both average value of t_i and average pore radius in each section. In the previous paper⁶⁾, their method was reasonably modified as follows.

When the section divided in Fig. 1 is so small that $V(r)$ is regarded as constant, the pore volume corresponding to the i -th section, V_i , is denoted by

$$V_i = V(r)(r_{i-1} - r_i). \quad (2)$$

Now

$$R_{c,i} = (r_{i-1} - r_i) / \int_{r_i}^{r_{i-1}} \left(\frac{r - t_i}{r} \right)^2 dr \quad (3)$$

and

$$M_{i,j} = \int_{r_j}^{r_{j-1}} \frac{(r - t_i)^2 - (r - t_{i-1})^2}{r^2} dr / (r_{j-1} - r_j) \quad (4)$$

are defined, then the pore volume is given by

$$V_i = R_{c,i} (\Delta v_i - \sum_{j=1}^{i-1} M_{i,j} V_j). \quad (5)$$

By means of Eq. (5), each pore volume may be estimated by starting with the first section, and in each step making use of the value of V_j ob-

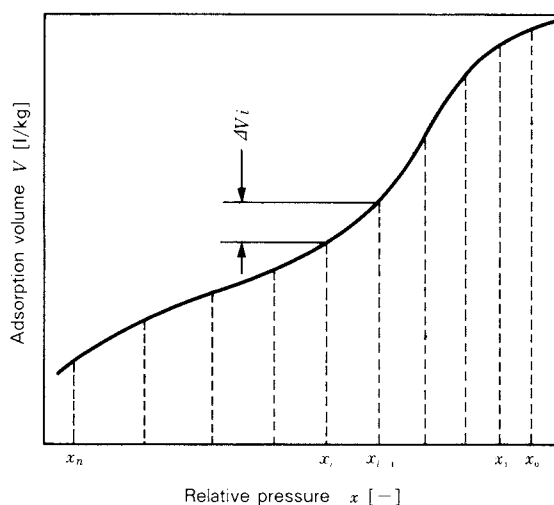


Fig. 1 Division of an isotherm. The vertical axis indicates the adsorption volume converted into liquefied volume of adsorbate.

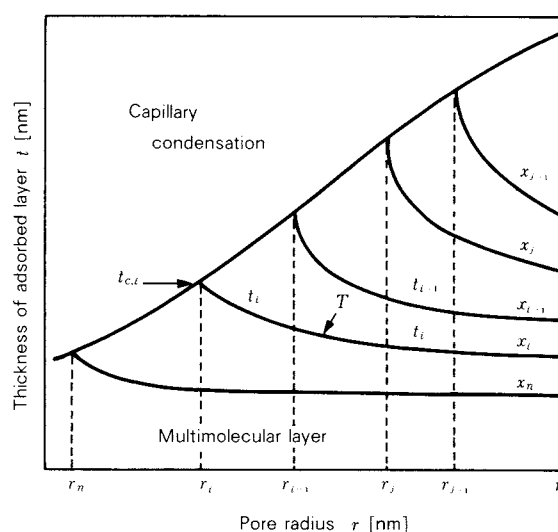


Fig. 2 The relations among thickness of adsorbed layer, pore radius and relative pressure.

tained from the preceding section.

The method above-mentioned is based on the calculation of pore volumes from an adsorption branch. In the case of desorption branch, the decrease in adsorption volume on account of capillary evaporation with decrease of relative pressure from x_{i-1} to x_i can be similarly represented by the first term of the right hand side in Eq.(1). Decrease of adsorbed layer is also indicated by the second term. Therefore, the calculations of pore volumes from desorption branch also refer to Eq.(5).

According to Broekhoff *et al.*⁴⁾, although the thickness of adsorbed layer in a pore is not necessarily the same as that of t -curve which depends only on adsorbate, it is possible to evaluate the thickness from t -curve.

Since R_c and M defined by Eqs.(3) and (4) respectively are the functions of both pore radius and thickness of adsorbed layer, the values of R_c and M can be calculated from t -curve for a given radius, regardless of the characteristics of adsorbents. If these values have been prepared, the calculation of pore volume can be reduced merely to that of Eq.(5).

2. 2 Calculation method of R_c and M

When the pore volumes are calculated by means of Eq.(5), the relative pressure at which capillary condensation takes place, R_c and M must have been known in advance.

The relative pressure can be evaluated on the basis of the method proposed by Broekhoff *et al.*⁴⁾ When the adsorption branch of a porous material is used for measuring the pore volume, the thickness of an adsorbed layer in a pore, for example, $t_{c,i}$ shown in Fig. 2 is given by

$$RT df(t_{c,i})/dt = \gamma M_v / (r_i - t_{c,i})^2 \quad (6)$$

for a given radius, r_i , where $f(t)$ means t -curve, while using the desorption branch, $t_{c,i}$ is given by

$$2RT \int_{t_{c,i}}^{r_i} f(t)(r-t)dt - RT f(t_{c,i})(r_i - t_{c,i})^2 = \gamma M_v (r_i - t_{c,i}) \quad (7)$$

instead of Eq.(6). By the use of these $t_{c,i}$, the relative pressure, x_i is obtained from

$$RT f(t_{c,i}) - RT \ln x_i = \gamma M_v / (r_i - t_{c,i}). \quad (8)$$

After x_i has been determined, the curve, T in Fig. 2 is drawn by

$$RT f(t) - RT \ln x_i = \gamma M_v / (r - t) \quad (9)$$

for r over r_i . Since the curve, T means t_i in Eqs. (3) and (4), R_c and M can be evaluated for a given pore radius.

2. 3 Measurement of t -curve of water vapor adsorption

There are many studies on the pore distributions by the water vapor adsorption method, and a few t -curves have been reported⁷⁾. But these t -curves may not be useful for calculating t_i in Eq.(3) or (4) because of insufficient measured points in neighborhood of the saturated pressure. Therefore, the t -curves were measured at 25°C^{8,9)}.

Making use of the nonporous materials shown in Table 1, the isotherms of water vapor adsorption were measured by a volumetrical adsorption apparatus. Since BET's plot gave a good straight line, specific surface area, S_{H_2O}

Table 1 Specific surface area, S and BET's constant C of nonporous materials.

	$S \times 10^{-3} \text{ [m}^2/\text{kg]}$			BET-C [-]	
	H ₂ O	N ₂	S_{H_2O}/S_{N_2}	H ₂ O	N ₂
BaSO ₄	2.42	3.39	0.71	120	300
anatase	10.5	11.5	0.91	57	210
rutile	16.3	14.1	1.16	84	220
Ca ₃ (PO ₄) ₂	65.6	71.8	0.91	50	240
SiO ₂	0.48	—	—	23	—
graphite	11.2	11.1	1.01	17	110

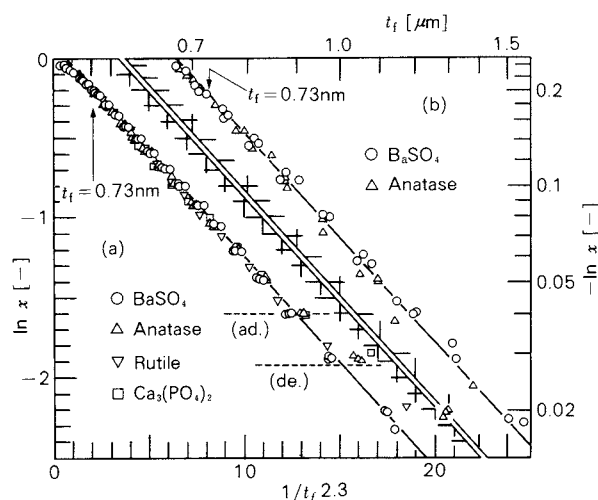


Fig. 3 The relations between thickness of adsorbed layer and relative pressure.

Table 2 R_c and M values for calculation of the pore volume from adsorption branch, which has BET's constant C over about 50.

r [nm]	x [-]	$R_{c,i}$ [-]	$M_{ij} \times 10^3$ [-]										
			$j = 1$	2	3	4	5	6	7	8	9	10	11
15.0	0.956	1.28											
10.0	0.931	1.39	51.7										
7.5	0.904	1.49	21.7	58.9									
6.0	0.875	1.60	13.7	26.4	62.4								
5.0	0.846	1.73	6.91	12.1	21.2	49.1							
4.5	0.826	1.78	7.07	11.8	18.9	32.5	67.0						
4.0	0.801	1.84	7.35	11.7	17.8	27.0	40.5	71.9					
3.5	0.768	1.91	8.25	12.5	17.6	24.5	32.8	44.3	78.0				
3.0	0.723	2.00	9.38	14.0	19.3	25.4	31.5	38.1	50.1	85.8			
2.5	0.660	2.11	10.9	16.0	21.5	27.7	33.5	39.2	47.7	61.9	100.5		
2.0	0.566	2.20	12.9	18.7	24.8	31.3	37.1	42.5	50.0	61.0	79.7	127.9	
1.5	0.420	2.26	15.4	22.1	28.9	35.8	41.9	47.3	54.4	64.2	78.6	102.9	164.7
1.0	0.203												

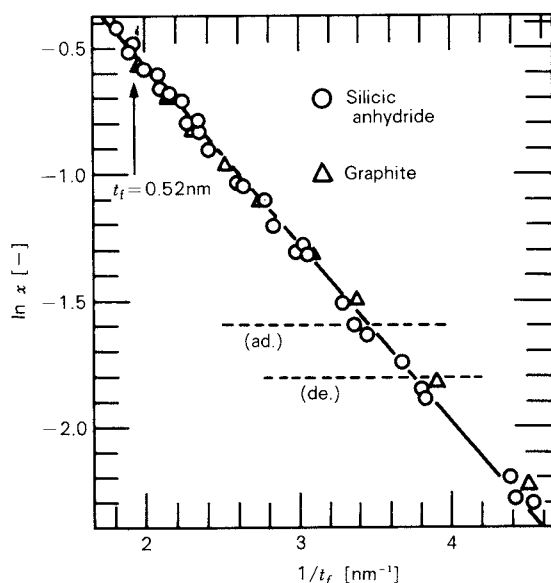


Fig. 4 t_f - $\ln x$ relations obtained from the isotherms of graphite etc.

was calculated by employing 0.108 nm^2 as the molecular cross-sectional area of water. The areas obtained and those by nitrogen adsorption method were shown in Table 1 together with BET's constant C .

The thickness of adsorbed layer on the surface of an adsorbent, t_f is evaluated as the ratio of an adsorbed volume of water to the specific surface area, $S_{\text{H}_2\text{O}}$. The relations between t_f and the relative pressures are shown in Figs. 3 and 4. Although the plots in Fig. 3 (a) shift to the right in lower pressure range, the regions over two dotted lines are useful for calculations of the pore distributions from the adsorption

and desorption branches. We regarded that measured points fell on a straight line in this regions, and then determined

$$\ln x = 0.08 - 0.132/t_f^{2.3} \quad t_f \leq 0.73 \text{ nm} \quad (10)$$

as t -curve. For higher pressure range, the following relation can hold from Fig. 3 (b).

$$\ln x = -0.069/t_f^{3.25} \quad t_f > 0.73 \text{ nm} \quad (11)$$

Eqs. (10) and (11) agree with each other at $t_f = 0.73 \text{ nm}$, that is, $x = 0.825$.

These two equations are based on the isotherms which have the values of BET- C over about 50 as shown in Table 1. On the other hand, the values became about 20 when silicic anhydride and graphite^{a)} were employed as adsorbent. The relationships between t_f and $\ln x$ for these samples are shown in Fig. 4. The straight line in the figure gives

$$\ln x = 0.85 - 0.708/t_f \quad t_f \leq 0.52 \text{ nm} \quad (12)$$

Eq. (12) agrees with Eq. (10) at $t_f = 0.52 \text{ nm}$.

2. 4 Values of R_c and M

In order to carry out the integrations in Eqs. (3) and (4), each section in Fig. 2 was divided further into twenty, and t_i for the each divided point was evaluated with the aid of Eqs. (9) to (12). Integral values were then calculated by

a) Value of $S_{\text{H}_2\text{O}}/S_{\text{N}_2}$ of graphite depends on the state of oxidation of its surface. Since the value of the graphite used in this study is 1.01, it may be suitable as the adsorbent for measuring t -curve.

Simpson's method. The values obtained are shown in **Tables 2 to 4**.

By reading of the adsorption volumes at the relative pressures shown in the second column of each table, the pore volumes can be easily evaluated by using of Eq. (5), and the calculations of the pore distributions refer to Eq. (2).

3. Equilibrium moisture contents

3. 1 Measurement methods

The equilibrium moisture contents of the porous materials were measured by the desiccator method.

Weighing bottles in which sample was contained were placed in a box made of stainless steel instead of the desiccator. The box was then submerged in a thermostat to keep it at a constant temperature. Humidity in the box was controlled by the use of saturated aqueous solution of a salt. A small fan was attached in the box, so as to keep humidity in the box uniform. According to the results of a few preliminary experiments, it was known that the weights of samples which were dried for 24 hours under the conditions of about 13 Pa and

130°C were able to regard as the weights of dry basis. The moisture contents of the samples laid in the box for two weeks, though they reached constant values for 3 to 7 days, were regarded as the equilibrium values.

In order to compare the equilibrium moisture contents with the amounts of water vapor adsorbed, adsorption isotherms were measured with a spring balance and with the glass wares as shown in **Fig. 5**. A sample was dried and weighed by using the left-halves of the wares. A saturated salt solution was poured into the right-halves to control the vapor pressure of water. After evacuating air in the wares under frozen state of the solution, the wares were maintained at a constant temperature in a thermostat. The adsorbed amount was obtained from the weight increment of the left-halves of the wares.

3. 2 Comparison of equilibrium moisture content curves with water vapor adsorption isotherms

Under the controlled humidity by the use of saturated solution of the salt shown in **Table 5^{b)}**, the equilibrium moisture contents of activated aluminas were measured at 25°C. Some of the results are shown by the solid lines in **Fig. 6**. The equilibrium moisture content of a sample was measured by utilizing three weighing bottles in a run. The solid lines in the figure represent the average values of three runs. The symbols on the lines such as I mean the greatest and least values of measured moisture contents. As is evident from **Fig. 6**, the magnitudes

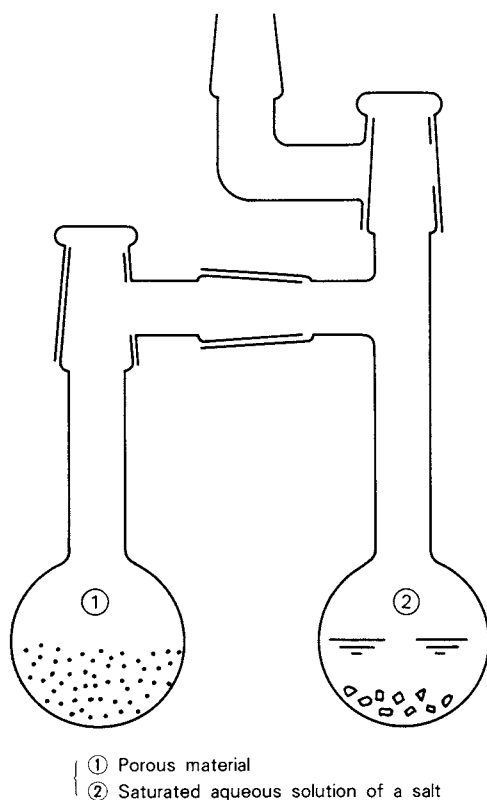


Fig. 5 Glass wares for measuring the amount of water vapor adsorbed.

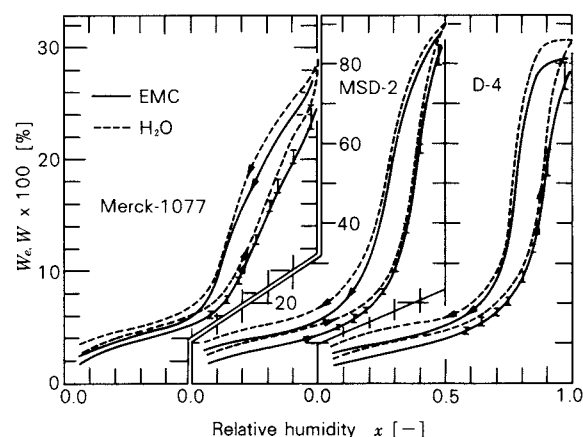


Fig. 6 Comparison of equilibrium moisture content curves (EMC) with isotherms of water vapor adsorption (H_2O)

Table 3 R_c and M values for calculation of the pore volume from desorption branch, which has BET's constant C over about 50.

r [nm]	x [—]	$R_{c,i}$ [—]	$M_{i,j} \times 10^3$ [—]										
			$j = 1$	2	3	4	5	6	7	8	9	10	11
15.0	0.925	1.18											
10.0	0.885	1.24	20.4										
7.5	0.845	1.30	12.6	21.6									
6.0	0.805	1.36	9.02	14.4	21.8								
5.0	0.765	1.41	5.05	7.70	15.2								
4.5	0.738	1.45	5.51	8.32	11.6	15.4	19.5						
4.0	0.705	1.50	5.66	8.44	11.6	15.2	18.8	22.6					
3.5	0.666	1.56	6.25	9.24	12.5	16.2	19.7	23.3	28.6				
3.0	0.616	1.63	7.04	10.3	13.8	17.6	21.2	24.6	29.5	37.3			
2.5	0.549	1.73	8.11	11.8	15.6	19.7	23.4	26.8	31.5	38.5	50.4		
2.0	0.459	1.86	9.74	14.0	18.4	23.0	27.0	30.6	35.5	42.3	52.7	71.9	
1.5	0.330	1.99	12.9	18.4	23.9	29.6	34.4	38.7	44.3	51.9	62.7	79.9	113.7
1.0	0.146												

of deviations in the measured values increased with increasing humidities, and the constant values of moisture contents were not obtained at the saturated humidity for powder samples.

The isotherms of water vapor adsorptions were measured by two methods mentioned above. The values obtained from both methods almost agreed. The results were also shown in Fig. 6 by the dotted lines. As shown in the figure, the curves of equilibrium moisture contents fell under the adsorption isotherms for all samples.

In order to obtain the specific surface areas, BET's plot was carried out after the conversion of the moisture weight into the volume of water vapor at the standard condition of gas. The results as well as BET-C were shown in Table 6^{c)}. The specific surface areas evaluated from moisture content curves were slightly smaller than those from other isotherms.

4. Pore distributions

4.1 Pore distributions from equilibrium moisture content curves

By means of the method described above, the pore distributions were calculated from the curves shown in Fig. 6.

The calculations of pore volumes were carried out by the use of numerical values in Table 2 or 3 from the isotherms of water vapor adsorptions except Wako-1525. From other curves, of which BET-C was less than 50, pore volumes were calculated by utilizing the values in Table 4. Results were shown in Figs. 7 and 8.

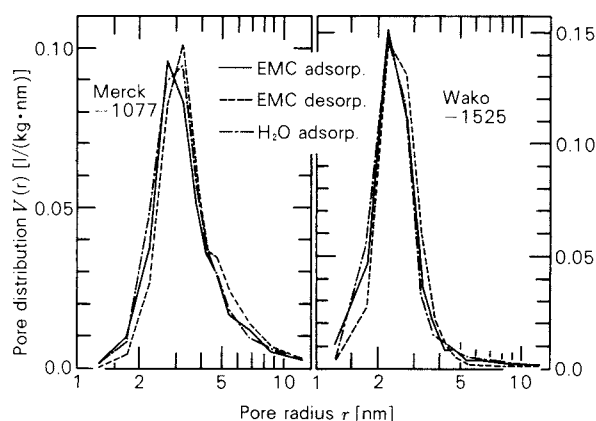


Fig. 7 Pore distributions obtained from the equilibrium moisture content curves and the water vapor adsorption isotherms.

In Fig. 7, the pore distributions obtained from ad- and desorption branches of the equilibrium moisture content curves (EMC) compared with those from the water vapor adsorption isotherms (H_2O). Fig. 8 shows the comparisons among the cumulative pore volumes evaluated from the adsorption branches.

Three pore distribution curves almost agreed with each other, despite there were differences between the moisture content curves and the water vapor adsorption isotherms. As the

b) Data at other temperatures have been shown in the references^{10,11).}

c) "Merck-1077" was provisionally named for activated alumina shown by catalog number 1077 in Merck Chemicals Reagents. Similarly, "Wako-1525" means activated alumina of 01525 in Wako Chemicals. "Neobead" is commercial name of activated alumina produced by Mizusawa Chemicals Co.

Table 4 R_c and M values for calculation of the pore volume from an isotherm, which has BET's constant C less than 50.

r [nm]	x [—]	$R_{c,i}$ [—]	$M_{i,j} \times 10^3$ [—]										
			$j = 1$	2	3	4	5	6	7	8	9	10	11
[adsorption]													
2.5	0.660	2.11	11.0										
2.5	0.566	2.20	14.4	20.8	27.2	33.9	39.8	45.2	52.6	63.4	81.6	129.0	
1.5	0.420	2.16	20.2	28.8	37.6	46.4	54.1	60.9	69.7	81.6	98.8	126.4	191.0
1.0	0.203												
[desorption]													
3.0	0.616	1.63	7.22	10.5	14.0								
2.5	0.549	1.73	8.94	12.8	16.8	21.1	24.8	28.1	32.7	39.5	51.1		
2.0	0.459	1.85	11.9	17.0	22.2	27.4	32.0	36.1	41.4	48.7	59.3	78.3	
1.5	0.332	1.92	16.0	22.8	29.6	36.6	42.5	47.8	54.7	63.9	77.0	97.4	136.0
1.0	0.163												

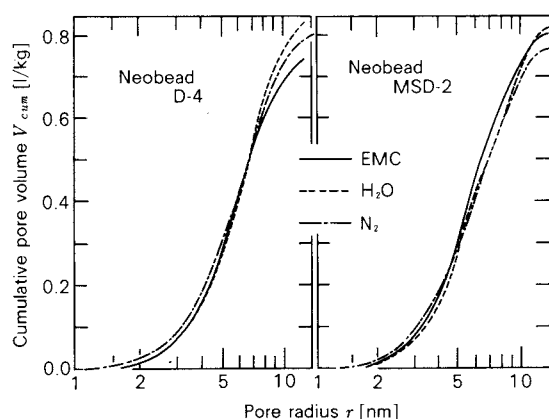


Fig. 8 Cumulative pore distribution curves obtained from adsorption branches.

reasons for the agreement, it may be considered that the values of Δv_i in Eq. (5) obtained from the moisture content curves were nearly equal to ones from the isotherms in higher pressure range, because both curves were in parallel with each other. In the lower pressure range, since the slope of the moisture content curves were larger than that of the isotherms, the values of Δv_i from the moisture content curves also became larger, while the values R_c in Table 4 are smaller than that in Table 2 or 3, and M is in opposite relation to R_c . By these effects, it was expected that the pore distribution was agreed with each other also in lower pressure range.

The total pore surface, ΣS was calculated from the pore distribution curve. Table 7^{d)} shows the comparisons of the results with the

specific surface areas from BET's method. The ratio of the two surface areas has been used to judge whether the pore distribution obtained was reasonable or not. It seemed that ΣS nearly agreed with the specific surface areas in any method.

4. 2 Discussions

In order to calculate the pore distribution from the equilibrium moisture content curve, the t -curve of the moisture content must be measured in principle. It is then desirable that R_c and M have been evaluated from the t -curve. But the amount of moisture content of nonporous material is very small as that in the case of water vapor adsorption. Although water adsorption isotherm can be volumetrically measured with good accuracy, the moisture contents cannot be measured with enough accuracy as shown in Fig. 6. Therefore, it is very difficult to measure the t -curve on the equilibrium moisture content.

If the t -curve of moisture contents could be measured on nonporous materials, the curve might differ from that of water vapor adsorp-

Table 5 Relative pressure over the saturated aqueous solution of salt at 25°C.

salts	x [—]	salts	x [—]
LiBr	0.067	NaBr	0.578
LiCl	0.111	NaNO ₂	0.643
CaBr ₂	0.162	KI	0.688
CH ₃ COOK	0.224	NaCl	0.754
MgCl ₂	0.328	KBr	0.808
NaI	0.378	KCl	0.842
K ₂ CO ₃	0.440	BaCl ₂	0.903
Co(NO ₃) ₂	0.490	K ₂ SO ₄	0.976

d) Blanks in the table mean no available data for the desorption branch. The powder of Wako-1525 is so fine that it scattered when the vapor pressure of water was decreased.

Table 6 Specific surface areas, S and BET's constant C of activated aluminas

Materials	$S \times 10^{-3} [\text{m}^2/\text{kg}]$			BET-C $[-]$		
	EMC	H ₂ O	N ₂	EMC	H ₂ O	N ₂
Merck-1077	108	123	130	20	60	102
Wako-1525	140	146	166	19	28	68
Neobead C-4	163	184	177	26	53	175
Neobead D-4	226	283	277	25	53	126
Neobead MSD-2	246	303	270	27	81	253

Table 7 Comparison of total pore surface areas, ΣS with BET's specific surface areas, S

Materials	$\Sigma S \times 10^{-3} [\text{m}^2/\text{kg}]$			$\Sigma S/S [-]$		
	EMC	H ₂ O	N ₂	EMC	H ₂ O	N ₂
Merck-1077	126	138	148	1.17	1.12	1.14*
	128	135	156	1.18	1.10	1.20**
Wako-1525	160	164	183	1.14	1.12	1.10
	156	—	195	1.11	—	1.18
Neobead C-4	164	182	191	1.01	0.99	1.08
	165	197	206	1.01	1.07	1.16
Neobead D-4	268	284	301	1.19	1.00	1.09
	333	332	337	1.47	1.17	1.22
Neobead MSD-2	292	280	308	1.19	0.92	1.14
	328	336	335	1.33	1.11	1.24

* upper row: calculated from adsorption branch

** bottom row: from desorption branch

tion as easily expected from Fig. 6, in which the results on the porous samples were depicted, though. But, the pore distributions could be obtained from the moisture content curves by employing t -curve of water vapor adsorption which had the different value of BET-C. The distributions were reasonable as shown in Table 7, and agreed with those obtained from isotherms of water vapor adsorption. Furthermore, in our previous papers^{6,8)}, it was shown that the pore distributions in Figs. 7 and 8 agreed well with the ones measured by the mercury penetration method, and by the nitrogen adsorption method.

From these results, we concluded that values of R_c and M shown in Tables 2 to 4 were also useful for the equilibrium moisture content curves.

5. Conclusion

Investigations on the calculation and the measurement of the pore distribution were carried out, and it was shown that pore volume could be easily evaluated by Eq. (5). The equation contains two coefficients, R_c and M ,

which can be calculated by the aid of t -curve.

The values of R_c and M obtained for the water vapor adsorption were applicable also to the determination of the pore distributions from the equilibrium moisture content curves.

Acknowledgement

The authors would like to acknowledge the continuing guidance and encouragement of Dr. Takeo Yano, Professor emeritus of University of Osaka Prefecture.

Nomenclature

C	: BET's constant	$[-]$
$f(t)$: t -curve	$[-]$
M	: coefficient defined by Eq. (4)	$[-]$
M_v	: molar volume of adsorbate	$[\text{nm}^3/\text{mol}]$
R	: gas constant	$[\text{J}/(\text{mol} \cdot \text{K})]$
r	: pore radius	$[\text{nm}]$
R_c	: coefficient defined by Eq. (3)	$[-]$
S	: specific surface area	$[\text{m}^2/\text{kg}]$
T	: temperature in measurement	$[\text{K}]$
t	: thickness of adsorbed layer in a pore	$[\text{nm}]$
t_f	: thickness of adsorbed layer on the flat surface	$[\text{nm}]$
V	: pore volume	$[\text{g}/\text{kg}]$
v	: adsorbed volume	$[\text{g}/\text{kg}]$
V_{cum}	: cumulative pore volume	$[\text{g}/\text{kg}]$
$V(r)$: distribution function of pore volume	$[\text{g}/(\text{kg} \cdot \text{nm})]$
W	: adsorption amount of water vapor	$[\text{kg-H}_2\text{O}/\text{kg-solid}]$
W_e	: equilibrium moisture content	$[\text{kg-H}_2\text{O}/\text{kg-solid}]$
x	: relative pressure	$[-]$
γ	: surface tension of adsorbate	$[\text{J}/\text{nm}^2]$
ΣS	: total pore volume	$[\text{g}/\text{kg}]$

Subscripts

H₂O : adsorption of water vapor

N₂ : nitrogen adsorption

References

- 1) Kondoh, R., ed.: "Takoh-Zairyo", p.47, Gihoh-do, Tokyo (1973).
- 2) Cranston, R.W. and F.A. Inkley: *Adv. in Catalysis*, **9**, 143 (1957).
- 3) Dollimore, D. and G.R. Heal: *J. appl. Chem.*, **14**, 109 (1964).
- 4) Broekhoff, J.C.P. and J.H. De Boer: *J. Catalysis*, **9**, 8 (1967).
- 5) Broekhoff, J.C.P. and J.H. De Boer: *ibid.*, **9**, 15 (1967).
- 6) Arai, C., K. Yamazaki and Y. Sano: *Kagaku*

- Kogaku Ronbun-shu*, **8**, 39 (1982).
- 7) Hagymassy, J., Jr. S. Brunauer and R. Sh. Mikhail: *J. Colloid Interface Sci.*, **29**, 485 (1967).
- 8) Arai, C., T. Mizutani, Y. Murase, T. Hanakawa and Y. Sano: *J. Soc. Powder Technology, Japan*, **20**, 115 (1983).
- 9) Arai, C., K. Onda, K. Kajiyama and Y. Sano: *ibid.*, **20**, 599 (1983).
- 10) Arai, C., S. Hosaka, K. Murase and Y. Sano: *J. Chem. Eng., Japan*, **9**, 328 (1976).
- 11) Arai, C., Y. Wakabayashi, A. Mizuno, I. Komatsu and Y. Sano: *Kagaku Kogaku Ronbun-shu*, **9**, 241 (1983).

Effects of Tensile Strength and Tensile Breakup Energy on Mulling Processes of Wet Powders

Keijiro Terashita*, Teruo Kimura*,
Hideyo Tsukaguchi* and Kei Miyanami*
Department of Chemical Engineering
University of Osaka Prefecture

Abstract

The dynamic mixing power required for mulling process of green mold sands was measured by using various types of kneaders and binding materials. A series of tensile tests for the green mold sands were carried out. The surface structures of the sands were also observed by a scanning electron microscope.

The state of mulling of the sands was found to be successfully correlated with the tensile strength, the tensile breakup energy and the compression characteristics of the sands. It was also found that the completeness of mulling process could be assessed by observing the steadiness of the power for mulling, and that it could be evaluated in terms of the tensile breakup energy. The more the power for mulling was required, the better the state of mulling was.

1. Introduction

Mixing of wet powders in the pendular and funicular states is usually achieved by mulling operation. This operation is extensively utilized not only in chemical industry but also in various kinds of other industries such as food, ceramics and foundry. Despite its considerable importance from the engineering point of view, few studies on mulling engineering have been reported^{2,3,5,6}. Suitable design of mulling process, choice of kneaders and analysis of their operational data may be facilitated by a standardization of the methods for evaluating various properties of solid-liquid systems and mulling power requirement.

The author and his co-workers⁵ conducted a series of tensile tests on the solid-liquid systems in pendular, funicular and capillary states, and reported the characteristics of the wet powders in terms of the breakup displacement-moisture content relations. They also analyzed the relationship between the tensile strength

and the mixing torque of the wet powders. At the present stage, however, the state of mulling in wet powders is still evaluated in terms of the degree of mixing^{2,3} by human sensory judgement or rheological morphology, and these methods permit only a qualitative assessment. It can also be said that the relationship between the power requirement for mulling and the tensile breakup energy of the mixture product has not become clear yet.

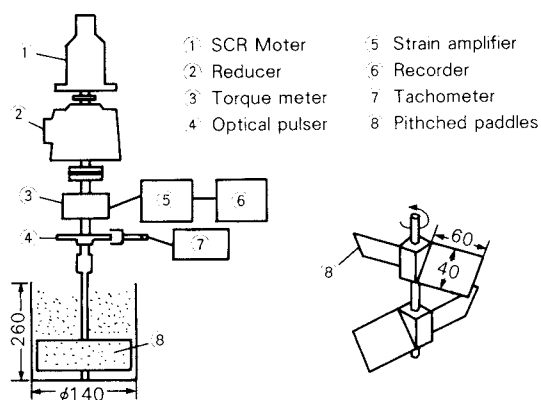
In this study, the mixing torque or the mixing power for mulling of green mold sands (silica sand-bentonite-water system) widely used in foundry, was measured to know the effect of moisture content on the tensile breakup characteristics of the green mold sands by using various types of binders and kneaders. The surfaces of green mold sands were observed by a scanning electron microscope to examine the state of mulling. This paper describes the interrelationships among the state of mulling, the tensile strength, the tensile breakup energy, the compression characteristics, the moisture content and the power requirement for mulling of the green mold sands.

* 4-804 Mozu-Umemachi, Sakai, Osaka, 591
TEL. 0722 (52) 1161

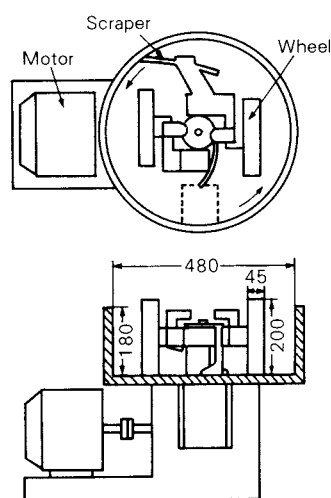
Received June 19, 1984

2. Materials and methods

A vertical cylindrical mixer with pitched paddles (Fig. 1(a)) and a Simpson mill (Fig. 1(b)) were used as kneaders. The vertical cylinder was made of methacrylic resin and had the inside diameter of 140 mm and the height of 260 mm. Two pitched paddles were attached crosswise to a vertical rotating shaft with the attack angle of the upper paddle of 60° and that of the lower one of 120° . The paddles (8) were driven by an SCR motor (1) which was controlled to maintain a constant rotational speed against load changes. The mixing torque was measured by a strain gauge torque meter (3) (capacity: 5 Kg-m). The mixing performance of this kneader had been already obtained⁴⁾.



(a) Vertical cylindrical mixer



(b) Simpson mill

Fig. 1 Experimental kneaders

The Simpson mill shown in Fig. 1(b) had a fixed pan with scrapers sweeping the pan wall and bottom. The rotational speed of the wheels of the mill was $N=0.62\text{s}^{-1}$. The power requirement for mulling was measured by the electric current intensity fed to the driving motor. Kneading was also carried out by hand to compare with the above result.

Figure 2 illustrates the outline of a hanging type adhesiveness tester used for testing of the tensile strength of binding materials and mulled mixtures (green mold sands)^{1,5)}. This tester was of a split cell type with vertical compression and horizontal tension mechanism. The movable cell (2) was hung by three phosphor bronze plates (6). The cell measured 50 mm in inside diameter and 20 mm in height. The tension velocity was $3.33 \times 10^{-5} \text{ m/s}$. The relationship between the tensile stress $\bar{\sigma}_x$ and horizontal displacement δ_x was determined with a strain gauge (3) and a differential transformer (4) and recorded on an X-Y recorder. This tester was equipped with an operational amplifier (7) to subtract the stress due to bending of the phosphor bronze plates so that only the tensile stress exerted onto the powder bed could be recorded. The porosity \bar{e} of the powder bed in the cell was adjusted by changing the precompression load from 1.6 to 16.6 kPa. The tensile breakup testing was performed after release of the precompression load.

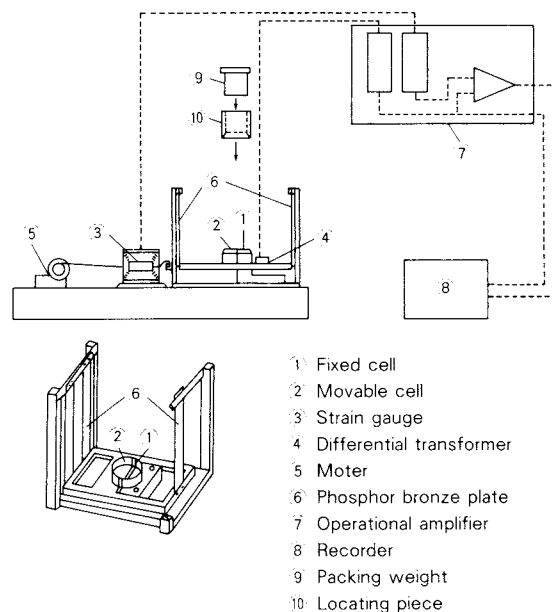


Fig. 2 Apparatus of tensile test

Table 1 Properties of powders tested

Sample	Particle density $\rho(\text{kg/m}^3)$	Apparent density $\rho_a(\text{kg/m}^3)$	Angle of repose $\Phi_r(\text{rad})$
Silica sand(Australia)	2610	1479	0.600
Na-Bentonite(U.S.A)	2370	832	0.742
Coal powder(Japan)	1370	523	0.723

The used powder consisted of the base material (silica sand) 100, the binder (bentonite) 7, the secondary binder (coal powder) 1.5 and the water 3, all in mass units. This composition was the same as that of the green mold sands employed in foundry industry. For mixing and mulling of the powder, the binder was first added to and mixed with the base material. A coal powder was then added to and mixed with the mixture, to which water was finally added at one time (refer Fig.3). The powder was mixed in the same manner throughout the experiments regardless of the type of kneaders and kind of binders used.

Table 1 is the list of the properties of the base material, the binder and the secondary binder used in experiments. The base material was Australian silica sand ($\sigma_g = 1.36$, $D_{50} = 345 \mu\text{m}$). The secondary binder was Japanese coal powder ($\sigma_g = 1.69$, $D_{50} = 120 \mu\text{m}$). Bentonite produced in Wyoming, USA (Na, $D_s = 7.2 \mu\text{m}$) was used as a binder. All the powder samples were dried at 110°C for 24 hours before experiments.

3. Results and discussion

3. 1 Mixing torque and tensile process curves of the mulled mixture during mixing and mulling processes

Figure 3 shows an example of the mixing torque T , changing with time during a mulling process of the mixture. The mixing torque T , after its monotonic increase with an addition of water as a mulling process proceeded reached a constant value T_s (Regardless of the type of kneaders and the kind of binders used, the mulling operation was continued considerably long even after the mixing torque reached a steady value T_s). To evaluate the state of mulling in the mixture, a portion of the mulled mixture in the kneader was randomly sampled during a course of mulling and its tensile break-

up moisture content was measured.

Figure 4 shows an example of breakup process curves (the relation between the tensile stress $\bar{\sigma}_x$ and the horizontal displacement δ_x) of the mulled mixture. The porosity $\bar{\epsilon}$ shown in this figure was obtained by evaporation of

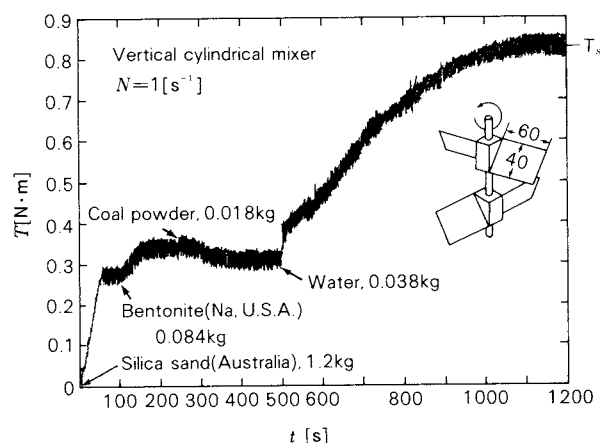


Fig. 3 Relationship between mixing torque and mixing time

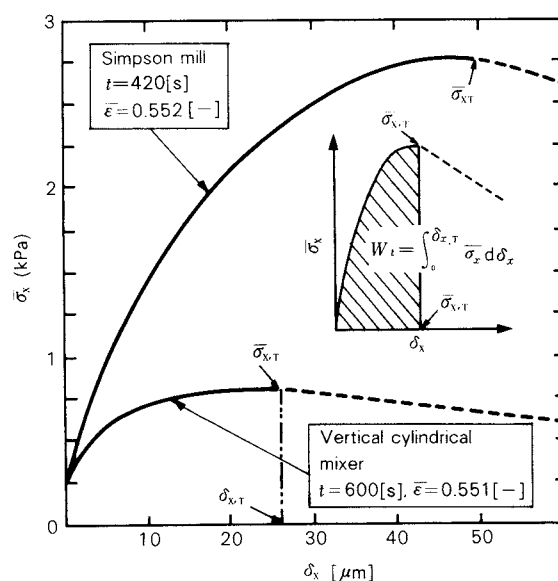


Fig. 4 Tensile process curves

the moisture contained within the mixture. As can be seen from Fig. 4, the tensile stress $\bar{\sigma}_x$ rapidly increases at the start of tension loading and a breakup occurs at a certain horizontal displacement δ_x showing the tensile strength $\bar{\sigma}_{x,T}$. For an evaluation of state of mulling in the mixture, two factors, the tensile strength $\bar{\sigma}_{x,T}$ and the tensile breakup energy W_t (refer to Fig. 4) were taken into consideration.

3. 2 Relationship between the mixing power (or mixing torque) and the tensile strength or standard deviation of the moisture content in samples.

Figure 5 shows a change in the mixing power P (effective value) with time during a mulling process. This figure also shows the tensile strength $\bar{\sigma}_{x,T}$ and the standard deviation S of the moisture content in the samples of mulled mixture taken at an arbitrary mixing time. It can be said that the lower the value of S is, the better the state of mulling is, since a small value of S means a uniformness of the moisture distribution in the mulled mixture. Namely, the value of S is equivalent to the degree of solid mixing. As is clear from Fig. 5, the mixing power P , after its monotonic increase with the progress of mulling, shows a constant value P_s (at $t \geq 420$ sec). The tensile strength $\bar{\sigma}_{x,T}$ of the mulled product also increased with the mulling time and reached a constant value at $t \geq 420$ sec. The standard deviation S also showed a constant value at $t \geq 420$ sec. This indicates that the mulling is possibly completed when

the mixing power is stabilized.

Figure 6 shows examples of scanning electron microscopic pictures of the mulled mixture. At the mulling time $t=150$ sec (Fig. 6 (a)), the mulling was incomplete because of agglomerate sticking of the binding material, bentonite, to the particle surface of the base material (silica sand). On the other hand, at $t=600$ sec when the mixing power P reached a steady value (Fig. 6(b)), the state of mulling was excellent as noted from the individual particles (silica sand) uniformly coated with the binder which could be seen as whitish cobweb in the photograph. It is further noted that, in the state of complete mulling, bentonite appears to be an inter-particle binder (Fig. 7). Figures 5 and 6, therefore, demonstrate that the constancy of the mixing power reflects the completeness of mulling macroscopically as

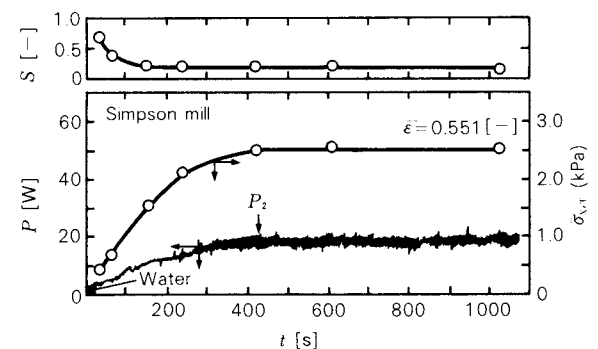
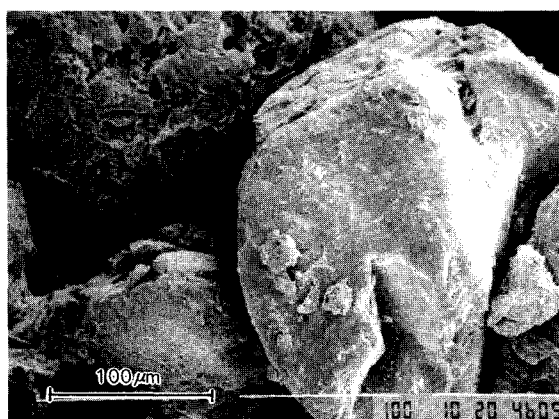
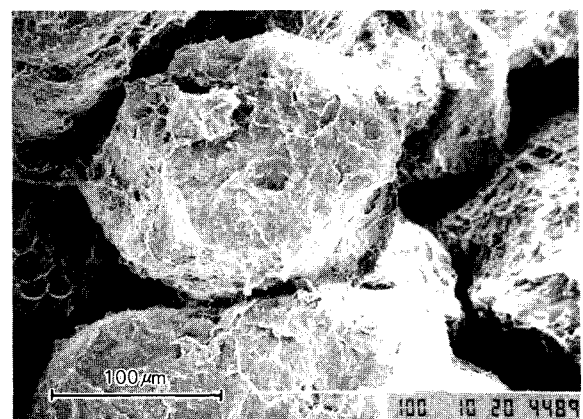


Fig. 5 Relationship between mixing power and tensile strength and standard deviation of moisture content in samples



t = 150 [s]
(a)



t = 600 [s]
(b)

Fig. 6 Scanning electron microscopic picture of mulling condition (Simpson mill)

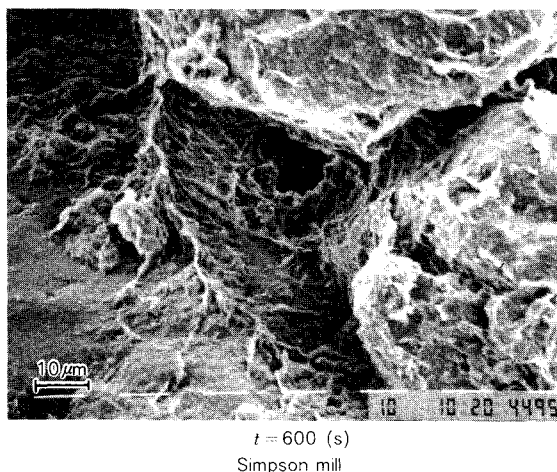


Fig. 7 Scanning electron microscopic picture of inter-particle binder

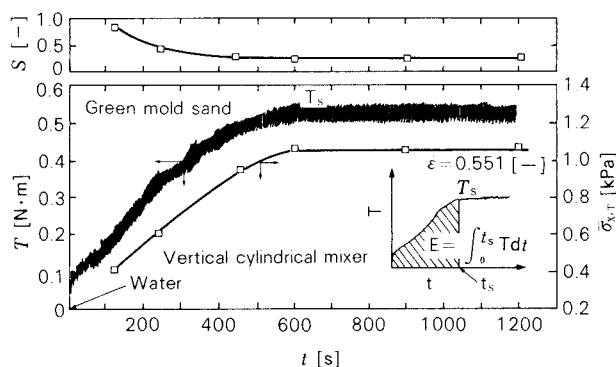


Fig. 8 Relationship between mixing torque and tensile strength and standard deviation of moisture content in samples

well as microscopically.

Figure 8 shows the relation among the mixing torque T , tensile strength $\bar{\sigma}_{x,T}$ and standard deviation S to the mulling time t obtained in the vertical cylindrical mixer. It was also found that a completion of mulling was not obtainable until the mixing torque reached a constant value T_s .

3. 3 Comparison of the kneader performances

Figure 9 shows the relationship between the tensile strength $\bar{\sigma}_{x,T}$ and the standard deviation S of the mulled mixture obtained by different mulling methods. The mixture was collected at 120 seconds later after stabilization of the mixing torque (or power) for tensile tests and moisture measurement. The figure also shows the tensile strength of silica sand-water mix-

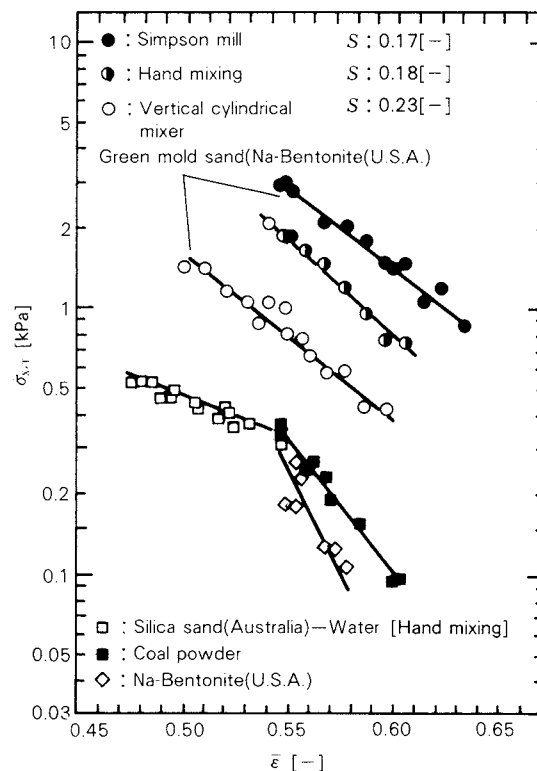


Fig. 9 Tensile strength-porosity relation by two types of kneaders

ture, dried bentonite and dried coal powder. As can be seen from the figure, the tensile strength $\bar{\sigma}_{x,T}$ of green mold sands (open circle) obtained by manual mulling is five times as large as that (open square) of the silica-water mixture. This difference may reflect the binding effect of water-impregnated bentonite. The value of tensile strength $\bar{\sigma}_{x,T}$ of the mulled mixture (green mold sands) decreased in the order of Simpson mill > hand mulling > vertical cylindrical mixer. The value of S is also smaller, when the tensile strength is larger. This, therefore, indicates that the Simpson mill provides excellent mulling of the mixture, which may be due to the effective contribution of the kneading, smearing and spatulate actions by the wheels.

Figure 10 shows the compression characteristics of the mulled mixture in terms of the vertical load $\bar{\sigma}_{x,w}$ and the porosity $\bar{\epsilon}$. At the vertical load of 15 kPa onto the mulled mixture, for instance, the porosity $\bar{\epsilon}$ indicates the values of approximately 0.506 for the mulled mixture obtained from the vertical cylindrical mixer and approximately 0.556 for that from

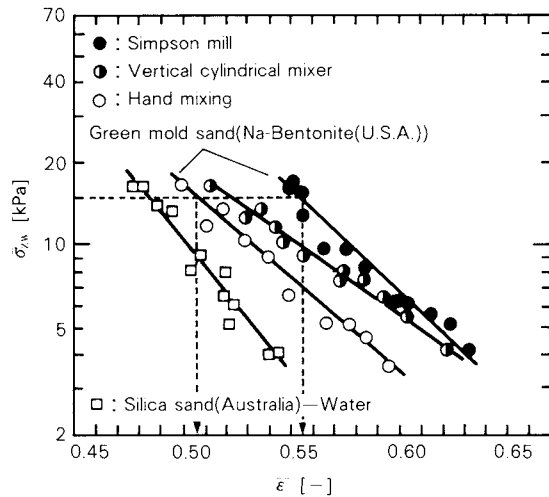


Fig. 10 Compression characteristics of mulled mixture

the Simpson mill. This suggests that the green mold sands kneaded by the Simpson mill are packed less tightly and thereby has a better permeability than that kneaded by the vertical cylindrical mixer.

The above findings demonstrate that the green mold sands obtained by the Simpson mill are sufficiently kneaded with a better permeability, thus satisfying the basic requirement for green mold sands. The data obtained by the tester may be interpreted to support the reasonableness of the wide-spread use of Simpson mill in industrial production of green mold sands.

3. 4 Relation between the tensile breakup energy and mulling power requirement

The energy needed for the tensile breakup of the mulled mixture can be expressed by Eq. (1) and the mulling power requirement by Eq. (2) (refer to Figs. 4 and 8).

$$W_t = \int_0^{\delta_{x,T}} \bar{\sigma}_x d\delta_x \quad (1)$$

$$E = \int_0^{t_s} T dt, \quad E_p = \int_0^{t_s} T dt / F \quad (2)$$

where E_p is the energy per unit mulled amount, and F designates a mulled amount. Figure 11 shows the relation between the tensile breakup energy W_t and the mulling power requirement E_p . It is noted that the breakup energy W_t for the mulled mixture produced by the Simpson mill is higher than that by the vertical

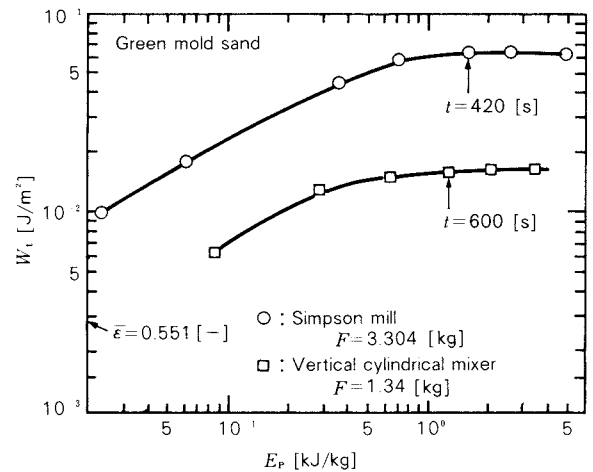


Fig. 11 Relation between tensile breakup energy and mulling power requirement by two types of kneaders

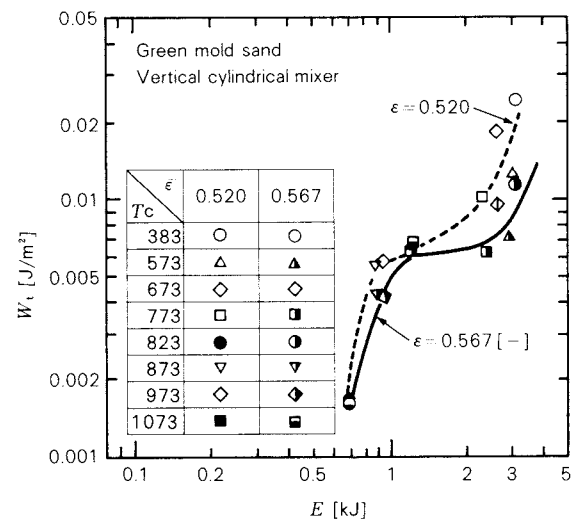


Fig. 12 Relation between tensile breakup energy and mulling power requirement for bentonites calcined at various temperatures

cylindrical mixer. This indicates the effectiveness of mulling energy in the Simpson mill. Figure 12 shows the relation between the tensile breakup energy W_t and the mulling energy requirement for the mulled mixture (green mold sands) prepared in the Simpson mill with the bentonite calcined at various temperature conditions as a binder. The use of calcined bentonite was intended to evaluate the effects of a binder heated by molten metal on the tensile breakup energy and mulling power requirement, because the green mold sands are usually repeatedly used in industrial processes. As can be seen from Fig.12, the mulling energy

(power) requirement increases with an increase in the tensile breakup energy irrespective of the calcinating temperature. Hence, the mulling power requirement for green mold sands (wet powder) can be evaluated in terms of the tensile breakup energy.

4. Conclusion

The state of mulling could be estimated on the basis of the tensile strength, the tensile breakup energy, the compression characteristics and the scanning electron microscopic observations of the mulled mixture. A well mulled mixture showed higher values of tensile strength and tensile breakup energy and lower value of the standard deviation of the moisture content in the mixture. The Simpson mill was proven its popularity in industrial production processes of green mold sands over paddle type mixers. Tensile breakup test could be utilized for an assessment of the state of mulling. The completeness of mulling in mixers could be estimated by observing a change with time in and a steadiness of the mixing torque or power. It was also confirmed that the power requirement for mulling of wet powders could be evaluated in terms of the tensile breakup energy.

Nomenclature

D_s	: surface mean diameter	[μm]
D_{50}	: 50%-radius particle size	[μm]
E	: mulling power requirement	[kJ]

E_p	: energy per unit mass of mulled amount	[kJ/kg]
N	: rotational speed	[sec^{-1}]
P	: mixing power	[W]
P_s	: steady mixing power	[W]
S	: standard deviation of moisture content in sample. $S = \sqrt{\frac{1}{15} \sum_{i=1}^{15} (C_i - \bar{C}_0)^2}$	[—]
T	: mixing torque	[N·m]
T_c	: calcinating temperature	[K]
T_s	: steady mixing torque	[N·m]
t	: mixing time	[sec]
W_t	: tensile breakup energy	[J/m ²]
δ_x	: horizontal displacement	[μm]
$\delta_{x,T}$: tensile breakup displacement	[μm]
$\bar{\epsilon}$: porosity	[—]
ρ	: particle density	[kg/m ³]
ρ_a	: apparent density	[kg/m ³]
$\bar{\sigma}_x$: tensile stress	[kPa]
$\bar{\sigma}_{x,T}$: tensile strength	[kPa]
$\bar{\sigma}_{z,w}$: vertical load	[kPa]

References

- 1) Fujii, K. and T. Yokoyama: *J. of the Society of Powder Technology, Japan*, **16**, 686 (1979).
- 2) Michaels, A.S. and V. Puzinauskas: *Chem. Eng. Progr.*, **50**, 604 (1954).
- 3) Mori, Y., G. Jimbo, M. Taki and F. Washio: *Kagaku Kōgaku*, **25**, 806 (1961).
- 4) Satoh, M., K. Miyanami and J. Yoshida: *J. of the Society of Powder Technology, Japan*, (in press).
- 5) Terashita, K., K. Miyanami and J. Yoshida: *J. of society of Materials Science, Japan*, **30**, 873 (1981).
- 6) Umeya, K., Y. Suzuki and Y. Aishima: *Kagaku Kōgaku*, **28**, 682 (1954).

A Review of the Investigations into Powder Bed Mechanics Based on a Microscopic View in Japan

Jun-ichiro Tsubaki*

Department of Chemical Engineering
Nagoya University

1. Introduction

Mechanical behaviors of powder beds have been investigated from different viewpoints with various methods according to their individual objects. In the present paper notable results of works in such a field published in several academic journals in Japan will be reviewed especially from a viewpoint of a microscopic analysis based on individual single particles.

As is widely recognized, a number of investigations have been developed to elucidate the mechanical behaviors of powder beds essentially based on two different viewpoints; taking powder beds as a uniform continuum and a discontinuum consisting of individual particles. Although these different approaches are popular to both fluid and solid mechanics, the case is slightly different with powder mechanics. It is because the mechanical behaviors of powder beds would depend on the specific properties of single particles which are constituent units not so small as those of the other continuums, i.e. molecules of the materials. This microscopic analysis of powder behaviors started nearly as early as the macroscopic analysis such as the measurement of an adhesive force^{5, 15)}, but there remain a number of unsolved problems in both of them.

This review, from a viewpoint of combining individual single particles with behaviors of powder beds, will outline as follows:

- relationship between the stress on powder beds and the local force at a contact point
- mechanical behavior at a contact point
- structure of powder beds
- relationship between the mechanics at a contact point and that of powder beds

2. Relationship between stress and force

Taking each individual particle into consideration, the analysis of a mechanical behavior of powder beds makes a demand for the information of forces acting on interparticle contact points. Unfortunately it is impossible in general to measure these forces directly, thus, if possible, the determination of them by measuring the corresponding stresses would provide sufficient convenience in the analysis.

A typical expression was presented by Rumpf⁴⁷⁾ based on the theoretical concept which referred the tensile strength as follows:

$$\sigma_z = \frac{1 - \epsilon}{\pi} k \frac{H}{d_p^2} \quad (1)$$

where σ_z = tensile strength

ϵ = porosity

k = average coordination number

H = cohesive force at a contact point

d_p = particle diameter

Based on the early concept of Rumpf^{45, 46)}, which involved a few mistakes in its derivation process, Molerus²⁵⁾ showed the stress – force relation might be expressed by Eq. (1) under the isotropic or hydrostatic pressure condition, and applied this conclusion to the analysis of shearing mechanism. On the other hand, Nagao²⁸⁾ derived a general expression of the stress – force relation assuming that a distribution of forces acting on interparticle contact points would be similar to that of stresses acting on powder beds. In addition Kanatani²⁰⁾ derived a similar expression of the correlation based on the principle of virtual displacement. These three expressions may have been considered to be essentially different since they are different in their forms.

The author *et al.*⁵⁸⁾ originally found that both expressions derived by Nagao and Kanatani would agree completely with Rumpf's

* Furo-cho, Chikusa-ku, Nagoya, Aichi, 464
TEL. 052 (781) 5111

Received April 3, 1984

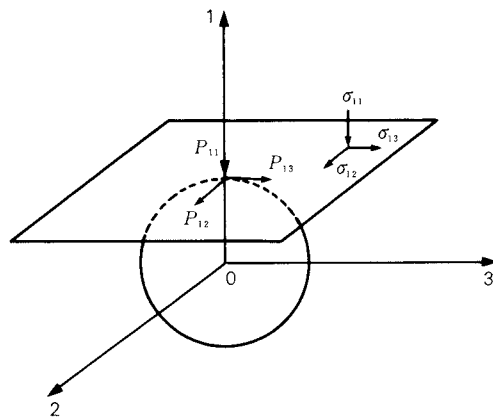


Fig. 1 Schematic representation of P_{ij} and σ_{ij}

equation. Consequently this can refer that the equation would be available in general to any expression of stress conditions. Therefore the stress acting on the plane vertical to i -axis, σ_{ij} can provide the j -axial component P_{ij} of the force acting on the contact point which is on the plane vertical to i -axis as shown in Fig. 1⁵⁸⁾, then Eq. (1) can be rewritten by:

$$\sigma_{ij} = \frac{1 - \epsilon}{\pi} k \frac{P_{ij}}{d_p^2} \quad (2)$$

Except the tensile test, very few applications of Rumpf's equation have been reported: Molerus²⁵⁾ made an analysis of the powder yield locus of cohesive powders and Naga^{26,27,28,29,30,32,34,36)} derived a general theory on the powder mechanics, which will be referred later. On the other hand the author *et al.*^{58,59)} established the way of analysis in which the effects of the porosity (the coordination number) on the powder layer mechanics and the force at a contact point separately discussed.

In general experimentally obtained results have been discussed using a relation of the porosity and the stress of powder beds. Eq. (2) can be rewritten assuming of $\pi \simeq k\epsilon$ as:

$$\sigma_{ij} = \frac{1 - \epsilon}{\epsilon} \frac{P_{ij}}{d_p^2} \quad (3)$$

It has been frequently shown that the relationship between a stress and a porosity in a consolidation test or between a tensile strength and a porosity could be a straight line on a semi-logarithmic paper. If the porosity ranges from 0.3 to 0.8, the term $(1 - \epsilon)/\epsilon$ in Eq. (3) can be modified using an exponential function

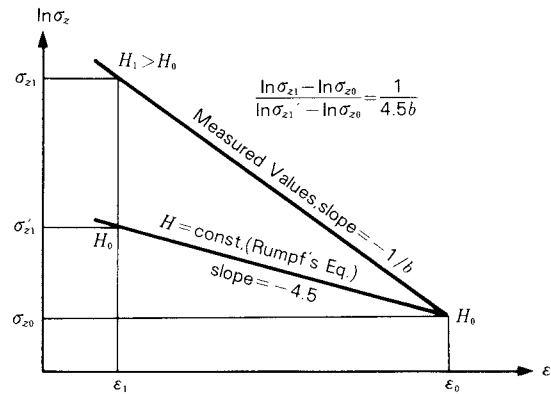


Fig. 2 Relationship between tensile strength σ and porosity ϵ

with an error of not over 10 percent;

$$\frac{1 - \epsilon}{\epsilon} \simeq 10 \exp(-4.5\epsilon) \quad (4)$$

Thus Eq. (3) transforms to

$$\sigma_{ij} = 10 \exp(-4.5\epsilon) \frac{P_{ij}}{d_p^2} \quad (5)$$

This equation is available to the analysis of tensile tests. A number of existing experimental data concerning them may correlate the tensile strength σ_z with the porosity ϵ by the equation of the form:

$$\sigma_z = k_1 \exp\left(-\frac{\epsilon}{b}\right) \quad (6)$$

where k_1 denotes a constant. The $\sigma_z - \epsilon$ relation is expressed by a straight line on a semi-logarithmic graph with a slope of $-1/b$ as shown in Fig. 2. It is also shown in this figure that a tensile strength can have a straight relation to the porosity ϵ with a slope of -4.5 , if a cohesive force is constant independently of a porosity. When the powder beds with the porosity of ϵ_0 and the cohesive force at a contact point H_0 are consolidated to the porosity of ϵ_1 , the tensile strength increases from σ_{z0} to σ_{z1}' if the cohesive force H_0 is kept constant, as shown in Fig. 2. It follows that this increase in the tensile strength can be expressed by nothing but the decrease in the porosity or the increase in the number of contact points. The ratio:

$$\frac{\ln \sigma_{z1} - \ln \sigma_{z0}}{\ln \sigma_{z1}' - \ln \sigma_{z0}} = \frac{1}{4.5b} \quad (7)$$

thus provides the way of quantitative estimation in which the change of the tensile strength

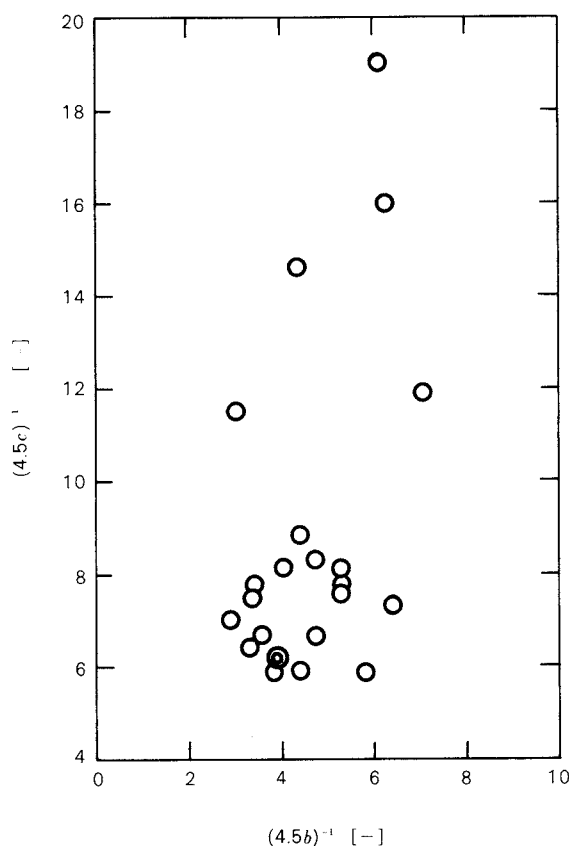


Fig. 3 Comparison of $(4.5c)^{-1}$ and $(4.5b)^{-1}$

due to the increase in the number of contact points and in the cohesive force at a contact point can be separately examined.

With respect to consolidation tests, a number of existing measurements may correlate the consolidation pressure p with the porosity ϵ using the following exponential function.

$$p = k_2 \exp\left(-\frac{\epsilon}{c}\right) \quad (8)$$

As is similar to the solution of Eq. (7), the

value $(4.5c)^{-1}$ refers how much the consolidation stress required to decrease the porosity is transmitted by increasing compaction force at a contact point.

Figure 3 shows the experimental results of the relationship between $(4.5b)^{-1}$ and $(4.5c)^{-1}$ which were obtained from 22 runs of tensile tests using adjusted porosity with pre-consolidation. Since it is remarkably seen that the value $(4.5b)^{-1}$ approximately ranges from 3 to 7 and the value $(4.5c)^{-1}$ from 6 to 19, it follows that the contribution of the porosity change is slight and the behavior will depend mainly on the force at a contact point.

3. Mechanical behavior at a contact point

As described above, the suitable method could be derived to obtain any force at a contact point. As the next step, here is discussed the mechanical behavior at a contact point resulted from such a force.

Most fundamental of the mechanical behavior at a contact point is a deformation of a particle. Nagao²⁶⁾, using grain model with surface roughness as shown in Fig. 4, related the elastic and plastic deformation w with the maximum vertical stress P_{N0} at a contact point, and thus presented the following equation:

$$w = b_m P_{N0}^{\frac{1}{m}} \quad (9)$$

The values of b_m and m for plastic deformation are indicated in Table 1. Nagao³⁶⁾ also derived the following expression which states a plastic recovery,

$$w_e = b_{em} P_{N0}^{1 - \frac{1}{2m}} \quad (10)$$

The values b_{em} and m are also indicated in Table 1.

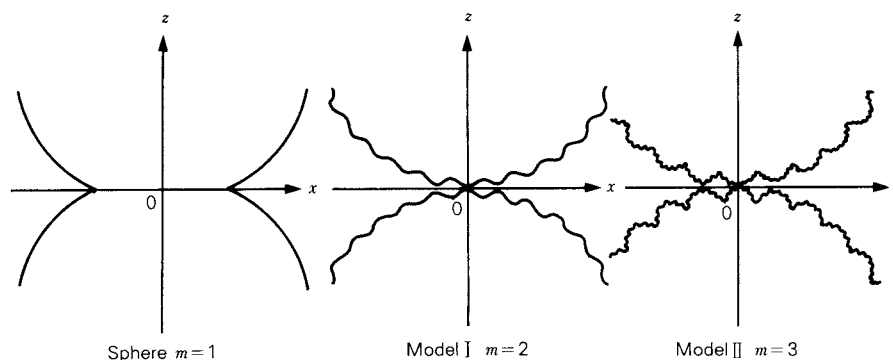


Fig. 4 Models of contact of grains

Table 1. The value of b_m , b_{em} and m for the interactions between the adjacent grains.

Shape of grain	m	b_m	b_{em}	Remarks
Plastic contact of spheres	1	$1/(2\pi p_m)$	$\frac{2(1-\nu^2)\sqrt{p_m}}{\sqrt{\pi} E}$	P_m : Yield pressure. N : Number of (small) asperities per unit area.
Plastic contact of Model I (Spheres with asperities)	2	$\frac{1}{2r} \left(\frac{2r}{\pi^2 N R p_m} \right)^{1/2}$	$\frac{8(1-\nu^2)}{3\sqrt{\pi} E} \left(\frac{N R p_m}{2r} \right)^{1/4}$	R : Mean radius of curvature of (small) asperities. N' : Number of large asperities per unit area.
Plastic contact of Model II (Spheres with large asperities covered by small asperities.)	3	$\frac{1}{2r} \left(\frac{6r^6}{\pi^3 N N' R R' p_m} \right)^{1/2}$	$\frac{16(1-\nu^2)}{5\sqrt{\pi} E} \left(\frac{N N' R R' p_m}{6r^2} \right)^{1/6}$	R' : Mean radius of curvature of large asperities. r : Mean radius of grains

As for the deformation or the flow behavior of powder beds, not only the deformation at a contact point but the friction there is of importance. Unfortunately, however, there have been few researches on the friction problems except that of Umeya^{11,62)} in which the friction factor between polystyrene pellets and the plane was measured. Nagao²⁹⁾, making use of Eq. (2) by which the distribution of forces at contact points could be obtained, quantitatively determined the surface area of spheres which would cause a slip or not.

Since the cohesive force relatively increases with a decrease in particle size, observed phenomena would become complicated. The adhesive force of single particles have been frequently measured using vibration^{17,18,19)} or impact method^{17,18,19)} as well as classical methods of balance^{3,6,66)} or centrifugal force^{5,8,13,48)}. It is because the obtained results are valid for actual applications such as dust collection and surface contamination.

The measurement of the adhesive force of a single particle was found to be greatly dependent on the particle shape and the surface roughness, which was pointed out by Jimbo^{14,16,17)}. Jimbo *et al.*⁵⁾ and Sano *et al.*⁴⁸⁾ experimentally found that the adhesive force between glass sphere and smooth glass plane is almost ten times larger than that between crushed glass particle and smooth glass plane, and the former distribution would be considerably broad. Sano *et al.*⁴⁸⁾ correlated the adhesive force to the shape factor defined by them. However in the case of discussing the shape factors from the viewpoint of particle separation mechanism, it should be necessary to pay

attention to the rotating moment around contact points, which Jimbo *et al.* pointed out in their reports^{18,19)}. Jimbo *et al.*^{18,19)} found that the separation force (adhesive force) of tangential direction is of an order to 1/10 of that of

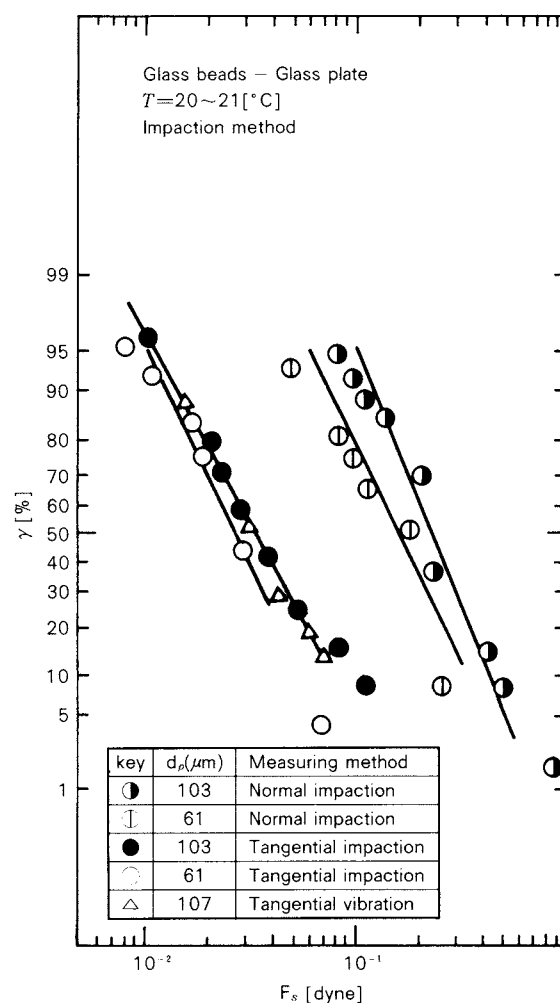


Fig. 5 The results of impactation separation method
Comparison of normal and tangential separation

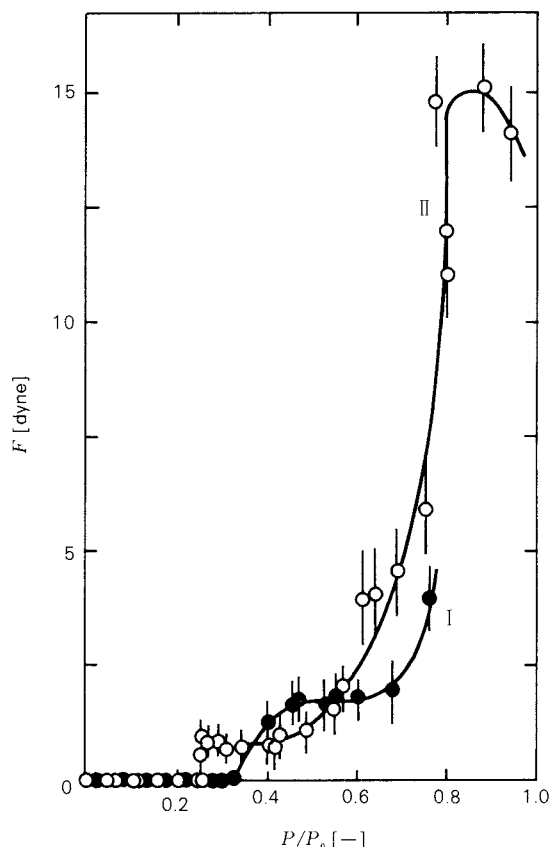


Fig. 6 Change in adhesive force of glass bead (GB503M) at a contact point with water vapor pressure
I : Glass bead—commercial plate glass
II : Glass bead—plate glass specimen prepared from glass beads

vertical direction as shown in Fig. 5.

Atmospheric conditions also have a significant influence on the adhesive force of a single particle. The measurement of a single particle adhesive force is also dependent on atmospheric condition such as humidity and temperature. As for humidity, the influence of vapor pressure or relative humidity of water and methylalcohol was experimentally examined in detail by Chikazawa *et al.*^{6,66)}. It is shown in Fig. 6⁶⁾ that the adhesive force rapidly increased when the relative humidity exceeded 60 percent or so at which the absorbed water formed liquid surface on particles^{6,8,39)} and it took a maximum value at about 80%, and it would decrease with increasing condensate water or p/p_0 . Similar tendency was obtained by other studies^{5,8,13,48)}.

As for temperature, on the other hand, the magnitude of a adhesive force was found to be greatly dependent on the kind of material.

Jimbo *et al.*^{17,18,19)} reported that the adhesive force of inorganic powder would increase with increasing temperature, with a minimum value at the temperature ranging from 100 to 150°C. As for organic powder, Danjo *et al.*⁷⁾ found that the adhesive force would increase with increasing temperature below $0.9 T_m$ K (T_m : melting point) and rapidly decrease over such a temperature.

4. Structure of powder layers

The combination of the mechanics at a contact point with that of powder beds should require the investigation into the structure of powder beds. A number of researches have been performed using a powder layer model in which monodispersed sphere particles were packed with isotropical and random arrangement. However the analysis based on such a primary hypothesis as described above might be unsatisfactory to obtain the detail information on mechanics of powder layers, and thus it follows that quantitative description of powder bed structure should be required from the micromechanical viewpoint.

Makino *et al.*^{21,22,23,51)} tried to develop a description of powder bed structure with the help of statistic mechanics. They²¹⁾ regarded random packing beds indicated in Fig. 7 (a) as statistic powder beds illustrated in Fig. 7 (b), in which individual particles were overlapped one another. They also presented a new concept called a particle density original function^{22, 23)} which could provide the particle density distribution of powder beds depending on time and space. From the viewpoint that a particle arrangement would have a significant influence on powder mechanics, also they derived the probability distribution of the first layer in

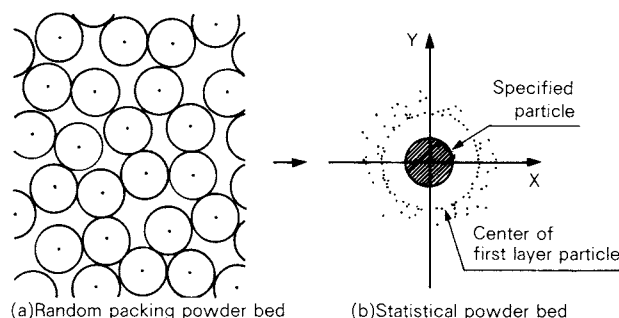


Fig. 7 Statistical representation of particle arrangement in powder bed

statistical powder beds⁵¹⁾ as shown in Fig. 7 (b).

A number of computer simulations for random packing beds have been performed to obtain radial distributions^{9,51)}, relationships between porosity and coordination number^{37,38,52,53,54)}, and other^{10,49)} which will be referred later. The porosity was related to the coordination number experimentally^{1,2)} and with model simulation^{42,44)}.

The bed structure of fine powders is more complicated due to the formation of secondary construction caused by agglomerated particles. It was experimentally found that effects of this secondary structure were considerable by Arakawa⁴⁾ and the author *et al.*⁵⁷⁾ using tensile tests, and by Hirota *et al.*¹²⁾ using shearing tests.

The change of powder bed structure is also important when the deformation or the flow behavior of powder bed is taken into account.

Makino *et al.*²¹⁾ described the deformation of packed particles using the first particle layer deformation in the statistical powder bed shown in Fig. 7 (b).

It is known that a shear deformation would destroy a isotropic structure of powder layers. This fact was ascertained experimentally by Umeya *et al.*⁶⁴⁾ (Fig. 8) and by Matsuoka²⁴⁾ with a shear test on a two-dimensionally packed bed model with a photoelastic rod, and by

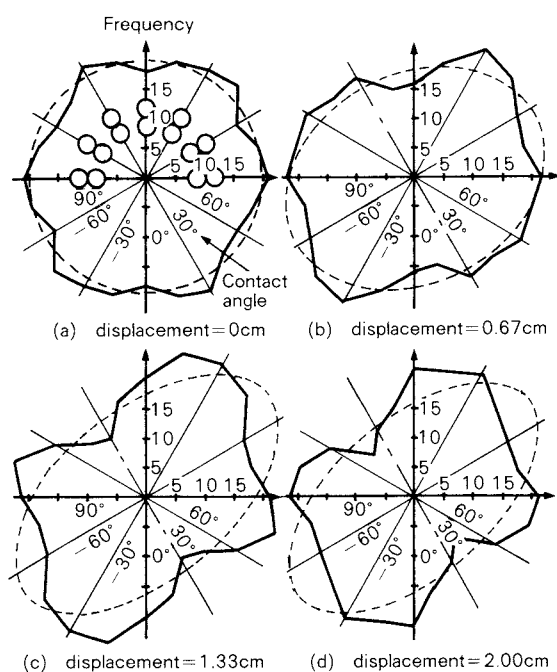


Fig. 8 The frequency distribution of contact angles (θ) (PVC rods)

Oda^{40,41)} with a two-dimensional visual observation of the yield behavior in a packed particles. Such a problem as an isotropy of powder bed structure is being discussed mainly in the field of soil mechanics.

It has been also reported that not only macroscopic but microscopic change of powder bed structure would have a significant influence on the rheological behavior such as stress-relaxation of powder beds.^{66,60,65)}

5. Relationship between mechanics at a contact point and that in powder beds

As above mentioned, works on mechanical behavior at contact points and structure of powder beds have been devoted to combine the macroscopic-microscopic relation of powder mechanics. Here it is shown to what extent the mechanics at contact points could form a connection with the mechanics of powder beds.

Nagao^{26,28,29,30,36)} and Makino *et al.*^{21,22,23,50)} presented the theoretical concepts which could be applied to more general problem of powder behavior.

Nagao, based on the stress-force relation²⁸⁾, Eq. (2) and deformation at contact points²⁶⁾, presented a theoretical relationship between stress and strain under the condition that; slip exists between individual contact particles^{29,30)}, it is negligible²⁸⁾, and consolidation pressure is released³⁶⁾. In the existence of slip motion²⁹⁾, the friction factor between individual particles was correlated with the internal friction factor in powder beds as illustrated in Fig. 9, which implies the internal friction angle could not decrease to less than 30°. He also performed

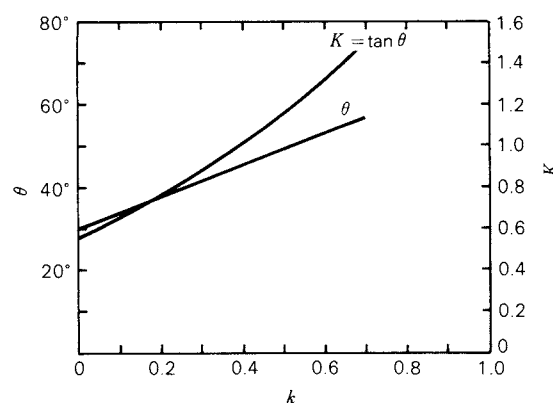


Fig. 9 Relationship between the macroscopic internal friction coefficient K and the friction coefficient between the adjacent grains k .

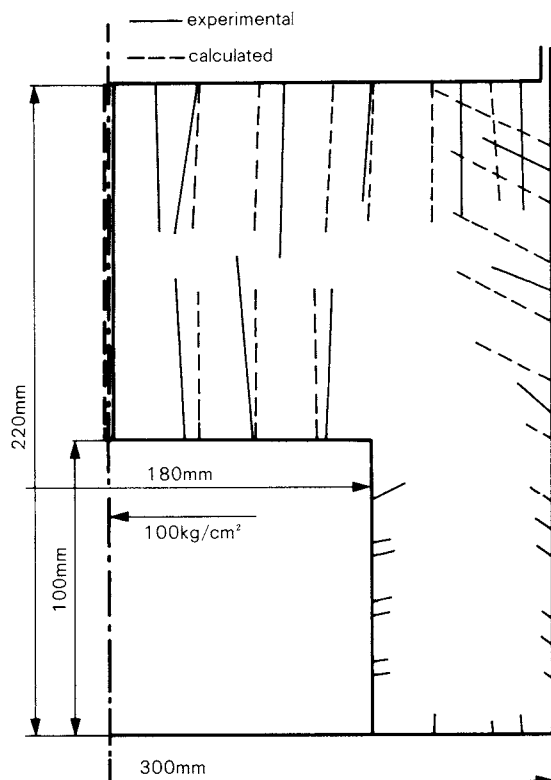


Fig. 10 Resultant stress distributions on the surface of the box (Silica sands are compressed under the mean pressure of 100kg/cm^2 on the lower surface of punch)

various consolidation tests^{27,31,32,33,34,35}) and ascertained his theories by experiments^{27,34}). The simulation of the finite-element approach based on the concept developed by Nagao could provide a stress distribution on the box surface in good agreement with measured results as illustrated in Fig.10³⁴). Although Nagao's concept made a frontal attack on the powder mechanics with rigorous logic, the problems of cohesive forces at constant points and a slip mechanism have not been made clear yet.

Makino *et al.* presented a theoretical model of powder bed yielding based on the following assumptions. One is the yield condition of constant displacement that powder beds yield when the specified particle reaches a point on the circular with a center of $S(0, s)$ and a radius of $d/2$ as shown in Fig.11²¹). The other is the Lennard-Jones typed potential energy which provides an interparticle force. They found the yield condition of constant displacement to be adequate using tests on consolida-

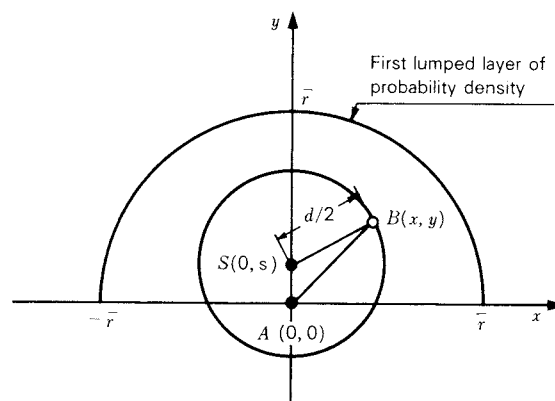


Fig. 11 Yield condition of constant displacement

tion, shear, and tensile strength, and estimated the PYL obtained from his concept as illustrated in Fig.12. Although the model made by Makino *et al.*⁵⁰) can be applied to any yield phenomenon of powder beds, it seldom seems to provide a sufficient information of the relationship between such a mechanism and the powder or particle properties which have been referred by a number of researchers. It is because the particle behavior at contact points and the strain of powder beds were daringly expressed using the potential function and the concept of statistical powder beds.

There have been several researches on individual powder bed behaviors. The author *et al.*⁵⁹) found by a semi-theoretical method that a compressive force would have a dominant effect on a tensile strength. Takahashi *et al.*⁵⁵) also made a similar point on the strength of a granule. Suzuki *et al.*⁴⁹) made a computer simulation for obtaining the relationship between a tensile strength and a porosity in the beds packed with spheres.

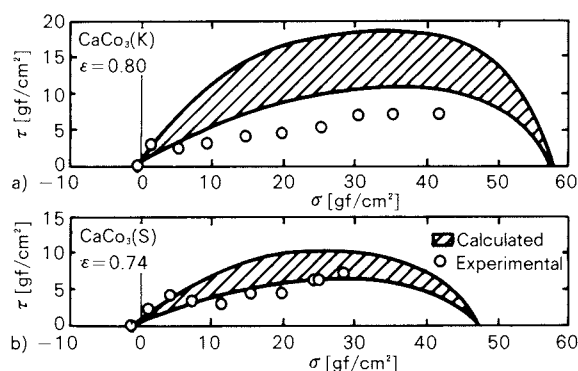


Fig. 12 Comparison between calculated yield loci and experimental results

It was shown by Gotoh *et al.*¹⁰⁾ using computer simulation that the unisotropic construction of the beds packed with spheres would result in the bottom weight distribution distorted to *M* shape. Danjo *et al.* indicated that a porosity of a powder bed packed by means of a centrifugal⁴³⁾ or an impact⁷⁾ force could be a function of the ratio of a force applied to a single particle to a cohesive force at a contact point. Basing his concept largely on the deformation at a contact point, Umeya *et al.*⁶³⁾ stated that PYL shape as well as a consolidation characteristic (the relationship between a porosity and a consolidation stress) might change at a certain consolidation stress. Umeya *et al.* investigated the qualitative relationship between stress and strain in two-dimensional model of packed beds using a straw⁶¹⁾. They⁶⁴⁾ also drew the conclusion that in a shearing two-dimensionally arrayed bed model with photoelastic rods, stress values calculated from a force at a contact point would tend to agree generally with measured results.

6. Conclusion

The present paper reviewed recent researches in Japan which microscopically investigated the mechanics of powder beds. Most of them have confined themselves chiefly to a microscopic analysis for specific objects. On the other hand Nagao and Makino *et al.* derived theoretical concepts relevant to general problems in powder mechanics which are highly estimated as a precursory investigation, though they have a few problems to be solved. The experimental researches by Umeya *et al.* are also valid because they have systematically analyzed the microscopic mechanics including rheological behaviors.

In order to develop the mechanics based on a microscopic view to more raised level, a model of powder bed structure should be required which is able to describe the deformation and/or the flow of a powder bed as the structure change. Investigations into beds structure have been actively performed in the field of soil mechanics as introduced partially in the present review.

It may be also essential to establish the appropriate measuring methods for mechanical or surface characteristics based on geometry and physical-chemistry of single particles. In par-

ticular fundamental works on friction should be required because their reports have been very few.

In this review the author tried to introduce as many studies performed in Japan as possible. Although this review involves the articles printed mainly in the field of powder technology, the author considers there are some other outstanding researches especially in the fields of pharmaceuticals, ceramics, and soil mechanics. As for soil mechanics, essential reports of powder bed structure have been printed in the English journal '*Soils and Foundation*' published by *The Japan Society of Soils Mechanics and Foundation Engineering*.

Acknowledgement

The author is grateful to Dr. Genji Jimbo, Professor of Nagoya University for valuable discussions and advice.

References

- 1) Arakawa, M.: *Journal of the Society of the Material Science, Japan*, **16**, 319 (1967).
- 2) Arakawa, M. and M. Nishino: *ibid*, **22**, 658 (1973).
- 3) Arakawa, M. and S. Yasuda: *ibid*, **26**, 858 (1977).
- 4) Arakawa, M.: *ibid*, **29**, 881 (1980).
- 5) Asakawa, S. and G. Jimbo: *ibid*, **16**, 358 (1967).
- 6) Chikazawa, M., W. Nakajima and T. Kanazawa: *Journal of the Research Association of Powder Technology, Japan*, **14**, 18 (1977).
- 7) Danjo, K. and A. Otsuka: *Yakugaku Zasshi*, **100**, 893 (1980).
- 8) Emi, H., S. Endo, C. Kanaoka and S. Kawai: *Kagaku Kogaku Ronbunshu*, **3**, 580 (1977).
- 9) Gotoh, K. and T. Chiba: *Journal of the Society of Powder Technology, Japan*, **16**, 179 (1979).
- 10) Gotoh, K., T. Chiba and A. Suzuki: *Kagaku Kogaku Ronbunshu*, **6**, 267 (1980).
- 11) Hara, R., H. Suzuki and K. Umeya: *Journal of the Society of the Material Science, Japan*, **30**, 867 (1981).
- 12) Hirota, M., Y. Iwamoto, T. Kobayashi and T. Oshima: *Journal of the Society of Powder Technology, Japan*, **21**, 69 (1984).
- 13) Jimbo, G. and S. Asakawa: *Journal of the Research Association of Powder Technology, Japan*, special issue, **6** (1966).
- 14) Jimbo, G.: *Journal of the Society of the Material Science, Japan*, **16**, 291 (1967).
- 15) Jimbo, G. and S. Asakawa and N. Soga: *ibid*, **17**, 177 (1968).
- 16) Jimbo, G.: *Kemikaru Enjiniyaringu*, **13**, 631

- (1968).
- 17) Jimbo, G. and R. Yamazaki: Preprints of European Symposium Particle Technology, B, 1064 (1980 Amsterdam).
 - 18) Jimbo, G., R. Yamazaki and G. Hong.: Semi-Annual Report of the Asahi Glass Foundation for the Contribution to Industrial Technology, **38**, 123 (1981).
 - 19) Jimbo, G. and R. Yamazaki: *KONA*, **1**, 40 (1983).
 - 20) Kanatani K.: *Journal of the Society of Powder Technology, Japan*, **17**, 504 (1980).
 - 21) Makino, K., K. Saiwai, M. Suzuki, T. Tamamura and K. Iinoya: *Kagaku Kogaku Ronbunshu*, **4**, 439 (1978).
 - 22) Makino, K.: *Journal of the Japan Society of Powder and Powder Metallurgy*, **28**, 269 (1981).
 - 23) Makino, K.: *ibid*, **28**, 276 (1981).
 - 24) Matsuoka, H.: *Soils and Foundations*, **41**, 29 (1974a).
 - 25) Molerus, O.: *Powder Technology*, **12**, 259 (1975).
 - 26) Nagao, T.: *Transactions of the Japan Society of Mechanical Engineers*, **33**, 229 (1967) or *Bulletin of JSME*, **10**, 775 (1967).
 - 27) Nagao, T.: *ibid*, **34**, 100 (1968).
 - 28) Nagao, T.: *ibid*, **43**, 4038 (1977) or *Bulletin of JSME*, **21**, 1077 (1978).
 - 29) Nagao, T.: *ibid*, **44**, 1912 (1978) or *Bulletin of JSME*, **22**, 148 (1979).
 - 30) Nagao, T.: *ibid*, **44**, 2967 (1978) or *Bulletin of JSME*, **22**, 636 (1979).
 - 31) Nagao, T., K. Chijiwa, Y. Hatamura, K. Takeuchi and E. Shinohara: *Journal of the Society of Powder Technology*, **15**, 643 (1978).
 - 32) Nagao, T., K. Chijiwa, Y. Hatamura, K. Takeuchi, N. Nakashima and H. Okamoto: *ibid*, **16**, 460 (1979).
 - 33) Nagao, T., K. Chijiwa, Y. Hatamura, K. Takeuchi and E. Shinohara: *ibid*, **16**, 625 (1979).
 - 34) Nagao, T. and S. Katayama: *Transactions of the Japan Society of Mechanical Engineers*, **46**, 355 (1980) or *Bulletin of JSME*, **23**, 1763 (1980).
 - 35) Nagao, T., K. Chijiwa, Y. Hatamura, K. Takeuchi, N. Nakashima and H. Okamoto: *Journal of the Society of Powder Technology, Japan*, **17**, 10 (1980).
 - 36) Nagao, T.: *Transactions of the Japan Society of Mechanical Engineers*, **47**, 1363 (1981).
 - 37) Nakagaki, M. and H. Sunada: *Yakugaku Zasshi*, **83**, 73 (1963).
 - 38) Nakagaki, M. and H. Sunada: *ibid*, **88**, 651 (1968).
 - 39) Nishino, M. and M. Arakawa: *Journal of the Society of the Material Science, Japan*, **22**, 663 (1973).
 - 40) Oda, M.: *Soils and Foundations*, **12**, 1 (1972).
 - 41) Oda, M. and J. Konishi: *ibid*, **14**, 25 (1974).
 - 42) Okazaki, M., T. Yamazaki, S. Gotoh and R. Toei: *Journal of Chemical Engineering of Japan*, **14**, 1983 (1981).
 - 43) Otsuka, A., H. Sunada and K. Danjo: *Yakugaku Zasshi*, **89**, 1013 (1969).
 - 44) Ouchiyama, N. and T. Tanaka: *Industrial and Engineering Chemistry, Fundamentals*, **19**, 338 (1980).
 - 45) Pietsch, W. and H. Rumpf: *Chemie Ingenieur Technik*, **39**, 885 (1967).
 - 46) Rumpf, H.: *ibid*, **30**, 144 (1958).
 - 47) Rumpf, H.: *ibid*, **42**, 538 (1970).
 - 48) Sano, S., F. Saito and S. Yashima: *Kagaku Kogaku Ronbunshu*, **10**, 17 (1984).
 - 49) Suzuki, A. and K. Gotoh: *ibid*, **7**, 628 (1981).
 - 50) Suzuki, M., K. Makino and K. Saiwai, H. Yamamoto and K. Iinoya: *ibid*, **5**, 481 (1979).
 - 51) Suzuki, M., K. Makino, T. Tamamura and K. Iinoya: *ibid*, **5**, 616 (1979).
 - 52) Suzuki, M., K. Makino, M. Yamada and K. Iinoya: *ibid*, **6**, 58 (1980).
 - 53) Suzuki, M. and T. Oshima: *Powder Technology*, **35**, 159 (1983).
 - 54) Suzuki, M. and T. Oshima: *ibid*, **36**, 181 (1983).
 - 55) Takahashi, M., T. Kobayashi and S. Suzuki: *Annual Report of Ceramic Engineering Research Laboratory (Nagoya Institute of Technology)* **8**, 25 (1981).
 - 56) Tanno, K., S. Kikuta and Y. Matsuda: *Journal of the Society of Powder Technology, Japan*, **18**, 887 (1981).
 - 57) Tsubaki, J., K. Kato and G. Jimbo: *ibid*, **18**, 873 (1981).
 - 58) Tsubaki, J.: *ibid*, **21**, 30 (1984).
 - 59) Tsubaki, J. and G. Jimbo: *Powder Technology*, **37**, 219 (1984).
 - 60) Tsubaki, J., G. Jimbo and K. Takagi: Proceedings of 3. European Symposium on Particle Characterization (1984 Nürnberg).
 - 61) Umeya, K., N. Kitamori, R. Hara and T. Yoshida: *Journal of the Society of the Material Science, Japan*, **18**, 489 (1969).
 - 62) Umeya, K., T. Isoda, R. Hara and J. Kikuta: *ibid*, **23**, 549 (1974).
 - 63) Umeya, K., T. Isoda, R. Hara and Y. Kato: *ibid*, **22**, 637 (1973).
 - 64) Umeya, K., R. Hara: *Journal of Chemical Engineering of Japan*, **8**, 56 (1975).
 - 65) Umeya, K., R. Hara and T. Kimura: *Journal of the Society of the Material Science, Japan*, **25**, 623 (1976).
 - 66) Yamaguchi, T., M. Tomita, M. Chikazawa and T. Kanazawa: *Journal of the Society of Powder Technology, Japan*, **16**, 514 (1979).

Informational Articles

The Symposium on Powder Technology

The Party of Powder Technology (Japan) held the 17th symposium at Kenpo-Kaikan in Tokyo on September 8th, 1983. This symposium was given with the theme "*Characteristics and application of ultra-fine particles*" which has awaken considerable interest in the ad-

vanced industries such as electronics, exotic ceramics, etc.

About 170 participants involving researchers and users filled the assembly hall, and discussed several subjects indicated in the following program.

Lecture topic	Lecturer
• Fineness and chemical characteristics of powders	Masafumi Arakawa (Institute for Chemical Research, Kyoto University)
• Production of ultra-fine particles by grinding and its application	Tohei Yokoyama (Hosokawa Micromeritics Laboratory)
• Separation of ultra-fine particles	Satoshi Okuda (Doshisha University)
• Agglomeration and separation efficiency of ultra-fine particles	Akira Suganuma (Tokyo University)
• Separation of submicron particles	Hitoshi Emi (Kanazawa University)
• Effective use of clean room	Yoshio Okuma (Hosokawa Environmental Engineering)
• General discussion	Naoya Yoshioka [Chairman] (Kyoto University)

The next symposium will be held in Osaka on August 8th, 1984 with the theme "*Interface at theory and practice in powder processing*".



Lecturers: Dr. N. Yoshioka, Dr. H. Emi, Dr. A. Suganuma and Mr. Y. Okuma from the left.



The participants in the assembly hall.

Photos: The 17th symposium on powder technology in 1983.

Academic publication concerning powder technology in Japan (printed in 1983)

Journal of the Society of Powder Technology, Japan Vol. 20 (1983)

Title	Author(s)	Page
• Studies on Closed-up Air Flows Out Through Porous Media	T. Issiki and K. Yaginuma	3–7
• The Sieving Rate of Cylinder Particles	S. Endoh, J. Koga and K. Yamaguchi	8–14
• Measurement of Wettability of Particles by the Constant Flow Method	K. Matsumoto, S. Omenyi and C.E. Capes	15–21
• The Uniformity and Physical Properties of Sodium Bicarbonate by the Addition of Coarser Particles	H. Hayashi, T. Kasano and K. Suhara	22–27
• A Consideration of Fracture with Compression Loading of Glass Bead	Y. Yamada	59–62
• Energy and Displacement Required to Split Power Bed	J. Tsubaki, K. Kato and G. Jimbo	63–68
• Experimental Study of the Power Required to Crush Wood and Bark	H. Endoh, H. Takahashi, K. Yamaguchi and K. Endoh	68–73
• Measurement of Pore Distribution by Water Vapour Adsorption	C. Arai, T. Mizutani, Y. Murase, T. Hanakawa and Y. Sano	115–121
• Grinding Characteristics and Mechanochemical Behaviors of Sericite Powder with Vibration Ball-Milling	K. Suzuki, S. Tomura and Y. Kuwahara	122–128
• Development of a Fineness Measuring Air Classifier (I)	Y. Yamada, M. Yasuguchi, E. Honma, M. Kabaya, H. Tomiyasu and K. Iinoya	128–134
• Simulation of Moving Granular-Bed Type Heat Exchanger	T. Minoura, S. Mizukami, T. Asami and H. Kohama	185–193
• The Properties of II-CaSO ₄ Obtained by Flash-Calcination	H. Tanaka, K. Uchida and Y. Kanesaki	194–202
• Behaviors of a Single Particle and Classification in Rotating Tilted Liquid Column	K. Ueda, K. Shirane and I. Aoki	202–210
• Atomization of Slurries Due to Pneumatic Nozzle	N. Yamada, H. Hirose, H. Ihara and T. Murayama	211–217
• Equilibrium Moisture Content of Porous Materials	C. Arai, K. Wani, T. Takahashi, H. Segawa and Y. Sano	265–270
• Computer Simulation of Pneumatic Conveying –The Case of the Presence of Pipe Branches–	Y. Tsuji, W. Seki and Y. Morikawa	270–279
• Electric Potential Distribution Profiles and Its Effects in Naturally Charged Fluidized Bed	M. Fujino, S. Ogata and H. Shinohara	280–290
• Energy Saving in a Suspension Preheater –Development of a High Performance Cyclone–	T. Fujisawa and T. Tanioka	337–346
• Viscosity Measurement of the Powder Plastic Body with a Parallel Plate Plastmeter	K. Uchida, M. Kuwamura, T. Ohtake and E. Ikazaki	347–351
• Reentrainment of Fine Particles from a Cylindrical Powder Layer Adhering on a Tube Wall	H. Masuda, S. Matsusaka, and Y. Sumiura	405–410
• Preparation of Active Powdery Materials by High Temperature Grinding	Y. Kanaya and M. Senna	411–415
• The Particle Growth Mechanism of Binapacryl in Aqueous Suspensions	M. Fujimoto, T. Nakamura and E. Muraoka	416–422

• Flow Behavior of Particles in a Storage Vessel of a Table Feeder	Z. Han, T. Kadowaki, H. Masuda and Y. Kawamura	479—485
• Transient State Simulation of Moving Granular-Bed Type Heat Exchanger	T. Minoura, S. Mizukami T. Asami and H. Kohama	485—492
• Proper Test Conditions for Measurement by a Direct Shear Tester with Parallel Plates	M. Hirota, T. Kobayashi and T. Oshima	493—498
• Azecotrope Prediction of Binary Liquid Mixtures on the Basis of a Random Packing Structure Model of Particulate Matters	H. Miyazaki and T. Tanaka	499—507
• The Packing Property and Adhesive Force of Heavy Calcium Carbonate Powder	M. Chikazawa and T. Kanazawa	543—547
• Selection of a Preferable Mulling Condition for Wet-Powder Using a Tensile Tester	K. Terashita, K. Miyanami T. Kimura and M. Mori	548—553
• Measurement of Pore Distributions by Equilibrium Moisture Content Curves	C. Arai, K. Onda, K. Kajiyama and Y. Sano	599—604
• Mixing of Wet Powders by Vertical Cylindrical-Type Mixer	M. Satoh, J. Yoshida and K. Miyanami	604—610
• Weight Control of a Hopper by Using a Microcomputer —Application of Finite Time Settling Control to Granular Materials which have a Good Flowability —	K. Wada, Y. Matsuzaki and N. Hayano	653—662
• An Analysis of Laboratory Hammer Screen Mill Based on a Grinding Rate Equation	S. Yashima and Y. Arai and S. Sano	663—670
• Deposition of Charged Aerosol Particles Flowing through Parallel Plates	S. Ikumi, T. Ito and H. Masuda	670—676
• Effects of Explosive Shock Treatment on Phase-Transition and Sinterability of Fine TiO_2 and ZrO_2 Powders	F. Ikazaki, K. Uchida, A. Goto, M. Kawamura and S. Fujiwara	717—722
• Process of Forming Seamless Capsules by a Concentric Nozzle System	T. Suzuki, H. Sunohara and R. Kamaguchi	723—727
• Molecular Interaction between Drugs and Cyclodextrins by Grinding	Y. Nakai, K. Yamamoto and K. Terada	728—733
• Effect of Binders on the Tensile Strength of Green Mold Sands	K. Terashita, T. Kimura, H. Tsukaguchi and K. Miyanami	733—738
• The Effect of Particle Size Reduction by Milling on Tablet Hardness	Y. Sagawa	738—743
• Surface Modification of Fine Powders and the Reactivity of the Surface Groups —The Surface-Treatment of Silica Gels with Organo-Silyl Chlorides and the Chemical Properties of their Surface Groups—	H. Utsugi and N. Suzuki	744—751

Funsai (The Micromeritics) No. 28 (1984)

Title	Authors	Page
• Triboelectric Separator for Plastics Sorting System	Y. Nakajima and T. Tanaka	4—13
• Performance Evaluation of Mixing and Mulling Process of Wet Powders	K. Terashita, H. Tsukaguchi, T. Kimura, N. Shinke and K. Miyanami	14—21
• Influence of Nozzle, Flow-corrective Insert and Voidage on Particle Flow in a Blow Tank Solids Conveyor	Y. Tomita and S. Makimoto	22—28

Kagaku Kogaku Ronbun-shu Vol. 9 (1983)

Title	Authors	Page
• Dispersion of Aggregated Airborne Dust by Orifice	H. Yamamoto and A. Suganuma	183–188
• Experimental Investigation of the Disintegrating Phenomena of Aggregates of Fine Powders in Air Flow	J. Tsubaki, K. Kato, N. Nagahiro and G. Jimbo	189–194
• Change in Aerosol Particle Charges in Stream from Charge Neutralizer	T. Takahashi and A. Kanagawa	295–301
• An Experimental Study of the Technics of Reducing Power Consumption in Pneumatic Conveying of Granular Materials —Effects of pulsating motion of conveying air and vibratory motion of conveying pipe—	T. Kano, F. Takeuchi, Y. Kondo, M. Utsumi, T. Maeda and K. Takemura	477–481
• A Pneumatic Classifier for Fine Powders Based on the Rapid Classification Principle	K. Yoshie, H. Yamamoto, Akira Suganuma and R. Aoki	530–535
• Collection Efficiency of Granular Bed Filters by Diffusion and Direct Interception	N. Kimura, H. Mori, T. Tomita, A. Yagi and M. Shirato	536–542
• Horizontal Jet Penetration into Powder Beds under Different Aeration Conditions	M. Horio, A. Nishiyama, J. Liu and I. Muchi	609–616

Journal of Chemical Engineering of Japan Vol. 16 (1983)

Title	Authors	Page
• Electrical Neutralization of Charged Aerosol Particles by Bipolar Ions	M. Adachi, K. Okumura and Y. Kousaka	229–235
• Water Transfer Coefficient in Adsorptive Porous Body	R. Toei, H. Imakona, H. Tamon and M. Okazaki	364–369

Journal of the Society of Materials Science, Japan Vol. 32 (1983)

Title	Author(s)	Page
• Preparation of Ultrafine Nitride Particles of Group IIIa, IVa, Va and VIa Elements by Reactive Gas Evaporation Technique	S. Iwasa, K. Hayakawa and T. Arizumi	943–947
• Analysis of the Effectiveness Factor on a Catalytic Reaction within Silica Alumina Pellets with Multi-Modal Pore Size Distributions	K. Mukaida	948–952
• Dependence of Tensile Strength of Compacted Powder Bed on Deformation Characteristics of its Granules	M. Takahashi, T. Kobayashi and S. Suzuki	953–957
• Effect of Tensile Strength and Tensile-Breakup Energy on Mulling Power Requirement of Green Mold Sands	K. Terashita, K. Miyanami and T. Kimura	958–961
• Characterization of α -FeOOH Powders and α -Fe ₂ O ₃ Derived Therefrom	T. Yamaguchi, T. Takahashi and S. Hirokawa	962–965
• Comparative Data of Particle Size Distribution on Flake Like Particles by Various Methods	M. Arakawa, T. Yokoyama, T. Yamaguchi and T. Minami	966–970
• Electric Resistance as a Measure for Estimating Randomness of Binary Solid Particles System —Effect of Extended System—	Y. Fujihara and Y. Yoshimura	971–976
• Measurement of Water Vapour Adsorption on Porous Materials by Means of Humidity Sensor	A. Takasaka, K. Hishinuma and Y. Matsuda	977–980

Vertical grinding machine

A new typed vertical grinding machine (Micron Vertech Mill) in **Photo. 1** was recently developed by Hosokawa Micron Corp. (Osaka, Japan) for the purpose of greater production capacities, improved products, stricter quality controls, and lower operating cost. This equipment is constructed of three sections; the lower section for a pulverizing chamber, the middle section for a primary air classifying chamber, and the upper section for a fine-classifying chamber. Ten types of the equipment are available for users: the smallest type is MVM-15 (11 KW required for grinding) and the largest type is MVM-500-6H (370 KW). This grinding machine features high capacity, compact unit, energy saving, stabilized operation, easy adjustment for adjustment for particle size, and easy maintenance.

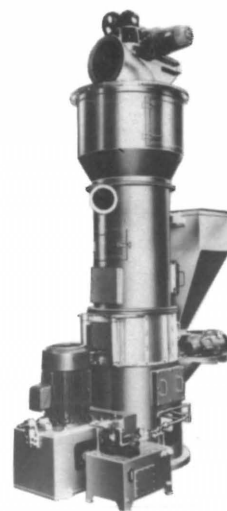


Photo. 1 *Hosokawa Micron Vertech Mill*

Automatic particle size distribution analyzer

An automatic particle size distribution analyzer based on the sedimentation principle (Sedimenputer SPT-G) was recently developed by Hosokawa Micron Corp. (Osaka, Japan). This analyzer shown in **Photo. 2**, which consists of the three parts such as measuring unit, analyzing unit with microprocessor, and X-Y plotter, automatically provides data of both differential and cumulative distributions. In addition this system can be connected with four measuring units for obtaining different data simultaneously.

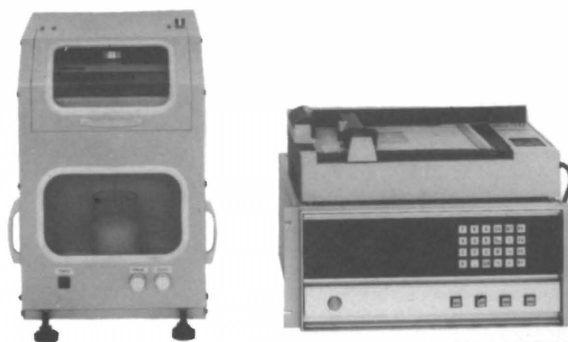
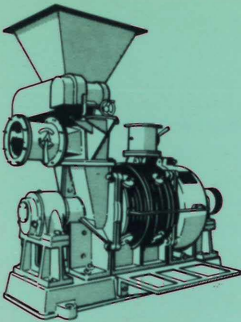
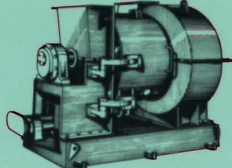
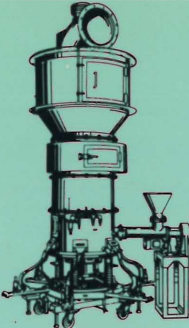
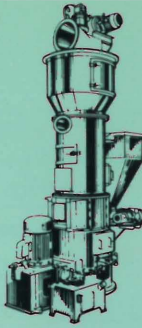
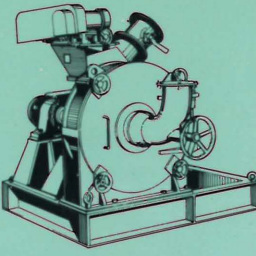
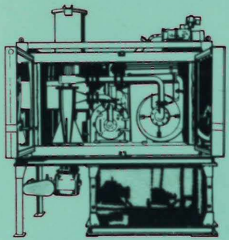
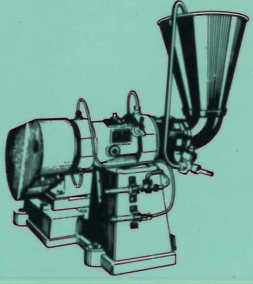
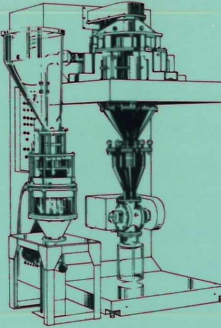
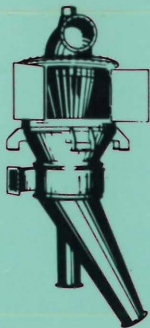
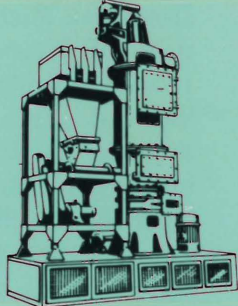
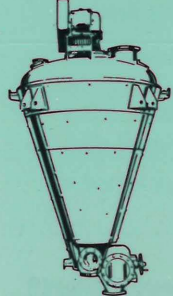
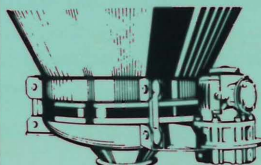
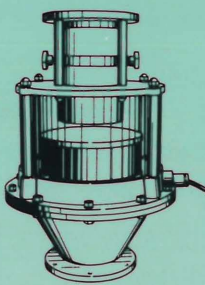
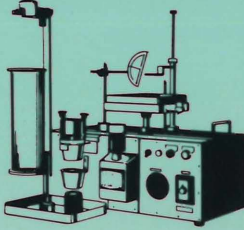
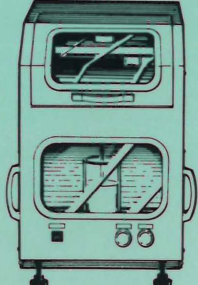


Photo. 2 *Hosokawa Micron Sedimenputer (SPT-G)*

Information from editors to readers

With regard to the units to be used in this journal, SI units will be employed from the next issue so that readers can understand mathematical expressions, figures, tables, etc. more easily.

				
Ultra-fine grinding Super Micron Mill	Ultra-fine grinding Fine Micron Mill	Ultra-fine pulverizing Micron Jet	Fine-grinding Micron Vertech Mill	Fine-grinding Fine Victory Mill
				
Cryogenic pulverizing Linrex Mill	Homogenizing Disperse Mill	Classifying Super Separator	Classifying Micron Separator	Drying Micron Dryer
				
Mixing/Drying Nauta Mixer-Reactor	Bridge Breaking/ Discharging Bin Activator	Feeding/Discharging Flo-tron	Measurements Powder Characteristics Tester	Particle Size Measuring Sedimenputer

HOSOKAWA

LEADER OF POWDER PROCESSING TECHNOLOGY

From a Single Unit to Complete Treatment System

Hosokawa has specialized in powder processing technology for over 65 years. Today, Hosokawa makes a complete line of advanced equipment for fine-grinding, classifying, drying, mixing, dust collection, measurement and so on. Yet, Hosokawa's most distinguished feature is

its capability of the system engineering that will satisfy a wide variety of industrial needs. Whenever you have a problem, planning, or project relating to powders, first consult with Hosokawa.

HOSOKAWA MICRON CORPORATION

Hosokawa Products are available from:

In Europe (Continent)
Hosokawa-Nauta Europa B.V.
2003 RT Haarlem, Holland,
P.O. Box 773, Nijverheidsweg 25
Telephone: (023) 31 9073
Telex: 41167
Facsimile: 23 318380

In the U.K.
Hosokawa-Nauta (UK) Ltd.
Hughenden Road, High Wycombe
Buckinghamshire, England.
Telephone: (0494) 443866
Telex: 837208
Facsimile: 494 443868

In the U.S.A.
Vibra Screw Incorporated
755 Union Boulevard,
Totowa, N.J. 07511
Telephone: (201) 256-7410
Telex: 685-3382

Other Areas
Hosokawa International Inc.
No.10, 2-chome, Minami-kyutaro Machi,
Higashi-ku, Osaka 541, Japan
Telephone: (06) 261-5141
Telex: J63837
Facsimile: (06) 266-9314